Statens strålevern
Norwegian Radiation Protection Authority

StrålevernRapport 2017:12

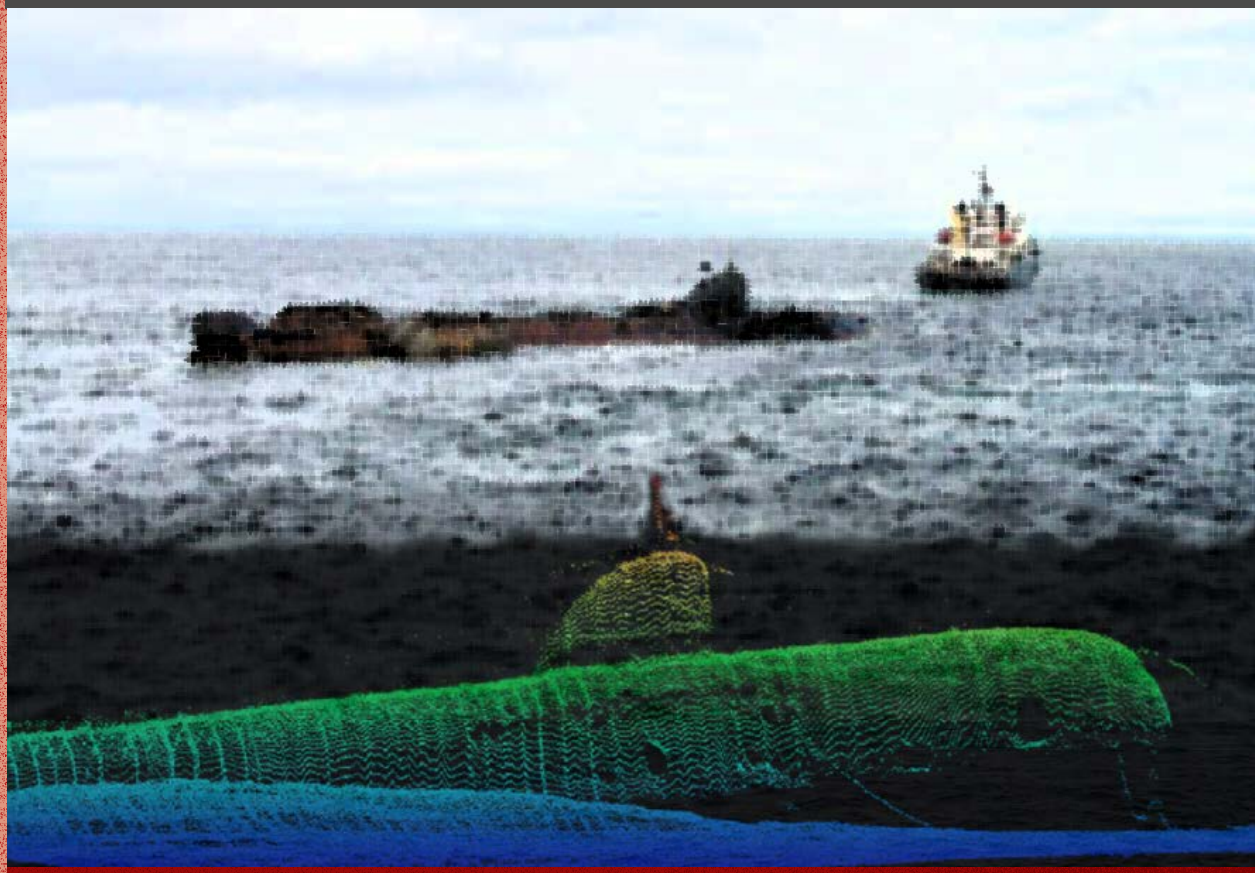

Radiological impact assessment for hypothetical accident scenarios involving the Russian nuclear submarine K-159

Reference:
Hosseini A, Amundsen I, Brown J, Dowdall M, Dyve JE, Klein H. Radiological impact assessment for hypothetical accident scenarios involving the Russian nuclear submarine K-159. StrålevernRapport 2017:12. Østerås: Statens strålevern, 2017.

Key words:
Sunken objects in the Arctic, Submarine K-159, Recovery of K-159, Contamination, Consequences, Concentration, Doses, Criticality scenarios.

Abstract:
The report presents a new and updated human health and environmental impact assessment for the sunken nuclear submarine K-159. The work is based on the development of different hypothetical accident scenarios resulting in releases of radioactivity into the environment and evaluating possible associated consequences for human and the environment.

Referanse:
Hosseini A, Amundsen I, Brown J, Dowdall M, Dyve JE, Klein H. Radiological impact assessment for hypothetical accident scenarios involving the Russian nuclear submarine K-159. StrålevernRapport 2017:12. Østerås: Statens strålevern, 2017.
Language: English.

Emneord:
Sunkne objekter i Arktisk, Atomubåt K-159, Kritikalitet scenarier, Løfting av K-159, Konsekvensvurderinger, Nedfall, Radioaktivitet, Doser

Resymé:
Rapporten presenterer en ny og oppdatert radiologisk konsekvensvurdering av den russiske atomubåten K-159. Arbeidet tar utgangspunkt i ulike hypotetiske ulykkescenarier som resulterer i utslipp av radioaktivitet til miljøet og evaluering av mulige konsekvenser for mennesker og miljø.

Head of project: Ali Hosseini
Approved:

Per Strand, director, Department of Emergency Preparedness and Environmental Radioactivity

141 pages.
Published 2017-11-24.
Printed number 50 (17-11).
Printed by 07 Media.
Cover illustration: Ali Hosseini

Norwegian Radiation Protection Authority, P.O. Box 55, N-1332 Østerås, Norway.
Telephone +47 67 16 25 00
E-mail: nrpa@nrpa.no
www.nrpa.no
ISSN 0804-4910 (print)
ISSN 1891-5205 (online)

StrålevernRapport 2017:12

Radiological impact assessment for hypothetical accident scenarios involving the Russian nuclear submarine K-159

Hosseini A,

Amundsen I,

Brown J,

Dowdall M,

Dyve JE,

Klein H.

Statens strålevern

Norwegian Radiation Protection Authority
Østerås, 2017

Contents

1	**Introduction**	**5**
1.1	K-159: Generic data and information	7
1.2	Accident and the sinking of K-159	8
1.3	Condition of Spent Nuclear Fuel (SNF) in the reactors of K-159 before sinking	10
1.4	Activity in the reactors of K-159 at the accident time and at present (2014)	10
1.5	Data on sea currents in the submarine sinking Area	13
2	**An overview of expeditions to the sinking site of the K-159 submarine**	**15**
2.1	Joint Norwegian-Russian expedition 2014	19
3	**Potential accident scenarios**	**20**
3.1	Release scenarios related to depressurization of the primary circuit	21
	3.1.1 Safety barriers of the submarine and characterization of their possible degradation	*21*
	3.1.2 Depressurization of the primary circuit and fuel claddings	*23*
	3.1.3 Radioactivity distribution inside the submarine's compartments	*24*
	3.1.4 Radioactivity releases to the sea	*25*
3.2	Accident scenarios involving initiation of Spontaneous Chain Reaction (SCR)	26
	3.2.1 General description of possible accidents involving SCR	*27*
	3.2.2 Estimates of radioactivity releases and consequences	*28*
4	**Marine dispersion modelling**	**32**
4.1	Water circulation in the Barents Sea	32
4.2	Features of the arctic ocean model	33
4.3	Setting a numerical experiment	34
4.4	Results of modeling dynamic characteristics of the Barents Sea	36
4.5	Modelling and analysis of the transfer by sea currents	39
	4.5.1 Statement of the problem	*39*
	4.5.2 Surface release at winter	*39*
	4.5.3 Bottom release at winter	*43*
	4.5.4 Surface and bottom releases at summer	*45*
5	**Atmospheric dispersion modelling**	**46**
5.1	Construction of a deposition database	46
5.2	Worst case source term	47
5.3	Concentrations in atmosphere and deposition	48
	5.3.1 Influence of thresholds and time on selection procedure	*48*
	5.3.2 Seasonal variation of air transport	*49*
5.4	Worst case run	50
5.5	Influence of release height and particle classes	52

6 Considerations regarding dose assessment methodology 54
6.1 Quantifying impacts to man and the environment 54
6.2 Modelling transfer of radionuclides through food-chains 56
6.3 Modelling doses to humans and the environment 56
6.3.1 Models used for human dose assessment 56
6.3.2 Models used for environmental impact assessment 59
6.4 Contextualising impacts to humans and the environment 61
6.4.1 Humans 61
6.4.2 Environment 62
7 Estimated activity concentrations and doses 64
7.1 Terrestrial ecosystem 64
7.2 Marine ecosystem 66
7.3 Human dose estimates 70
7.4 Dose estimation for non-human biota 71
7.4.1 Terrestrial 71
7.4.2 Marine 73
8 Dealing with uncertainty 75
9 Summary and concluding remarks 77
10 Acknowledgments 82
Appendix 1: Mathematical Formulation of the INM-IO Ocean Model 83
A. Approximation of spatial operators 85
B. Application of the model 85
Appendix 2: Marine dispersion modelling - assumptions and resultant concentration maps 86
Appendix 3: Derivation of a threshold for deposition assessment in atmospheric dispersion modelling 119
Appendix 4: Modelling transfer of radionuclides through food-chains 120
A. Marine food-chain model description 120
B. Terrestrial food-chain Model description 124
References 132

1 Introduction

From an environmental perspective, the Arctic is of great importance on both a global and regional scale. The Arctic influences the formation of global weather patterns and constitutes a sensitive indicator of climate change. For Norway, the Arctic is very important as one third of its land mass and 80% of its sea areas lie within the Arctic. Furthermore, fish is a major export goods for Norway, with a substantial amount originating from boreal-Arctic waters: the Barents and Norwegian Seas. The Arctic is perceived to be a pristine and vulnerable region of direct economic and socioeconomic importance for a number of countries.

From an environmental point of view, the Arctic has a unique position. For instance, the Barents Sea is home to some of the largest fish stocks in the world, e.g. the capelin (*Mallotus villosus*), the Northeast Arctic cod (*Gadus morhua*) and the Norwegian spring spawning herring (*Clupea harengus*) (IAEA 1998). In addition, , the Barents Sea plays an essential role as a feeding ground for fish populations harvested further south on the Norwegian shelf. The Norwegian shelf area from 62°N northwards is a spawning ground for the most important fish populations of the Northeast Atlantic. Fish eggs and larvae are transported via the Norwegian Coastal Current into the Barents Sea, where fish fry may benefit from abundant food (Stiansen et al., 2009).

The Barents Sea contains one of the largest concentrations of seabirds in the world as well as a diverse collection of marine mammals, including polar bears. A rich community of benthic invertebrates, more than 3000 species, inhabit the Barents Sea (Stiansen et al., 2009). It also contains a diverse community of planktonic algae and algae attached to sea ice, both of which contribute to primary production in the region. The Barents Sea is also home to some endangered species. The list of such species from the Barents Sea include 28 fish species, 9 bird species, and 18 mammal species (Stiansen et al., 2009).

With these considerations in mind, coupled to the fact that the Arctic contains several potential radionuclide sources (e.g. the Kola nuclear power plant, dumped radioactive waste, sunken reactor-driven submarines), it is quite understandable that there has been and continues to be concern over potential radioactive contamination of this region.

To address this concern, the Norwegian Government's Nuclear Action Plan was launched in April 1995. A key objective of the plan is to reduce the risk of serious nuclear accidents and radioactive pollution as well as the prevention of radioactive and fissile material falling into the wrong hands.

During the last two decades, the Norwegian Radiation Protection Authority (NRPA) has been involved in conducting health and environmental risk assessments for various Russian nuclear facilities and installations. Lately, in line with this practice and under activities initiated as part of the Norwegian Nuclear Action Plan, the NRPA initiated two studies where the main focus of investigation has been Russian dumped and sunken nuclear submarines in the Arctic.

Concern is raised over potential radioactive contamination of the Arctic due to the presence of a wide range of nuclear sources within this region, in particular, dumped and sunken nuclear submarines containing Spent Nuclear Fuel (SNF).

The Russian dumped submarine K-27 has been the subject of the first of the two aforementioned NRPA studies where different issues pertaining to health and environmental risk assessment have been explored and analysed (NRPA 2015 & 2016).

The focus of the present study is another Russian nuclear submarine, K-159, which is a sunken as opposed to a dumped object and which constitutes another major potential source of radioactive contamination in the Arctic seas. The Russian submarine K-159 sank on 30 August, 2003 at about 3:00 AM (Russian time), ca. 6 km northwest of Kildin Island. In this tragic accident, nine of the crew members went down with the submarine. The submarine was being towed from Gremikha to the Nerpa shipyard in the town of Snezhnogorsk in Murmansk Oblast for dismantlement. The submarine currently lies at a depth of 246 meters, less than 130 km from the border with Norway. In addition to its vicinity to Norway, the K-159 submarine lies close to fishing areas of the Barents Sea. It also represents the single largest potential source of radioactive contamination to the Arctic marine environment (NRPA 2014).

Shortly after the accident, NRPA conducted a study in which the issue of health and environmental risk assessment associated with K-159 was very briefly discussed (NRPA 2006). Now, 14 years after its sinking, more detailed information regarding potential source terms and possible recovery operations have come to light. These, in conjunction with the availability of more sophisticated modelling tools render a detailed assessment timely and more robust.

With these considerations in mind, the main objective of the present study was to provide a new and updated human health and environmental impact assessment for the sunken nuclear submarine K-159. The study is based on the development of different hypothetical accident scenarios and evaluation of possible associated consequences for human and the environment.

The present report is the product of a collaborative effort between the Norwegian Radiation Protection Authority and the Russian Energy Safety Analysis Centre of IBRAE RAN.

1.1 K-159: Generic data and information

Nuclear submarine No. 289, project 627A, was built in 1963 at PO 'Sevmash' shipyard (Severodvinsk, Arkhangelsk region). In October 1963, the submarine was commissioned and joined the Northern Fleet under the name of K-159. It was designed by the Malakhit Design Bureau and was a November class attack submarine (Figure 1.1a). This class belonged to the first generation of nuclear submarines build by the Former Soviet Union. The submarine's pressure hull was comprised of 9 compartments (Figure 1.1b). A list of the main characteristics of the submarine can be found in Table 1.1.

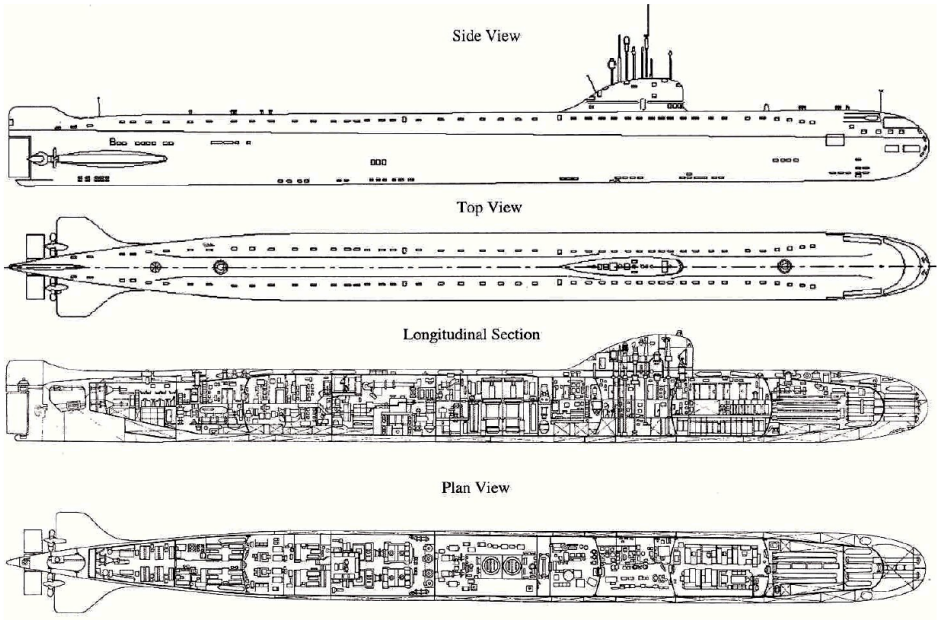

Figure 1.1a. November class submarines (Source: AMEC 2007).

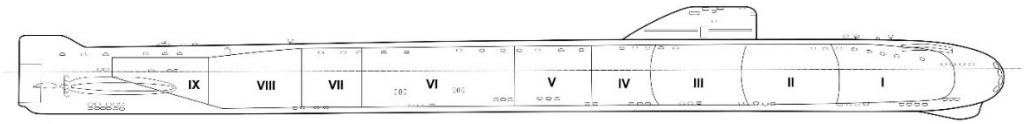

Figure 1.1b Schematic representation of K-159. I – torpedo section; II - residential and battery compartment; III – control room, IV – auxiliary equipment compartment; V – reactor compartment; VI – turbine compartment; VII – electromechanical compartment; VIII - residential compartment; IX - aft compartment.

Table 1.1. Main Characteristics of K-159.

Overall length, m	107.4
Overall width, m	7.9
Draft at normal displacement, m	5.72
Displacement (normal), t	3125
Displacement (underwater), t	4050
Main power installation, h.p.	2 x 19615
Thickness of the pressure hull casing, mm	26

In 1970-1972, during a scheduled repair, both reactor cores of K-159 were refueled. During 1963-1984, the submarine made 9 autonomous campaigns of 392 days total duration including 6 campaigns after the reactor reloading (253 days). In 1989 the K-159 submarine was withdrawn from service in the Navy and renamed as *B-159*[1]. Until 2003, the submarine was stored afloat in Yokanga basing station (Gremikha) awaiting to be sent to its final destination for defueling and dismantling Chernyaev et al. (2003).

There are 2 pressurized water reactors of 'VM-A'-type 70 MW thermal power each, located in compartment No. 5 (see Figure 1.1b). All equipment and primary coolant piping are designed for operation at internal pressures up to 200 kgf/cm^2, temperatures of 250-350 ºC and overload shocks up to 15 g[2] in vertical direction and up to 5 g in horizontal direction. The reactors and Control and Protection System (CPS) mechanisms were sealed within special enclosures.

As part of decommissioning procedures, both reactors of the submarine were shut down on October 25, 1988 and brought to a safe state in accordance with the Russian technical regulations and standards in effect at that time. The measures taken were aimed at ensuring the maintenance of the reactor cores in deep subcriticality even in the cases of extreme external impacts such as fire, flooding or capsizing of the submarine which could lead to destruction of the reactor compartment.

Accumulator batteries, variable loads and lubricants were unloaded from the submarine during its waterborne storage and preparation for towing.

1.2 Accident and the sinking of K-159

Under the Russia's submarine decommissioning program, by the end of August 2003, 12 nuclear submarines were towed from Yokanga base (Gremikha) to the shipyards of the Murmansk region.

The towing of K-159 commenced on August 28, 2003. The destination was the Nerpa shipyard in the town of Snezhnogorsk, where defueling and subsequent dismantling of the NS were intended to take place. The towing was carried out by the SB-406 rescue tug. To increase K-159's buoyancy, two pairs of pontoons (SSP-200 type) of 11 t weight and 200 t displacement each, were strapped to its bow and stern prior to towing. In accordance with the towing design, the pontoons were attached by ropes to steel plates welded to the submarine outer hull.

[1] However, to avoid confusion the notation K-159 will be used throughout the report.
[2] Here, g ≈ 9.8 m·s^{-2} is the Earth gravitational acceleration.

Figure 1.2. The nuclear submarine K-159 with the four floatation pontoons strapped to it prior to being towed. Photo: The Russian Northern Fleet.

On August 30, 2003 on its towing route K-159 was caught in a storm in the vicinity of Kildin Island (Barents Sea); wave heights were in the range of 1.25 to 4 m with wind speeds of up to 17 m/s. Under these conditions, the bow pair of pontoons were torn off and water ingress into Compartment No 8 resulted in its flooding. Simultaneously, the fastenings of the stern pair of pontoons also failed with loss of their support functions. At approximately 3 a.m. (Russian time), K-159 sank to a depth of 246 m at a distance of about 6 km from Kildin Island and about 26 km from the destination point. The sinking site lies at a distance of about 130 km from the Norwegian border.

Figure 1.3. The nuclear submarine K-159 being towed out on its route towards the Nerpa shipyard. (Source: AMEC 2007).

The sinking location of K-159 is shown in Figure 1.4.

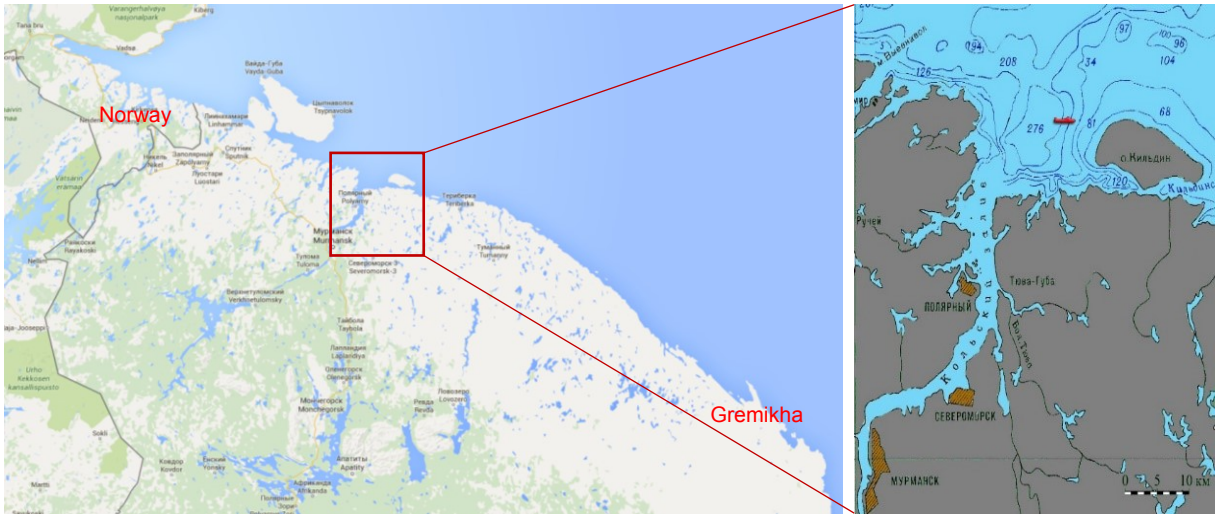

Figure 1.4. Sinking site of K-159.

1.3 Condition of Spent Nuclear Fuel (SNF) in the reactors of K-159 before sinking

Little is known about the general condition of *K-159* at the time of sinking, but since the submarine was kept afloat in Gremikha for so long (from 1989 to 2003), there is reason to believe that the submarine was in very poor condition. This impression is confirmed by the many pictures taken of the submarine just before and during the towing (see Figures 1.2 and 1.3).

The nuclear fuel present in the reactors of K-159 is of a uranium oxide type, within an aluminum matrix. The fuel elements use stainless steel cladding. The ^{235}U enrichment of the fuel is ~ 20% corresponding to a total load of 50-60 kg of ^{235}U in both reactors.

Before sinking, the primary circuits of both reactors were sealed. The volume of water in the primary circuit of each reactor was about 5.0 m^3 and pressure was 10-25 kgf/cm^2. Furthermore, the specific activity of water in the primary-circuit was: $1.3\text{-}1.4 \cdot 10^4$ Bq/l in the bow side reactor and $5.5\text{-}8.5 \cdot 10^2$ Bq/l in the stern side reactor.

1.4 Activity in the reactors of K-159 at the accident time and at present (2014)

According to the data available, the reactors of K-159 were not defueled and hence the SNF present in the submarine is the main source of potential contamination of the environment. The activity induced in equipment and structures of the reactor compartment is more than two orders of magnitude less than that of fission products present in the SNF of the two cores of the submarine.

The activity of fission products in SNF and the induced activity in materials of steam-producing installation equipment and structures were estimated considering the following operating conditions:

1. Total power production of the reactors over their operating period:

- bow reactor – 144% of the design power capacity;
- aft reactor - 145% of the design power capacity.

2. Last loading of the cores:

- bow reactor – 1972;
- aft reactor – 1971.

3. Both reactors were shut down in 1988 in accordance with standard procedures.

4. Power production of each core over the last operating period was approximately the same, being taken equal to about 87% of the design power capacity (a mean value according to different sources).

5. Mean power of the reactors – 25-30 % (of full capacity).

6. A capacity factor[3] of about 0.1.

7. In accordance with the description of the submarines lifecycle, it was assumed that its active operation lasted from mid-1973 till mid-1987.

8. When setting the time intervals for the reactors operating power history, the periods of sea campaigns, repairs and mooring were accounted for.

The activity accumulated in the reactor compartment of K-159 was estimated using the 'SCALE - 4.3' software code (Rearden and Jessee, 2016) with due account taken for the operating conditions and duty cycle.

Table 1.2 provides the estimates for radionuclide concentrations in SNF of the two reactors at the time of sinking (note that only radionuclides whose contributions to the total concentration exceed about 0.01% are presented) and those calculated for induced activity present in the RC equipment and structures. The table shows only those radionuclides with a half-life greater than two years.

The main fraction of induced activity (> 99%) can be found in the reactor internals, reactor vessels and structures located within the reactor enclosures.

[3] The net capacity factor of a power plant is the ratio of its actual output over a period of time, to its potential output if it were possible for it to operate at full capacity continuously over the same period of time.

Table 1.2. Estimated activities of anthropogenic radionuclides present at the reactors of K-159.

Group of nuclides	Nuclide	Half-life (y)	Activity as of 09.2003 (TBq)	Activity as of 09.2014 (TBq)
Fission products	H-3	12.3	3.21E+00	1.74E+00
	Kr-85	10.7	7.28E+01	3.59E+01
	Sr-90	28.2	1.51E+03	1.16E+03
	Cs-134	2.06	2.76E+00	7.03E-02
	Cs-137	30.0	1.60E+03	1.24E+03
	Pm-147	2.62	4.57E+01	2.55E+00
	Sm-151	90.0	1.63E+01	1.50E+01
	Eu-152	13.3	1.49E+00	8.44E-01
	Eu-154	8.8	9.11E+00	3.76E+00
	Eu-155	4.96	2.06E+00	4.08E-01
	Total		3.26E+03	2.45E+03
Actinides	Pu-238	87.7	5.83E+00	5.35E+00
	Pu-239	24060	3.56E+00	3.56E+00
	Pu-240	6537	2.07E+00	2.07E+00
	Pu-241	14.4	8.30E+01	4.89E+01
	Am-241	432	4.10E+00	5.15E+00
	Total		9.85E+01	6.53E+01
Activation products	Fe-55	2.7	7.44E+00	4.42E-01
	Co-60	5.27	3.23E+01	7.61E+00
	Ni-59	75000	3.31E-01	3.31E-01
	Ni-63	96	3.52E+01	3.25E+01
	Total		7.52E+01	4.09E+01
Total activity			3.44E+03	2.57E+03

According to the data in Table 1.2 the current total inventory of potential contamination is about 2.6 E+03 TBq and is mainly comprised of ^{90}Sr and ^{137}Cs (> 90%).

1.5 Data on sea currents in the submarine sinking Area

There are permanent and tidal currents in the area of K-159. Wind currents are also observed. Owing to the combined effect of these currents, the resulting cumulative currents are very changeable in the littoral areas.

Permanent currents: The warm North Atlantic Current, upon passing along the coast of Norway, divides into two branches near 70º N, one going to the western coast of Spitsbergen (the West Spitsbergen Current) and the other is deflected to the Barents Sea (the North Cape/Nordkapp Current) where it encompasses the entire southern part of the sea. When proceeding to the east, the North Cap Current is in its turn divided into branches - one of them going along the coast of the Kola Peninsula and being called the Murmansk Littoral Current. Near the cape Kanin Nos, this branch merges with the current coming from the White Sea and goes east. A branch flowing along the western coast of Novaya Zemlya is called the Novaya Zemlya Current.

From the Arctic Ocean, cold arctic waters penetrate to the Barents Sea. The major part of them moves from northeast to southwest to Bear Island, whereas their smaller part goes to the Greenland Sea skirting the southern tip of West Spitsbergen Island.

Through the Kara Gate Strait, cold waters of the Kara Sea penetrate to the Barents Sea and form the Litke Current. This current, going along the southwest coast of the southern island of Novaya Zemlya, is directed north-west. Affected by the Barents Sea waters, it is warmed and is no longer traceable north of 72º N. There is also a system of local circular currents in the central part of the Barents Sea. Generally, the average speed of permanent currents is less than 0.5 knots, reaching1 knot in places. A diagram of the permanent currents of the region is shown in Figure 1.5.

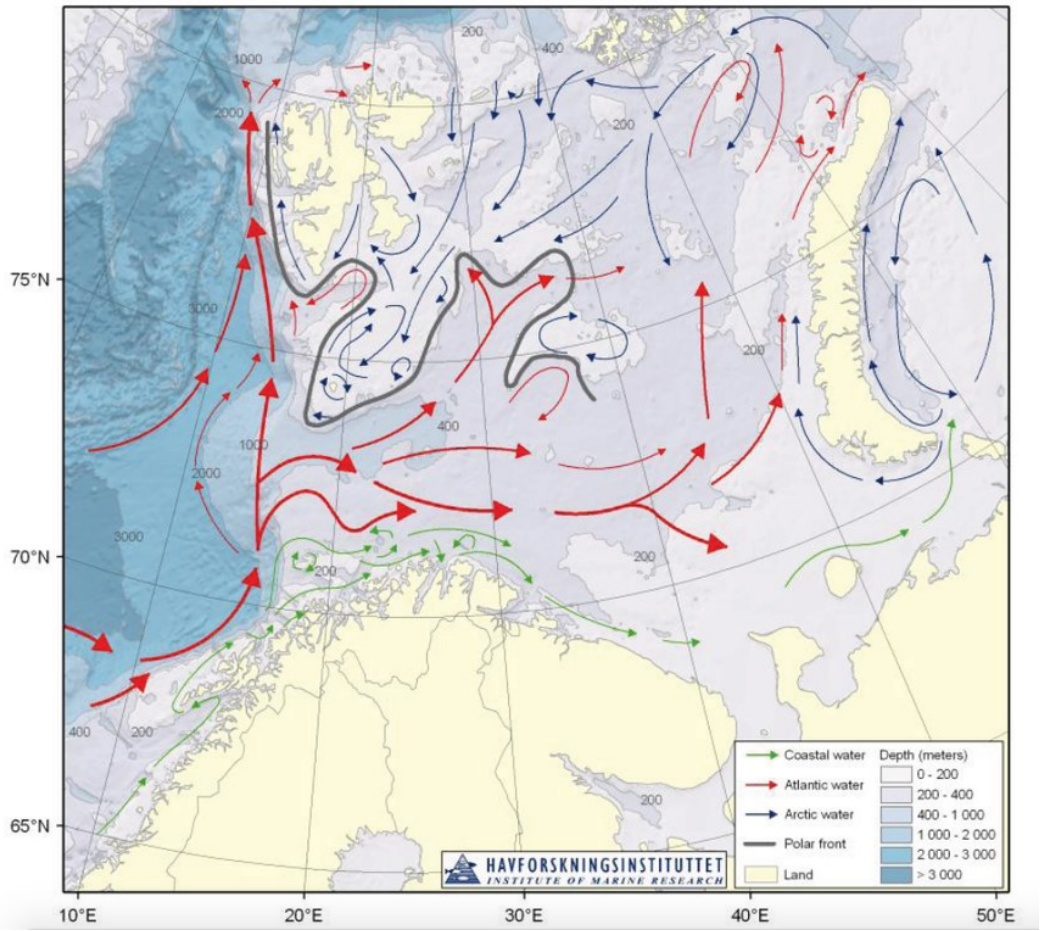

Figure 1.5. Main features of circulation and bathymetry in the Barents Sea (taken from JNRESR, 2009).

Tidal currents: In most of the Barents Sea tidal currents are semidiurnal and reversible in the littoral zone: generally, flood currents are directed from W to E, whereas ebb currents have the opposite direction, though in some areas deviations from these directions may be observed. In the open sea, the average speed of tidal currents does not usually exceed 0.5 kt; in the south-east part of the sea it attains 06.-0.8 kt, and in the western part it is 0.6-1 kt. Westerly/Easterly winds increase the speed and duration of flood/ebb currents, respectively.

Wind currents: These currents are instable due to changes in wind direction. At wind speeds of 12-19 kt over open sea, the speed of wind currents is 0.3-0.4 kt; at wind speeds of 21-33 kt this increases to 0.6 kt. In the littoral zone and in narrow areas, the speed of wind currents may exceed 1 kt.

2 An overview of expeditions to the sinking site of the K-159 submarine

Table 2.1 provides an overview of the major expeditions conducted to study the sunken submarine K-159.

Table 2.1. Major expeditions to the K-159 submarine sinking site.

Period	Organizations	Vessel	Purpose
03.10-09.10.2003	RCBPS NF[4], IBRAE RAN[5]	*'Horizont'* HV*	Radiation survey of the submarine site
23.10-02.11.2003	NRC KI[6], NIKIET[7], RCBPS NF, IBRAE RAN	*'G.Titov'* RV** SAS-34	Radiation survey close to the NS hull
13.02-19.02.2004	RCBPS NF	*'Vizir'* HV*	Radiation survey of the submarine site
25.12-26.12.2004	RCBPS NF	HV*-87	Radiation survey of the submarine site
16.05-21.05.2005	RCBPS NF	*'Krillon'* HV*	Radiation survey of the submarine site
11.11-13.11.2005	RCBPS NF	HV*-278	Radiation survey of the submarine site
30.01-01.02.2007	RCBPS NF	HV*-278	Radiation survey of the submarine site
27.06 – 11.07.2007	AMEC[8]	*'Alliance'* research ship, NSRS ROV***	Technical and Radiation survey of the submarine, environmental sampling
Aug/ Sep 2014	NRPA[9], IMR[10], NMBU[11], ROSHYDROMET[12], NRC KI, RPA[13]	*Ivan Petrov*	Radiation survey of the submarine site, environmental sampling

* Hydrographic Vessel; **Rescue Vessel; *** Remotely Operated underwater Vehicle

[4] Radiation, Chemical and Biological Protection Service of the Northern Fleet
[5] Nuclear Safety Institute of the Russian Academy of Sciences
[6] National Research Center 'Kurchatov Institute'
[7] N.A. Dollezhal Research and Development Institute of Power Engineering
[8] The Arctic Military Environmental Cooperation
[9] Norwegian Radiation Protection Authority
[10] Institute of Marine Research
[11] Norwegian University of Life Sciences
[12] Federal Service for Hydrometeorology and Environmental Monitoring
[13] Research and Production Association "Typhoon"

It is worth noting that, according to the results of radiation surveys carried out by the Radiation, Chemical and Biological Protection Service of the Northern Fleet (RCBPS NF), the gamma dose rates in air, seawater and bottom sediments in the sinking area of the submarine did not differ from the radiation background.

During the first survey of 2003, the following monitoring activities were conducted: a visual inspection, video filming of the hull and initial radiation survey Chernyaev et al. (2003). The submarine was found in upright position on the seabed with its aft partially submerged within the sediment such that the submarine's bottom made a 5 degree angle with the seabed.

For 50 minutes, a remotely operated underwater vehicle passed over the K-159 submarine from the aft to the bow at a distance of 2-4 meters from the outer hull. At the level of sensitivity of the used submersible gamma spectrometer (~ 0.1 Bq/l for ^{137}Cs) no radionuclide release from the submarine was observed.

Towing, mooring and fastening cables and air hoses were scattered in disarray on the hull of the submarine and over the surrounding seabed. Two damaged pontoons were found near the submarine. The piles of cables and hoses as well as engineering structures welded to the outer hull significantly hampered the delivery of radiation monitoring devices and their installation on the submarine hull without the risk of damaging the ROV.

In 2007, within the framework of The Arctic Military Environmental Cooperation (AMEC) Program, specialists of National Research Center 'Kurchatov Institute'(NRC KI) with the Rescue Service of the U.K. Royal Navy jointly conducted a detailed radiation survey of K-159 (Shishkin et al. (2007), MALACHITE (2007) and Kazennov (2007)).

The main goals of the 2007 radiation survey were to obtain reliable experimental data on the dynamics of the radiation situation since the last survey (November 2003), to investigate the radioactivity of water in the RC and just above the outer hull of the submarine, to detect leakages in the primary circuit and determine the condition of inner safety barriers.

During the survey the following tasks were conducted:

- searching for locations of possible radioactivity release from the NS to the marine environment and measuring identified leaks;
- measuring gamma levels over the pressure hull and outer hull directly above the RC to estimate the volume concentration of radionuclides inside the reactor compartment;
- installation of long-term monitoring devices at the NS to determine the dynamics of possible radioactivity releases and estimate gamma dose rates on the outer hull and pressure hull just above the reactor compartment; and
- determination of radionuclide composition and concentrations in seawater and bottom sediments near the sunken NS.

Using the *Triton* ROV, the submarine was cleared of fragments of rope that fixed pontoons, mooring ropes and other small items. An acoustic scan was performed and based on its results, a 3-D model of the NS location on the sea bottom was generated (Figures. 2.1 - 2.2).

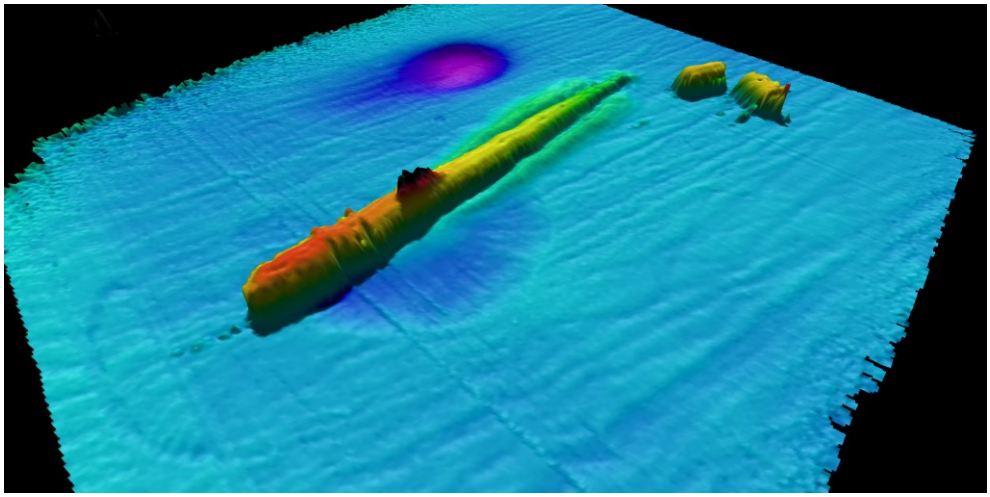

Figure 2.1 Acoustic model: a general view of the submarine on the sea bottom; two damaged pontoons are visible on the right.

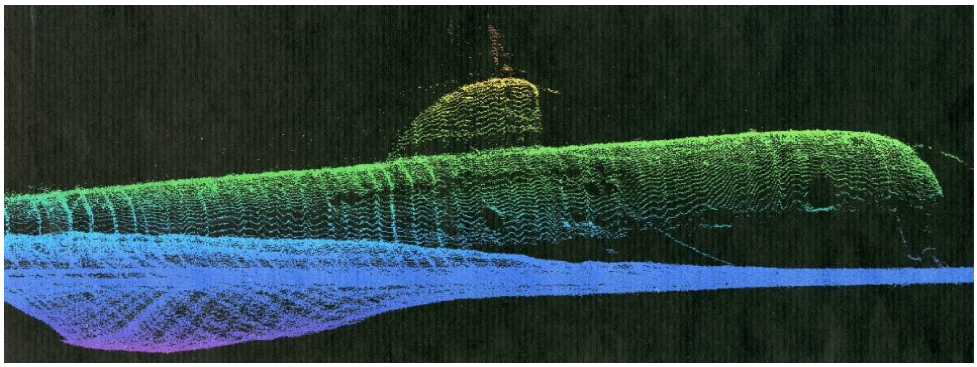

Figure 2.2 Acoustic model: a view of the starboard of the submarine.

The survey revealed no changes in the positions of the submarine and the sediment pile along the submarine outer hull compared to 2003. There was no significant biofouling or silting of the hull.

The video data demonstrated the following:

- minor biofouling of the NS hull;
- no apparent corrosion damage caused by seawater;
- the closed position of the 'commander's shield' (breakwater shield) in the conning tower;
- one broken pane in the breakwater shield;
- confirmation of the destruction of the aft portion of the submarine, starting from rib N° 166. Technical capabilities of the used acoustic equipment did not allow concluding as to whether it was crushed or broken off;
- no sign of the horizontal stabilizers, rudders and marine propellers – apparently located under a layer of sediments;
- a lack of sheets in the lower belt of plating associated with the superstructure's bow;
- two torn off pontoons found at a distance of 8-10 meters from the aft end, on the portside; and
- visible tears and dents on the outer hull at pontoon fixing points.

During the 2007 expedition, a search for any possible leakage from the submarine was conducted using an ROV equipped with a gamma-spectrometer ('REM-25') that recorded gamma spectra along the ROV's path. In total, 1669 gamma-spectra were recorded during 10 ROV dives in the immediate vicinity of K-159.

Analysis did not reveal any evidence of anthropogenic radionuclides (^{137}Cs and ^{60}Co) in concentrations that exceeded the gamma-spectrometer detection limits (0.5 Bq/l and 0.4 Bq/l measured over 90 s, respectively).

No evidence of anthropogenic radionuclides above the detection limits (in particular, ^{137}Cs at a level above 0.1 Bq/l), in the immediate vicinity of the submarine, was observed.

Simultaneously, a second gamma-spectrometer ('REM-26') was installed on the K-159 superstructure, the most likely place for radionuclide release, for the purpose of long-term monitoring of ^{137}Cs and ^{60}Co release to the surrounding seawater. In the spectra recorded, no anthropogenic radionuclides were found in concentrations exceeding the gamma-spectrometer detection limit over 8.5-hour exposure time: 0.04 Bq/l for ^{137}Cs and 0.03 Bq/l for ^{60}Co.

No gamma radiation, which could originate from anthropogenic radionuclides located inside the RC, was detected outside the submarine's pressure hull. The results of all measurements above the RC indicated that the primary circuit of the reactor installation was still intact.

The specific activities of radionuclides in samples of bottom sediments taken from around the submarine are presented in Table 2.2.

Table 2.2. Activity of radionuclides in bottom sediments sampled in vicinity of the K-159, Bq/kg fresh weight.

Samples	^{137}Cs	Natural radionuclides		
		^{238}U series	^{232}Th series	^{40}K
1	4.6±0.7	22.6±1.5	31.7±1.9	770±41
2	<0.8	20.3±1.8	42.7±3.2	740±45
3	3.3±0.6	19.4±1.9	39.4±2.5	770±44
4	3.7±0.7	19.1±1.6	34.2±2.8	800±45
5	<0.8	18.8±1.6	40.9±2.8	740±42
6	<0.8	16.3±1.5	40.2±3.1	680±42

Analysis of the results shows that the activity of ^{137}Cs in samples of bottom sediments near the submarine does not exceed the background levels which are characteristic of the Kola Bay and the Barents Sea.

After 2007, there were no expeditions to the submarine. In September 2014, a new joint Russian-Norwegian sea expedition was conducted with the aim of radiation monitoring of the sunken K-159 submarine. The results of this expedition are currently being processed and therefore are not included in this report although a brief overview of the expedition's activities and some key findings are given below.

2.1 Joint Norwegian-Russian expedition 2014

In the summer of 2014, after a 7 year pause, an expedition (under the auspices of the joint Norwegian-Russian Expert Group) visited the site. The purpose of the expedition was to obtain new, up-to-date information about the level of radioactive contamination in the marine environment in the immediate vicinity of K-159 and in adjacent areas of the Barents Sea.

The expedition took place on the Russian research vessel *Ivan Petrov* and lasted for approximately 3 weeks. From Norway, the Norwegian Radiation Protection Authority (NRPA), the Institute of Marine Research (IMR) and the University of Life Sciences (NMBU) participated. From Russia, there were participants from the Federal Service for Hydrometeorology and Environmental Monitoring (Roshydromet), the National Research Center 'Kurchatov Institute' (NRC KI) and the Research and Production Association "Typhoon" (RPA). In addition, the International Atomic Energy Agency (IAEA) also participated as observers.

The sunken nuclear submarine K-159 was inspected with the use of a Remotely Operated Vehicle (ROV) equipped with a video camera and spectrometer. Video pictures show that K-159 lies upright on the seabed with the deck of the submarine covered in a layer of sediment. A number of different fish species and other biota were observed around the submarine. The inspection of the outer hull showed a number of missing hatches and some damage to the deck and stern. It was not possible to visually assess the status of the inner pressure hull. Measurements with the spectrometer on the ROV were taken next to K-159 including critical locations such as above the reactor compartment. Sediment samples were recovered with the ROV close to the bow, stern and on either side of the reactor compartment.

The preliminary conclusions of the joint Norwegian Russian expedition stated that: based on the analysis of the ROV spectrometer data and onboard sample measurements, radiation levels showed to be of the same order as those typical for the Barents Sea. A similar picture for the radiological situation around the sunken nuclear submarine K-159 was observed in 2007. According to the results obtained so far, the conclusion of the Russian/Norwegian expedition is that no leakage has occurred from the reactors of the submarine to the marine environment.

3 Potential accident scenarios

As long as K-159 lies on the sea bottom, penetration of water into the vessel due to corrosion of structural materials would be the triggering event for an emergency situation. This is particularly the case for the primary circuit of the submarine as, following its depressurization, seawater would be in contact with fuel element claddings and nuclear fuel in the reactor core. Such a situation would result in degradation of the fuel matrix and fuel element claddings and, consequently, in release of radionuclides accumulated in the reactor to the reactor compartment and subsequently to the environment (Dozhdikov et al.1991).

In addition, swelling and subsequent sloughing of fuel to reactor lower part with the generation of fuel spillage cannot be ruled out (ENES, 2003). As a result, changes in the core geometry might significantly reduce the efficiency of the absorber system. Under certain conditions, this can trigger a criticality accident – the ignition of a self-sustained chain reaction.

Considering the possible processes mentioned above, two groups of potential accident scenarios can be envisaged. The first group of accident scenarios is associated with the release of radionuclides owing to a loss of fuel integrity. The second group includes the cases of possible fuel spillage to the reactor vessel lower head and hence criticality related scenarios. Potential accidents related to the last group of scenarios will be discussed in Section 3.2. These scenarios belong to the category of accidents with the maximum potential impact.

For the first group, the following types of accident scenario may be considered:

- depressurization of the primary circuit, dispersion of radionuclides inside the vessel and their release to seawater when the submarine is lying on the sea bottom; and
- a release of radionuclides to the environment owing to pressure changes and the generation of flows in the submarine compartments during its lifting and transportation.

It is also worth noting that water which has penetrated the submarine compartments from the core might attain high contamination levels. Such water should be drained prior to lifting and transportation of the submarine, and internal surfaces should be decontaminated prior to defueling and dismantling.

In general, all the accident scenarios considered in the present work, can be grouped into three categories: ‘in situ’, ‘lifting’ and ‘docking’. “In situ” refers to release scenarios which might occur as a result of the submarine being submerged over a long period and hence due to loss of fuel integrity as barriers age and degrade. “Lifting” refers to all possible accident scenarios that might take place during, or because of, raising activities. The last category refers to release accident scenarios that could occur during docking of the submarine. It has been assumed that, while releases from the first two groups would be to the sea, the releases from the latter would be to the atmosphere. For the present assessment, as discussed in chapter 7, we have assumed that while all releases from both in situ and lifting accident scenarios would end up in the sea, the releases associated with the docking scenarios would only be to the atmosphere.

3.1 Release scenarios related to depressurization of the primary circuit

3.1.1 Safety barriers of the submarine and characterization of their possible degradation

During operation of a nuclear submarine, radiation and environmental safety is ensured by confinement of radioactive substances contained within the reactor installation equipment through the use of several safety barriers. Such safety barriers may include: the pressure hull; reactor compartment bulkheads; sealed enclosures of reactor compartment rooms; the primary circuit of the reactor cooling system; and fuel element claddings.

Multi-barrier shielding of the environment from leaks of radionuclides generated during operation of nuclear submarine reactors is depicted in Figure 3.1 (Kazennov, 2007).

When a fueled nuclear submarine is stored afloat, the doors of the bulkheads are battened and sealed. However, in the case of sinking, damage to operating-room bulkhead elements is possible, resulting in loss of integrity and seal failure. Before the K-159 sinking, its pressure hull and reactor compartment bulkheads lost their shielding capabilities because the deckhouse and bulkhead hatches were not battened down in all compartments.

Following the observations and findings of the latest surveys conducted in 2007 and 2014, investigations of the radio-ecological situation around the submarine indicates that the primary circuit of the submarine remains sealed.

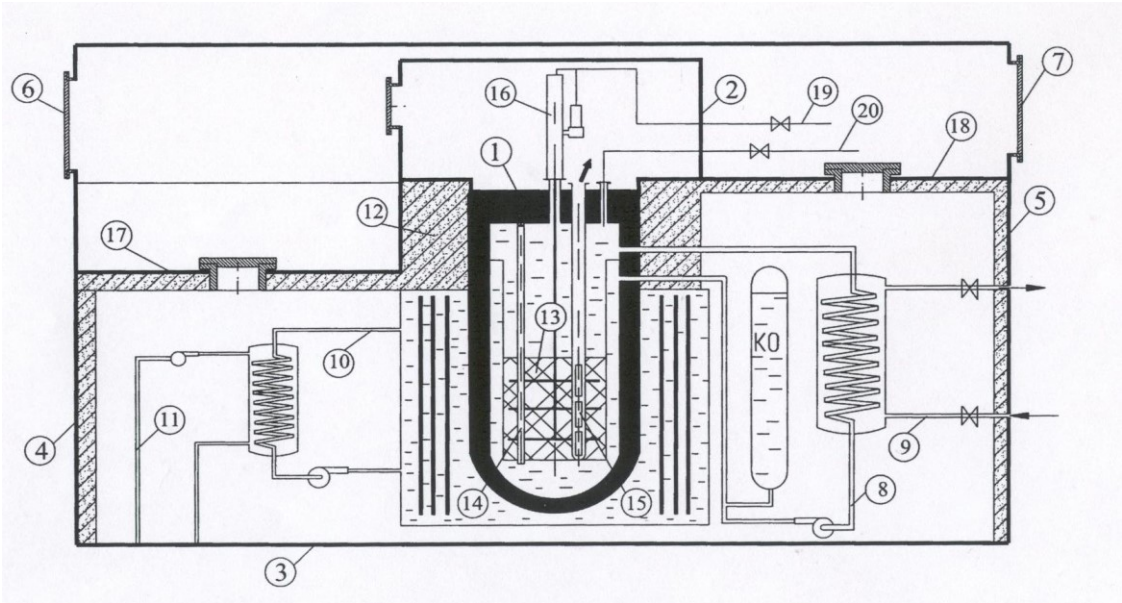

1 – Reactor

2 – Reactor reflection shield

3 – Pressure hull

4 & 5 – Intercompartment bulkheads

6,7 – Intercompartment doors

8 – Pipes and equipment of the 1st circuit

9 - Pipes and equipment of the 2nd circuit

10 - Pipes and equipment of the 3rd circuit

11 - Pipes and equipment of the 4th circuit

12 – Biological shielding

13 – Reactor core

14 – Fuel element

15 – Absorber rod

16 – CPS mechanisms

17 &18 – Sealed floorings

19 – Release valve of the CPS drive (1st circuit)

20 – Release valve of the reactor

Figure 3.1. Safety barriers of steam producing installation.

The construction of nuclear submarines and their Steam Producing Installation (SPI) provide multi-barrier protection of the environment from a release of radionuclides produced during operation of submarine's reactors. In particular:

- Walls of sealed equipment and primary-circuit pipes prevent the release of radionuclides accumulated in the primary circuit;
- In the case of depressurization of the primary circuit, sealed flooring and bulkheads prevent further radionuclide spreading into the reactor compartment;
- In a case of a seal failure in the reactor compartment bulkhead, the release of radionuclides to seawater is hindered by the inter-compartment bulkheads of the adjacent compartments and the sealed pressure hull of the submarine.

Radionuclide release to seawater is therefore only possible in the case of seal failures in all of the above-mentioned safety barriers as well as in the submarines pressure hull itself. As already mentioned, in the case of K-159 the two last barriers (the pressure hull and the reactor

compartment bulkheads) are not capable of fulfilling their function as before the sinking, the deckhouse hatch and all hatches in inter-compartment bulkheads were open.

There is a risk of seal failure in all of the safety barriers over time; though any assessment of the risk level is a difficult task because the technical condition of the K-159's SPI is unknown (acquisition of accurate information regarding the SPIs condition is impossible).

According to data acquired indirectly through radio-ecological monitoring of the marine environment close to the submarine and over its hull, no release of ^{137}Cs to seawater has been recorded since the submarine sank in 2003.

3.1.2 Depressurization of the primary circuit and fuel claddings

The condition of the submarine's SPI at the time of sinking can be described as follows:

- the reactor cores were deemed to be in a sub-critical state;
- The primary circuits of both reactors were sealed, and an anticorrosion preservative was introduced to the primary circuit water;
- The sorbent filters of the primary circuit were disconnected;
- The steam generators were drained of water and filled with nitrogen; and
- The third SPI circuit was sealed.

Furthermore, the following measures were taken:

- maintenance of the submarine reactor cores in a state of deep sub-criticality to withstand cases of extreme external impacts which could result in reactor compartment destruction and causes fire, sinking or turning-over; and
- technical measures were taken to make it physically impossible to perform any unauthorized changes in the core layout and content (e.g. by moving or extracting the CPS rods); therefore, both cores would stay deeply subcritical with high degree of certainty.

Nevertheless, it is possible that after the submarine's sudden sinking and its consequent collision with the sea bottom, unpredictable processes could take place that would accelerate depressurization of the primary circuit followed by activity release to the submarine compartments and the sea.

In such a situation it is assumed that when seawater penetrates into a nuclear submarine, hydrostatic pressure in the reactor compartment increases. Consequently, significant damage to or destruction of operating room enclosures is possible that may result in degradation and depressurization of the outlet pipes (in particular, those of small diameter allowing for gas release from the reactor and CPS driving mechanism during repair work) as well as of the cooling system.

The modeling outcomes demonstrate that depressurization of broken pipes of small diameter, if this did not happen at the time of submarine sinking, might occur subsequently owing to various reasons (partial failure of seals and welds, cracking of pinched or distorted ducts, accelerated corrosion, *etc.*). In such cases, radionuclide release to seawater may occur at any time before a

complete corrosive destruction of reactor-supporting structures (100-200 years) and the submarine pressure hull (200-300 years) take place.

After failure of one of the key SPI safety barriers it is assumed that the shielding function of the primary circuit is lost (a rather conservative assumption) and that seawater will penetrate into the core. After that, active corrosion of the fuel element claddings and later the fuel itself may be expected to occur. Under such conditions, the fuel element claddings would lose integrity within a few months and unprotected fuel would corrode and its structure would change. The radionuclide leaching process would start, some remaining in seawater and the other part being deposited on surfaces of the reactor compartment and equipment.

Gradually, water containing anthropogenic radionuclides would penetrate from the reactor through leaks in the primary circuits to the reactor compartment and other compartments of the submarine and subsequently to the sea.

3.1.3 Radioactivity distribution inside the submarine's compartments

Radionuclide release from K-159 to seawater would occur mainly via the open hatch of the deckhouse in the 3rd compartment and partially (up to 10%) via the 8th and the 9th compartments at the locations where the pressure hull seal failures occurred before the submarine sinking accident.

About 2200 m^3 of seawater contained in the submarine's compartments could be involved in inter-compartmental water exchange (Table 3.1).

Table 3.1. Free volumes of K-159 compartments.

Compartment	Volume, m^3
1	235
2	265
3	222
4	187
5	289
6	352
7	285
8	210
9	125
Total	2170

In the following, only ^{137}Cs release (as a tracer) was considered. The release processes of other significant radionuclides, such as ^{90}Sr, are similar to cesium, and the partial fractions of the environmental contamination level for the main radionuclides are approximately constant in the close vicinity of the source.

To establish the redistribution of ^{137}Cs inside the submarine and its release to the sea, a multi-compartmental model was used wherein fuel, water, compartment surfaces and equipment, and the sea were considered as 'compartments'.

The redistribution of ^{137}Cs between such 'compartments' inside the submarine was determined by a bidirectional water exchange i.e. seawater release and ingress due to tidal processes. The deposition of ^{137}Cs from water to any surface was assumed to be unidirectional (after a dynamic equilibrium establishment) the rate of this process being characterized by appropriate coefficients.

The results of evaluating the amount of ^{137}Cs that accumulates in the various compartments of the submarine over time obtained using the aforementioned multi-compartmental model, are presented in Table 3.2 (the data for one reactor are provided; for the second reactor almost identical data are achieved).

Table 3.2. Activity of ^{137}Cs (TBq) accumulated in seawater contained in the K-159 compartments depending on the time after depressurization of spent fuel assembly canisters.

Compart. nr.	***Time after depressurization (year)***					
	0.25	*0.5*	*1*	*2*	*5*	*10*
1st	7.33E-07	3.09E-05	1.02E-03	2.09E-02	4.11E-01	1.50E+00
2nd	3.64E-05	7.51E-04	1.19E-02	1.16E-01	9.55E-01	2.29E+00
3rd	6.73E-04	6.99E-03	5.70E-02	3.09E-01	1.43E+00	2.62E+00
4th	2.29E-02	1.25E-01	5.66E-01	1.90E+00	5.51E+00	7.99E+00
5th	1.04E+00	2.85E+00	6.59E+00	1.24E+01	2.19E+01	2.64E+01
6th	9.99E-03	5.77E-02	2.90E-01	1.17E+00	5.22E+00	1.13E+01
7th	1.44E-05	1.73E-04	1.84E-03	1.57E-02	1.85E-01	8.07E-01
8th	3.05E-08	7.36E-07	1.59E-05	2.72E-04	7.40E-03	5.51E-02
9th	1.32E-10	6.51E-09	2.89E-07	1.01E-05	6.81E-04	9.44E-03

Note that in a few years, accumulation of ^{137}Cs on the submarine internal surfaces may be 10-30% of its content in seawater.

3.1.4 Radioactivity releases to the sea

To estimate the concentrations of ^{137}Cs in seawater (close to the submarine) after its release the following approach was taken. It was assumed that sea currents flow around the submarine, and that the released ^{137}Cs was uniformly distributed in a horizontal cylindrical water plume of about 8 m diameter.

The mean flow velocity in the bottom layer of seawater was taken as being equal to 0.1 m/s corresponding to a flow rate of approximately 5 m^3/s. The concentration of ^{137}Cs in seawater in the initial area of the plume will be equal to the ratio between the rate of release of its activity to seawater and this volumetric flow rate. According to the performed calculations, permanent water leakage from the deckhouse to the sea would be ca. 1.0E-05 l/s. To determine the content of ^{137}Cs in water of the deckhouse, its volume was taken to be about 2 m^3. As a result, the rate of ^{137}Cs release to seawater was estimated – see Table 3.3.

Table 3.3. Estimate of ^{137}Cs release rate out of K-159 to seawater after depressurization of its spent fuel assemblies over time.

Time after depressurization (year)	Release rate (TBq/h)	^{137}Cs concentration (Bq/l)		Activity released to the sea (TBq)
		In the deckhouse	In the plume	
0.25	1.20E-07	1.60E+03	0.01	2.56 E-05
0.5	1.27E-06	1.71E+04	0.07	5.77 E-04
0.75	4.55E-06	6.14E+04	0.2	3.26 E-03
1	1.04E-05	1.41E+05	0.6	1.05 E-02
1.5	2.95E-05	4.00E+05	1.6	4.81 E-02
2	5.70E-05	7.70E+05	3.2	1.32 E-01
3	1.25E-04	1.68E+06	6.9	4.85 E-01
4	1.98E-04	2.66E+06	11.0	1.10 E+00
5	2.65E-04	3.57E+06	14.7	1.99 E+00
6	3.25E-04	4.40E+06	18.1	3.11 E+00
8	4.22E-04	5.70E+06	23.4	5.88 E+00
10	4.85E-04	6.55E+06	27.0	9.18E+00

The data of Table 3.3 indicate a certain tendency towards stabilization of the rate of ^{137}Cs release to seawater out of the damaged reactor at a level of ~ (4-5) E-04 TBq/h, 8-10 years after the depressurization event. Such a release would result in contamination of the surrounding seawater to concentrations of approximately 20-30 Bq/l. By that time, about 6-9 TBq of ^{137}Cs would have been released to seawater from the submarine.

In a case of a more active degradation of the submarine's safety barriers subsequent changes/ increases in the rate of ^{137}Cs release to seawater could reasonably be expected. Taking into account the rate of ^{137}Cs release from SNF of about 1 % per year, one may conclude that this process will proceed towards completion over approximately one hundred years (Sivintsev et al., 2005).

3.2 Accident scenarios involving initiation of Spontaneous Chain Reaction (SCR)

During the submarine waterborne storage period, on the basis of joint decisions of agencies as well as design and operational documents developed in accordance with those decisions, the SPIs of both sides were brought to a safe condition through following measures:

- All compensating and control mechanisms of reactor cores were transferred to the lowermost position;
- Hand drives of compensating gratings were locked by welding at their location on the lower stop; access hatches to reactor enclosures were locked and sealed;

- The possibility of reestablishment of power supply to the CPS actuator drives was excluded (safety devices were removed from the control stations, and cable sections were disconnected from the terminal block and cut off); and
- The possibility of forced circulation in the primary circuits and reestablishment of water supply to the reactors from external systems was eliminated (sections of power-supply cable to the main and auxiliary pumps, makeup systems *etc.* were cut off).

The above measures ensured the maintenance of the reactor cores in a state of deep sub-criticality even in cases of extreme external impacts (reactor compartment destruction; fire, sinking and capsizing of the submarine; terrorist attacks, *etc.*).

However, the sinking of the submarine and its prolonged stay under water would inevitably lead to degradation of the safety barriers in the submarine. As already mentioned, if there is seal failure of the primary circuit and seawater ingress to the reactors, the process of active corrosion of the fuel element claddings and subsequent corrosion of the fuel will begin. Under such conditions, in cases of an external impact (e.g. torpedo hit, terrorist attack, major earthquake, *etc.*) the probability of fuel transfer to the bottom of the seawater filled reactor vessel would increase and, under specific conditions, could ultimately lead to the initiation of a SCR.

Regarding the initiation of a SCR incident, the following scenarios might be envisaged:

1. As a result of fuel transfer from the spent fuel assemblies to reactor lower part a critical mass of fuel may arise.
2. In the process of raising the submarine, agitation of transferred fuel may occur upon release from the sea bottom or due to a sudden rupture of a supporting rope(s)/ wire(s).
3. During raising, a critical mass of transferred fuel and seawater could be formed as a result of shaking (in a case of rope breaking, hook rupture, *etc.*) and rocking (overturning, sharp emergency submersion, *etc.*) when the submarine reaches the water surface.
4. During docking, a sudden jolt or a collision with a support ship may lead to a mixing of transferred fuel and water with generation of a critical mass.

The first two scenarios involve a release of activity to seawater, the third scenario to water and the atmosphere, and the fourth scenario to the atmosphere only.

3.2.1 General description of possible accidents involving SCR

The development of events under Scenarios 1 and 2 might be considered as accidents with the most serious adverse effects that could arise while the submarine is submerged or afloat. In such situations, hull structures are degraded and an instantaneous release of activity to the environment occurs. Under Scenarios 3 and 4, a release of radionuclides to the atmosphere could occur which constitutes a hazard to humans and the environment. It is assumed that following the initiation of a SCR, with resultant changes in the fuel geometry and destruction of structural components, the whole system would return to a sub-critical state again.

In determining the SCR parameters, an assessment of its most important parameter - the number of fissions in the nuclear fuel – is the most relevant starting point. This parameter directly affects both the degree of destruction of the safety barriers and the total release of radionuclides to the environment. Note that not only radionuclides generated in the course of the SCR but also those accumulated in the reactor during its operation would be released.

To assess the power of a potential SCR, data from the Chazhma Bay accident of 1985 during refueling of a water-moderated submarine reactor in the Russian Far East may be usefully employed. This accident occurred in a similar-type reactor of a first generation nuclear submarine at the pier in Chazhma Bay. As a result of a thermal explosion, a fuel assembly with fresh fuel was ejected from the reactor vessel. According to estimates of the radiation effects and consequences of that SCR, the total number of fissions was estimated as being of the order of 5.0E+18. According to observations at the time, the radioactive cloud height varied between 20 and 50 m following the Chazhma Bay accident (Sivintsev et al. (1994) and (2005)).

Conservatively, it is here assumed that an initiation of a SCR in one of the reactors of K-159 would result in 1.0E+19 fissions.

It should be borne in mind that the 'conservative' assumption made regarding the SCR power influences the generation and release of short-lived fission products. The generation, the rate and amount of long-lived fission products released depends much less on the SCR power, though radionuclides such as ^{137}Cs and ^{90}Sr, make a prominent contribution to the long-term contamination of the environment and determine the radiological consequences of the accident.

3.2.2 Estimates of radioactivity releases and consequences

By setting the power of the SCR event at 1.0E+19 fissions and using ORIGEN-2 software, which is a part of the SCALE Code (Rearden and Jessee, 2016), the activities of fission products formed in the nuclear fuel were calculated (Table 3.4).

The data of Table 3.4 indicates that the total activity of fission products generated during the initial moments of the SCR event is comparable to the previously accumulated activity, though one hour later the activity is an order of magnitude less due to decay of the short-lived radionuclides. Note that the activity of newly formed ^{137}Cs and ^{90}Sr is more than 5 orders of magnitude lower than the same radionuclides accumulated during reactor operation.

Table 3.4. Activity of main fission products (TBq) in reactor fuel at various time points following a SCR accident of 1.0E+19 fission power.

Time	**0**	**1 hour**	**3 hours**	**12 hours**	**24 hours**	**7 days**	**28 days**
NG (Kr, Xe)	7.92E+03	8.07E+01	3.08E+01	9.88E+00	5.14E+00	5.51E-01	3.44E-02
Iodine, Bromine	7.62E+02	1.13E+02	5.66E+01	1.15E+01	5.81E+00	4.44E-01	3.03E-02
Ru, Te	3.77E+02	1.69E+02	2.86E+01	2.63E+00	1.34E+00	3.21E-01	4.63E-02
^{140}La	2.65E-03	9.51E-03	2.29E-02	7.70E-02	1.35E-01	2.93E-01	1.02E-01
^{140}Ba	3.56E-02	4.03E-01	4.03E-01	3.96E-01	3.85E-01	2.78E-01	8.84E-02
^{143}Ce	1.87E-02	3.36E+00	3.40E+00	2.82E+00	2.19E+00	1.06E-01	2.68E-06

^{143}Pr	2.82E-07	5.14E-03	1.98E-02	7.81E-02	1.39E-01	2.72E-01	9.69E-02
^{141}Ce	1.07E-06	1.49E-02	5.40E-02	1.29E-01	1.44E-01	1.29E-01	8.25E-02
^{144}Ce	2.11E-04	1.58E-02	1.58E-02	1.57E-02	1.57E-02	1.55E-02	1.47E-02
^{144}Pr	7.07E-04	1.53E-02	1.57E-02	1.57E-02	1.57E-02	1.55E-02	1.47E-02
^{147}Nd	4.18E-05	1.73E-01	1.80E-01	1.76E-01	1.71E-01	1.17E-01	3.10E-02
^{89}Sr	5.51E-04	9.21E-02	9.84E-02	9.81E-02	9.73E-02	8.95E-02	6.73E-02
^{91}Sr	5.59E-01	1.14E+01	9.88E+00	5.11E+00	2.14E+00	5.96E-05	6.88E-21
^{91}Y	1.36E-05	3.57E-03	1.30E-02	4.63E-02	6.73E-02	7.70E-02	6.03E-02
^{93}Y	2.64E-01	7.81E+00	6.85E+00	3.68E+00	1.62E+00	8.25E-05	7.84E-20
^{95}Zr	9.62E-04	8.44E-02	8.58E-02	8.55E-02	8.51E-02	7.99E-02	6.36E-02
^{97}Zr	1.25E+00	6.29E+00	5.81E+00	4.00E+00	2.45E+00	6.70E-03	7.03E-12
^{95}Nb	2.39E-06	5.55E-05	1.96E-04	8.21E-04	1.65E-03	1.07E-02	3.11E-02
^{137}Cs	1.20E-05	4.70E-04	4.70E-04	4.70E-04	4.70E-04	4.70E-04	4.70E-04
^{137m}Ba	3.05E-01	4.44E-04	4.44E-04	4.44E-04	4.44E-04	4.44E-04	4.44E-04
^{90}Sr	2.92E-06	4.70E-04	4.70E-04	4.70E-04	4.70E-04	4.70E-04	4.66E-04
^{90}Y	1.31E-05	1.79E-05	2.76E-05	6.85E-05	1.17E-04	3.96E-04	4.66E-04
Total	9.07E+03	3.92E+02	1.43E+02	4.07E+01	2.19E+01	2.81E+00	7.66E-01

Based on experience from the Chernobyl accident, it is known that the release of fission products from a reactor in case of an SCR is determined by their volatility. Table 3.5 summarizes release fractions of various radionuclide groups from the fuel according to the data found in Russian sources.

Table 3.5. Release fraction of various radionuclide groups from the fuel following an accident.

Group of radionuclides	Release fraction, %
NG (krypton, xenon)	100
Iodine, Bromine	50
Cesium	20
Ruthenium, Tellurium	10
Others	5

Taking into account the experience of similar accidents, no more than 20% of the generated radionuclides would be released to the environment (Table 3.6).

Table 3.6. Activity of main fission products released (TBq) from a reactor of K-159 during an SCR accident of 10^{19} fission power as a function of the time elapsed after the accident (case of instantaneous release).

Time	0	1 hour	3 hours	12 hours	24 hours	7 days	28 days
NG(Kr, Xe)	1.58E+03	1.61E+01	6.16E+00	1.98E+00	1.03E+00	1.10E-01	6.88E-03
Iodine, Bromine	7.62E+01	1.13E+01	5.66E+00	1.15E+00	5.81E-01	4.44E-02	3.03E-03
Ru, Te	7.54E+00	3.38E+00	5.72E-01	5.26E-02	2.68E-02	6.42E-03	9.26E-04
^{140}La	2.65E-05	9.51E-05	2.29E-04	7.70E-04	1.35E-03	2.93E-03	1.02E-03
^{140}Ba	3.56E-04	4.03E-03	4.03E-03	3.96E-03	3.85E-03	2.78E-03	8.84E-04
^{143}Ce	1.87E-04	3.36E-02	3.40E-02	2.82E-02	2.19E-02	1.06E-03	2.68E-08
^{143}Pr	2.82E-09	5.14E-05	1.98E-04	7.81E-04	1.39E-03	2.72E-03	9.69E-04
^{141}Ce	1.07E-08	1.49E-04	5.40E-04	1.29E-03	1.44E-03	1.29E-03	8.25E-04
^{144}Ce	2.11E-06	1.58E-04	1.58E-04	1.57E-04	1.57E-04	1.55E-04	1.47E-04
^{144}Pr	7.07E-06	1.53E-04	1.57E-04	1.57E-04	1.57E-04	1.55E-04	1.47E-04
^{147}Nd	4.18E-07	1.73E-03	1.80E-03	1.76E-03	1.71E-03	1.17E-03	3.10E-04
^{89}Sr	5.51E-06	9.21E-04	9.84E-04	9.81E-04	9.73E-04	8.95E-04	6.73E-04
^{91}Sr	5.59E-03	1.14E-01	9.88E-02	5.11E-02	2.14E-02	5.96E-07	6.88E-23
^{91}Y	1.36E-07	3.57E-05	1.30E-04	4.63E-04	6.73E-04	7.70E-04	6.03E-04
^{93}Y	2.64E-03	7.81E-02	6.85E-02	3.68E-02	1.62E-02	8.25E-07	7.84E-22
^{95}Zr	9.62E-06	8.44E-04	8.58E-04	8.55E-04	8.51E-04	7.99E-04	6.36E-04
^{97}Zr	1.25E-02	6.29E-02	5.81E-02	4.00E-02	2.45E-02	6.70E-05	7.03E-14
^{95}Nb	2.39E-08	5.55E-07	1.96E-06	8.21E-06	1.65E-05	1.07E-04	3.11E-04
^{137}Cs	4.80E-07	1.88E-05	1.88E-05	1.88E-05	1.88E-05	1.88E-05	1.88E-05
^{137m}Ba	3.05E-03	4.44E-06	4.44E-06	4.44E-06	4.44E-06	4.44E-06	4.44E-06
^{90}Sr	2.92E-08	4.70E-06	4.70E-06	4.70E-06	4.70E-06	4.70E-06	4.66E-06
^{90}Y	1.31E-07	1.79E-07	2.76E-07	6.85E-07	1.17E-06	3.96E-06	4.66E-06
Total	1.67E+03	3.11E+01	1.27E+01	3.35E+00	1.73E+00	1.76E-01	1.74E-02

Thus, the expected activity of radionuclides released from the submarine to the environment, taking into account their prior accumulation and production during SCR, may reach 45 TBq (Table 3.7).

Table 3.7. Activity of radionuclides (TBq) with half-lives >2 years (both accumulated and newly produced) that may be released to the environment following a SCR accident in one of the reactors of K-159.

Nuclide	T½	Activity, TBq
^{3}H	12.3 y	1.74E-02
^{85}Kr	10.7 y	7.18E+00
^{90}Sr	28.2 y	1.15E+01
^{134}Cs	2.06 y	1.40E-03
^{137}Cs	30.0 y	2.49E+01
^{147}Pm	2.62 y	2.55E-02
^{151}Sm	90.0 y	1.50E-01
^{152}Eu	13.3 y	8.44E-03
^{154}Eu	8.8 y	3.76E-02
^{155}Eu	4.96 y	4.08E-03
^{238}Pu	87.7 y	5.33E-02
^{239}Pu	24060 y	3.55E-02
^{240}Pu	6537 y	2.07E-02
^{241}Pu	14.4 y	4.88E-01
^{241}Am	432 y	5.14E-02
^{55}Fe	2.7 y	4.40E-03
^{60}Co	5.27 y	7.59E-02
^{59}Ni	75000 y	3.31E-03
^{63}Ni	96 y	3.24E-01
Total		**4.50 E+01**

Note that ^{137}Cs and ^{90}Sr will constitute the main contribution to environmental contamination (> 80%).

4 Marine dispersion modelling

For the modelling of radioactivity distribution in the Barents Sea, a joint model of sea dynamics 'INM-IO' and ice dynamics 'CICE5' (Hunke et al. 2015) was used. The horizontal resolution of the INM-IO model is 3 km. Atmospheric forcing is defined based on CORE-I[14] protocol. A brief description of the model, settings and implementation of numerical experiments on the transport of activity and the results achieved is provided below.

The 'INM-IO' ocean model has been developed at the Institute of Numerical Mathematics of the Russian Academy of Sciences (INM RAS) since the mid 1980s. After 2007, the work was simultaneously conducted at INM RAS and P.P. Shirshov Institute of Oceanology of RAS. The 'INM-IO' ocean model was developed for numerical modeling of the ocean state over a wide range of space-time variability. The model is based on the solution of a 3D equation system of oceanic thermo-hydrodynamic processes making use of hydrostatics, seawater incompressibility and Boussinesq approximations. The dynamics of the ocean upper boundary, allowing for the mass flux (atmospheric precipitation, evaporation and ice melting), is described by an ocean free-surface equation.

A finite-volume method (box method), applied for the first time to ocean models by Chernyaev et al. (2003), provides the methodological background for constructing approximations of the differential equations of the model. The equations are formulated in a curvilinear orthogonal coordinate system. This makes it possible to solve the equations in the Cartesian or spherical system of coordinates depending on the size of the modelled region. For the case of the global ocean model, the equations are solved in a tripolar system of coordinates. More details on the INM-IO ocean model and its application in this study can be found in Appendix 1.

4.1 Water circulation in the Barents Sea

When developing a water-circulation model for a marginal sea such as the Barents Sea, assignation of the boundary conditions at open boundaries of the sea is required. The availability of an open artificial boundary of the domain necessitates solving two problems: first, providing for the impact of external processes on the dynamics of the sea within the domain; and, second, ensuring unimpeded outward passage of signals from the domain (waves, vortices, *etc.*) so that no artificial boundary layer is formed along the interface. The second problem may be solved with a certain accuracy. For example, Marchesiello et al. 2001 developed an approach for adaptive open-boundary conditions where inward and outward fluxes are considered separately. Solution of the first problem requires information on the sea state at the open boundaries taken e.g. from the global model.

For the matter being considered here, the dispersion of radionuclides, one more aspect exists: the temporal scale. When estimating short-term (1-5 days) consequences of a radionuclide release from radiation sources in the Barents Sea, a sea model would be obviously sufficient. However, to assess long-term, seasonal and inter-annual effects of a radionuclide release, a much larger

[14] CORE: Coordinated Ocean-Ice Reference Experiment.

simulation domain – the entire Arctic Ocean – should be considered owing to the existence of evident interrelation of the long-term water circulation throughout the ocean including marginal seas. Thus, to solve the posited problem, an Arctic Ocean water-circulation model was developed. The computational grid of the Arctic Ocean model coincides with that of the World Ocean dynamic model north of 56,95°N (Ibrayev et al. 2012). The World Ocean Model, with a resolution of 1/10° horizontally and 49 vertical levels (WOM 1/10 × 1/10 × 49), is based on the system of equations mentioned above (see Appendix 1). The equations are written in a tripolar coordinate system. Figure 4.1 displays the computational grid of the WOM 1/10 × 1/10 × 49.

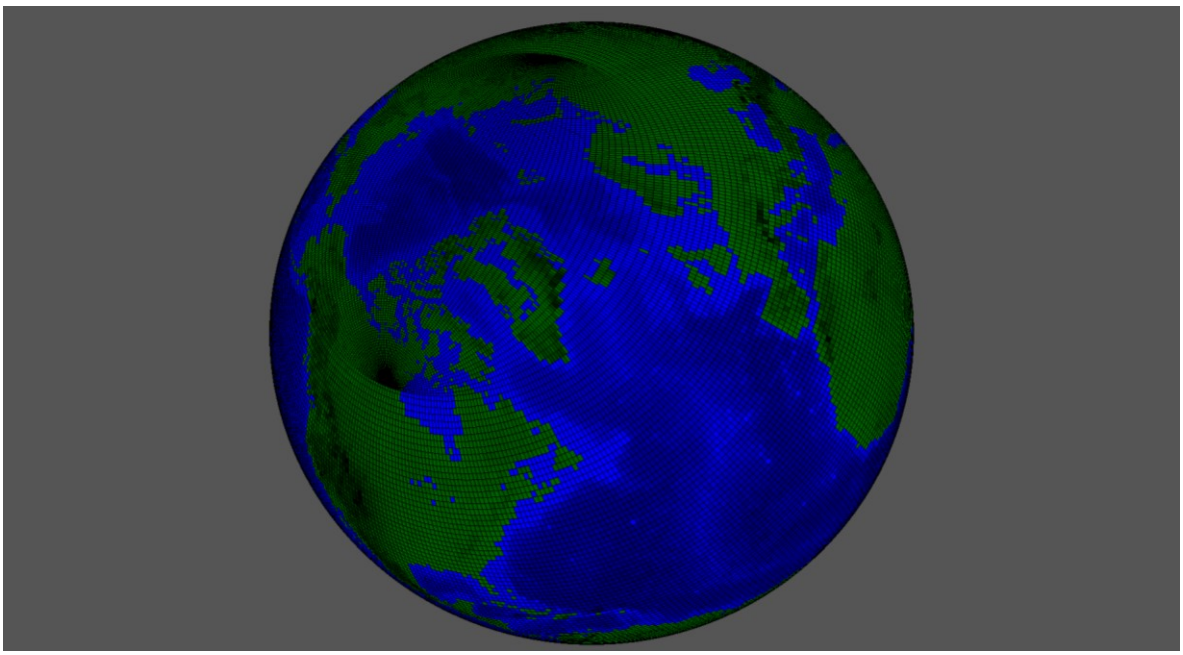

Figure 4.1. Tripolar grid of the World Ocean Model (WOM) with a resolution of 1/10°. Every tenth coordinate line is displayed. The Earth topography is taken from the ETOPO5[15] data.

4.2 Features of the arctic ocean model

A new parameterization of sub-grid turbulent processes was used in the Arctic Ocean model as compared to that addressed in Ibrayev et al. 2012.

The model of the horizontal, turbulent mixing assumes that turbulent flow is proportional to the gradients of transferred substances (temperature, salinity, and momentum). These fields are further smoothed by a bi-harmonic filter. The relevant coefficients of diffusion and viscosity are assumed to be constants.

Description of vertical mixing uses an empirical K-Profile Parameterization (KPP) scheme of turbulence described in detail in Large et al. 1994. In this model, the values for turbulent viscosity and turbulent diffusion in the upper ocean boundary layer are determined on the basis of the similarity theory for turbulence in stratified fluids (Obukhov, 1946 and Monin, 1956). KPP is the

[15] Earth topography five minute grid (ETOPO5) is a gridded data base of worldwide elevations derived from several sources at a resolution of 5 minutes of latitude and longitude.

most frequently used parameterization scheme in the World Ocean models with vortex-resolving resolution under which long-term (in the model time scale) calculations are performed.

The water-air interface is free with explicit description of the flows of water, heat, salt and momentum. At the atmosphere boundary, the flows of heat, salt, momentum and water are computed using a boundary-layer model (Large and Yeager, 2004).

Sea ice conditions are described by the CICE model (Hunke and Lipscomb, 2010), Version 5.0 (CICE 5.0).

4.3 Setting a numerical experiment

The performed numerical experiment is a several-year iterative calculation. Iterations are repeated until the calculated year-long cycle converges to the yearly seasonal cycle of key Arctic Ocean characteristics resulting under the impact of a cyclically repeated 'normal' annual variation of atmospheric and solar radiation parameters. More details are given in Large and Yeager (2009). The parameters are determined by the CNYFv2 database of the CORE-I Protocol (Large and Yeager, 2009). Wind speed, air temperature and humidity at 10 m are set at 6-hour intervals; surface long-wave and short-wave radiation are taken as daily averages; atmospheric precipitation and continental runoff are monthly averages.

The initial fields of temperature and salinity are taken as equal to yearly average fields from the World Ocean Database 2009 (WOA, 2009); the initial velocities of currents are zero; and sea ice is absent at the start of the experiment.

The sea bottom topography is taken from the 5 Minute Gridded Earth Topography Database (ETOPO5, 1988).

Vertical discretization includes 49 horizons with their thickness varying from 6 m in the upper layer to 250 m in the depth. The calculated horizons are given in Table 4.1.

Table 4.1. Horizons and their location at water column as used in INM-IO ocean model.

Horizon nr.	Depth (m)	Horizon nr.	Depth (m)
1	3	26	650
2	9	27	775
3	15	28	900
4	25	29	1050
5	35	30	1250
6	45	31	1500
7	55	32	1750
8	65	33	2000
9	75	34	2250
10	90	35	2500

Horizon nr.	Depth (m)	Horizon nr.	Depth (m)
11	105	36	2750
12	120	37	3000
13	135	38	3250
14	150	39	3500
15	165	40	3750
16	185	41	4000
17	205	42	4250
18	230	43	4500
19	255	44	4750
20	280	45	5000
21	310	46	5250
22	350	47	5500
23	400	48	5750
24	475	49	6000
25	550		

The mean horizontal resolution of the computational grid in the domain is 3 km. The time step is 3 minutes.

The coefficients of horizontal viscosity for shallow-water equations are equal to 1 m^2/s; the coefficients of horizontal bi-harmonic viscosity and diffusion are only applied to baroclinic equations and are equal to $-9\cdot10^9$ and $-27\cdot10^9$ m^4/s, respectively. The background values of vertical viscosity and diffusion are equal to 10^{-4} and 10^{-6} m^2/s.

Hereafter, only the model solution for the Barents Sea will be analyzed.

Figure 4.2 presents the model topography of the sea bottom.

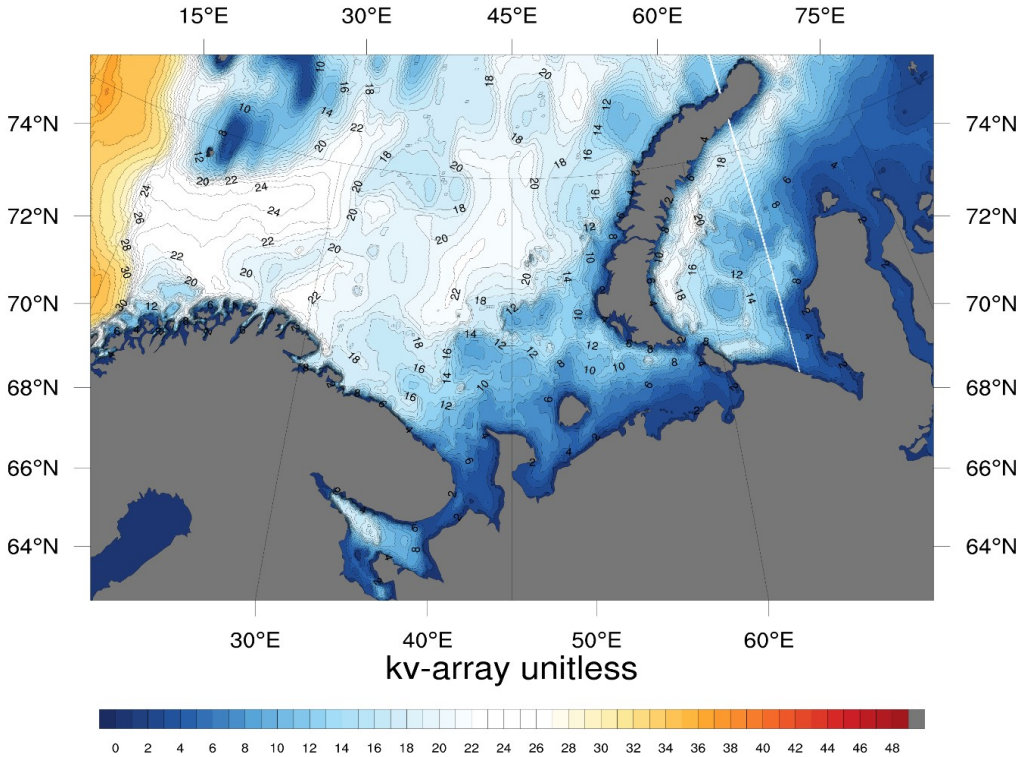

Figure 4.2. Model topography of the Barents Sea bottom. Isoline values enumerate the horizons (See Table 4.1).

4.4 Results of modeling dynamic characteristics of the Barents Sea

Integration of the equations of the Barents Sea dynamics model was repeatedly performed until establishment of a quasi-periodic yearly cycle. After 4-5 years of the model time, key parameters of the solution reached the quasi-periodic regime. The solution addressed below corresponds to the 6th model year.

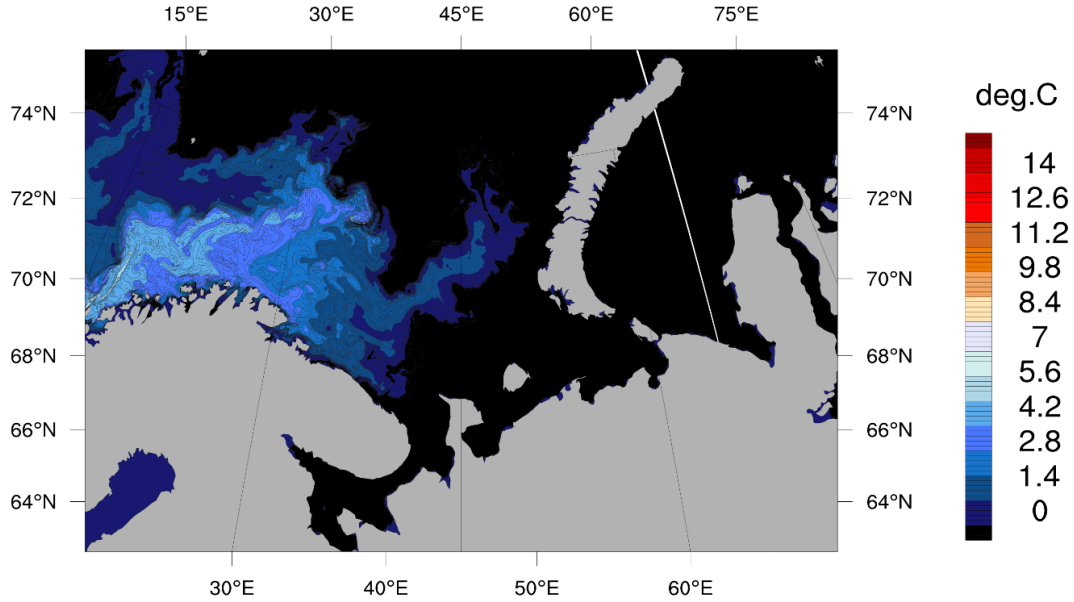

Figure 4.3a. Water temperature on the sea surface as of March 22 – the model solution.

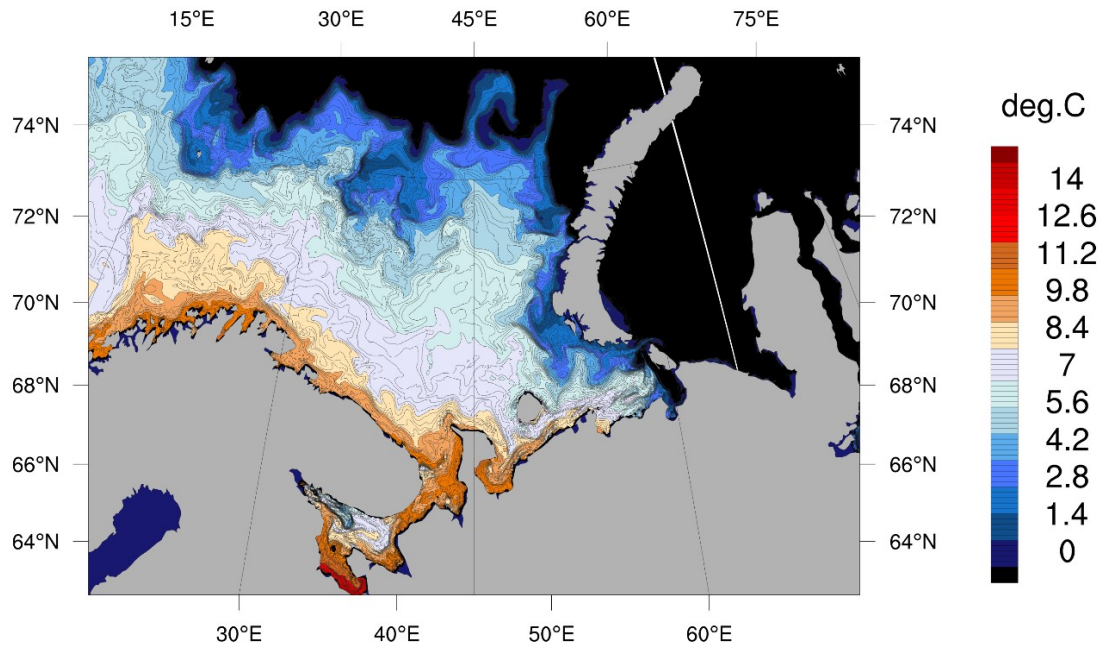

Figure 4.3b. Water temperature on the sea surface as of September 3 – the model solution.

Figure 4.3 shows the sea surface temperature, which corresponds to the total heat content. The figure clearly indicates the temperature variations in winter and summer seasons. In winter, the northern and the north-western parts of the sea are covered with ice. In summer, seawater temperature is significantly higher, and in the sea center the seasonal difference reaches 5-6 ºC. Throughout the year, persistent transport of relatively warm Atlantic waters along Scandinavia and the Kola Peninsula eastward is observed. In summer, a transfer of warm waters along the mainland eastward to the Kara Gate is clearly traced.

Sea currents are characterized by strong spatial and temporal variability. Sea surface currents of the central part of the sea are significantly affected by the wind. Figure 4.4 demonstrates an

example of surface currents simulated in the model. Maximum velocities of sea currents often reach 1.5-2 m/s. It should be remembered that the atmospheric forcing is synoptic[16] and includes, among other phenomena, storm winds.

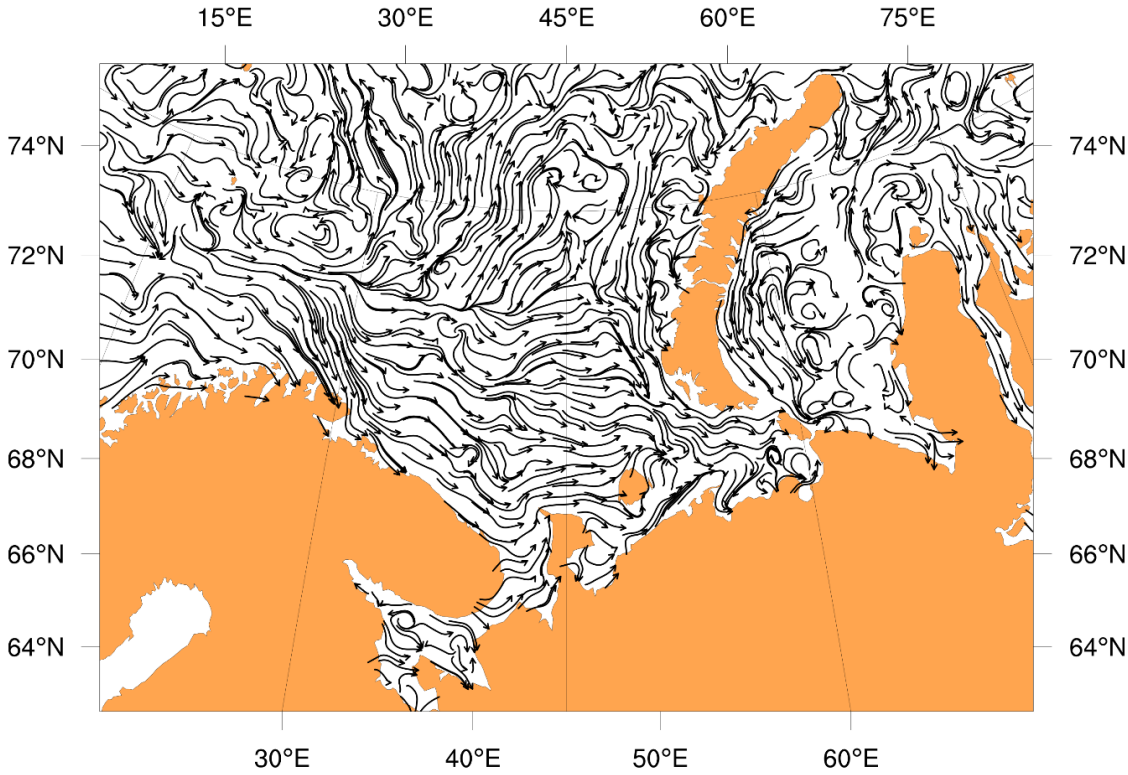

Figure 4.4. Currents on the sea surface as of January 6 – the model solution.

A more detailed analysis which was conducted later show that the circulation simulated in the model is in good agreement with the observational data, in particular, by those provided in (Terziev et al., 1990).

[16] Considering a variety of large scale weather variables over a wide area at the same time.

4.5 Modelling and analysis of the transfer by sea currents

4.5.1 Statement of the problem

The pertinent problem is the prediction of the oceanic transportation of ^{137}Cs released from K-159. The input data were the total activity release from the source, 50 TBq, during 12 hours at the source coordinates (69°22.64'N and 33°49.51'E). As discussed in Section 3.2.2, the estimated maximum activity released upon an accident would be in the order of 45 TBq. However, this value was rounded up to 50 TBq and was used as a starting point for all considered accident scenarios.

The following four release scenarios were considered:

Winter surface release scenario: The source is at the sea surface. The model depth of the source is located at the horizon nr. 1 corresponding to 3 m (see Table 4.1). The emergency release occurs in early January.

Winter bottom release scenario: The source is under the sea surface. The model depth of the source is located at the horizon nr.17 corresponding to 205 m (see Table 4.1). The emergency release occurs in early January.

Summer surface release scenario: The source is at the sea surface. The model depth of the source is located at the horizon nr.1 corresponding to 3 m (see Table 4.1). The emergency release occurs in early July.

Summer bottom release scenario: The source is under the sea surface. The model depth of the source is located at the horizon nr.17 corresponding to 205 m (see Table 4.1). The emergency release occurs in early July.

All simulated concentration maps obtained upon considering these four release scenarios are shown in Appendix 2.

4.5.2 Surface release at winter

The highest contaminant concentrations are obviously observed during the first few days following the release in the horizons where the release occurred. Figures 4.5 and 4.6 display the contaminant concentrations in the horizon depth of 3 m and 45 m for 5, 10, 15 and 360 days of the model time following the release. Cs-137 activity concentrations exceeding the maximum permitted level (MPL)[17] of 1 kBq/m^3 are observed at the sea surface and at horizon depth of 45 m within the first 10 days following the release. Under this scenario, no concentrations above 1 kBq/m^3 are observed at lower horizons provided 5-day discretization in the model calculations.

[17] This is the level introduced by the departmental document of the USSR Navy in 1990 (the latest available document). The document is referred to in the "White Book-2000" (Sivintsev et al. 2005) as RKVS-90 (Russian).

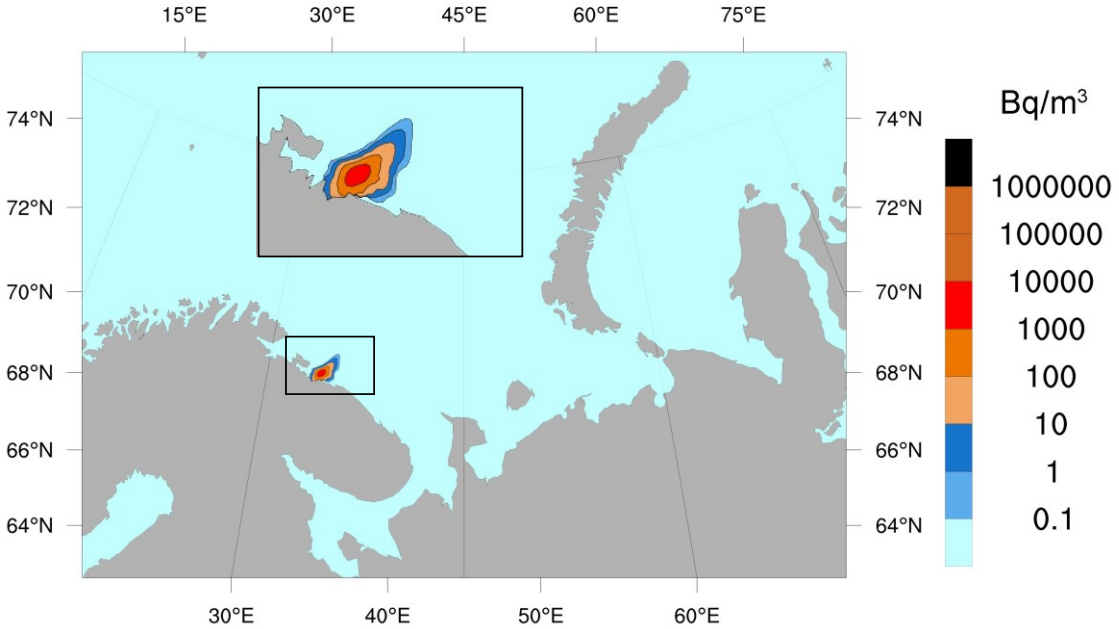

Figure 4.5a. Dispersion of radioactive contamination (^{137}Cs) following an emergency release of 50 TBq in early January from K-159 (surface position). Concentrations (Bq/m^3) at the horizon depth of 3 m, 5 days following the release.

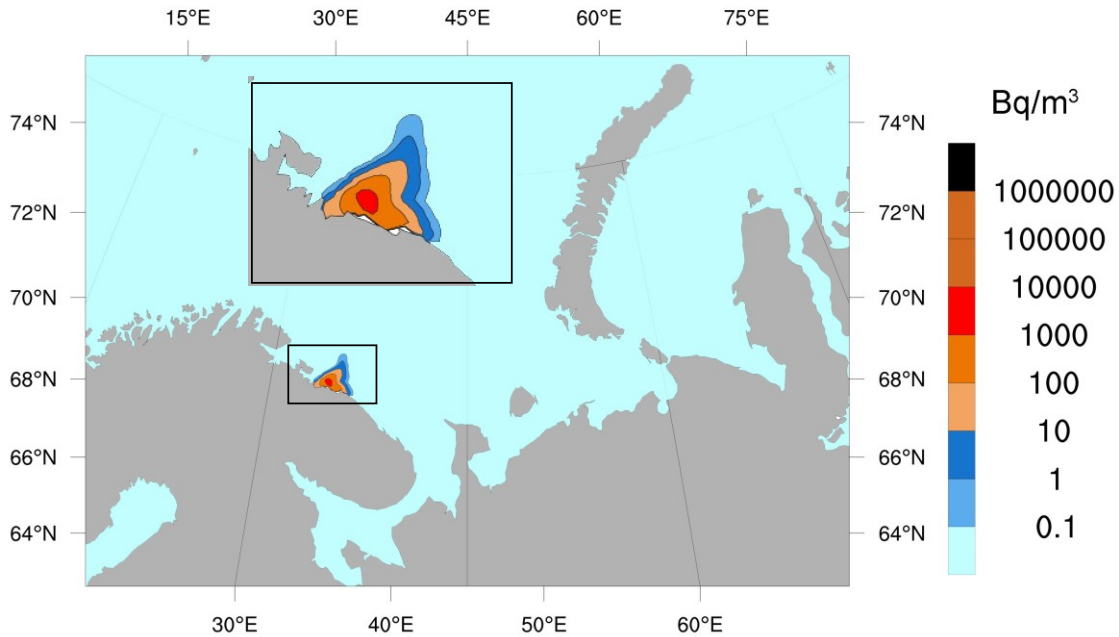

Figure 4.5b. Concentrations (Bq/m^3) at the horizon depth of 3 m, 10 days following the release.

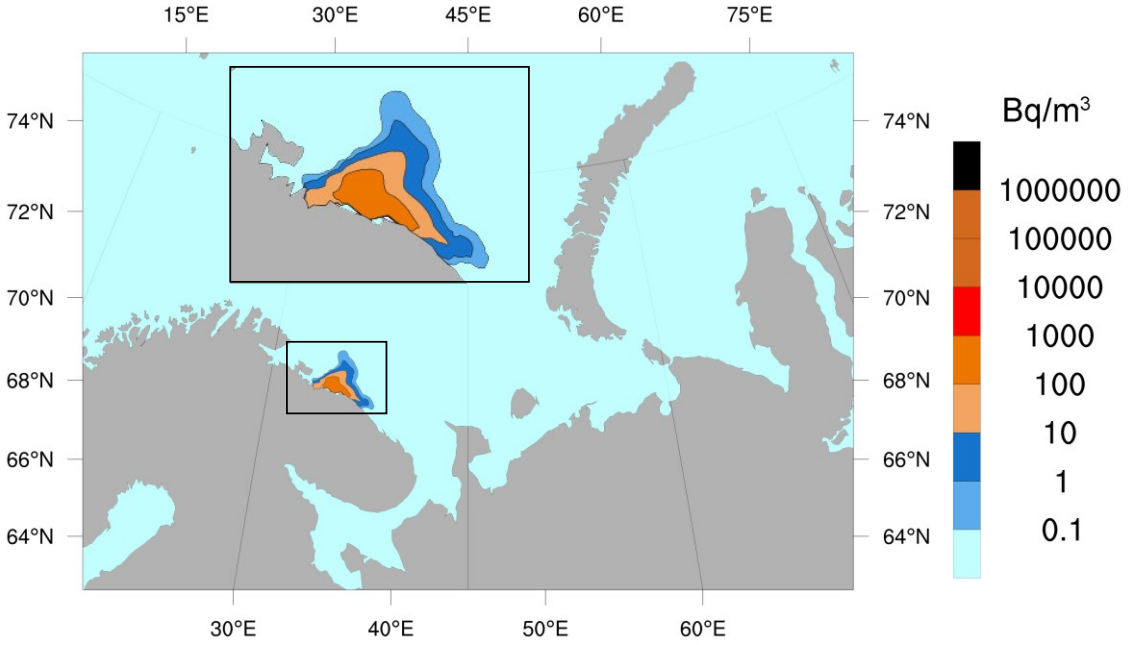

Figure 4.5c. Concentrations (Bq/m^3) at the horizon depth of 3 m, 15 days following the release.

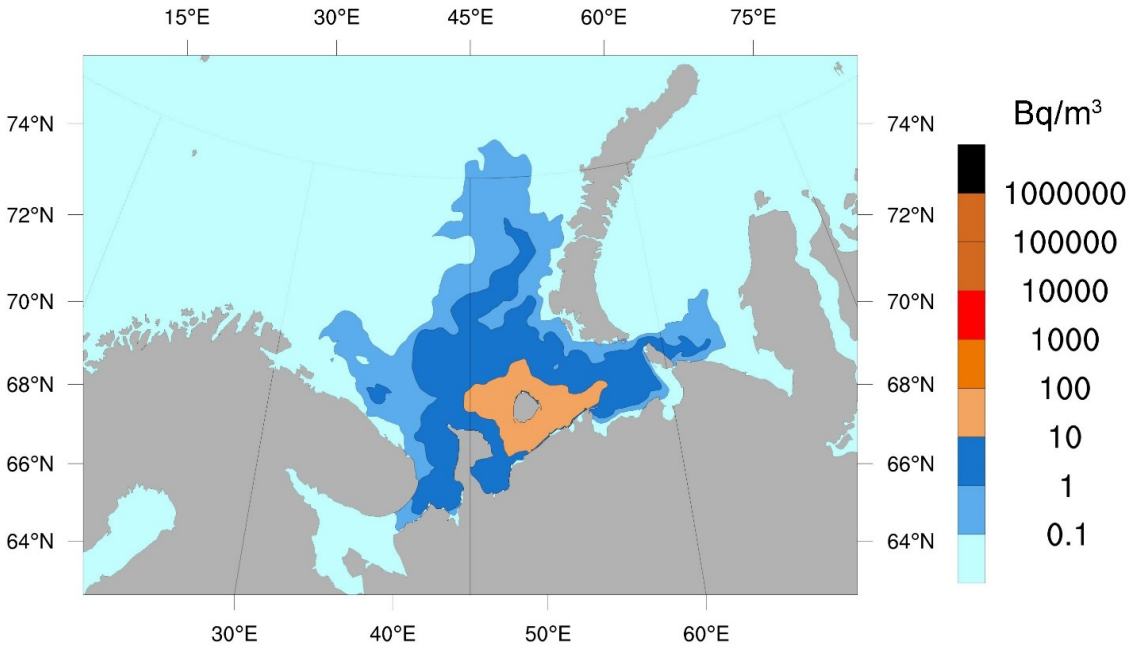

Figure 4.5d. Concentrations (Bq/m^3) at the horizon depth of 3 m, 360 days following the release.

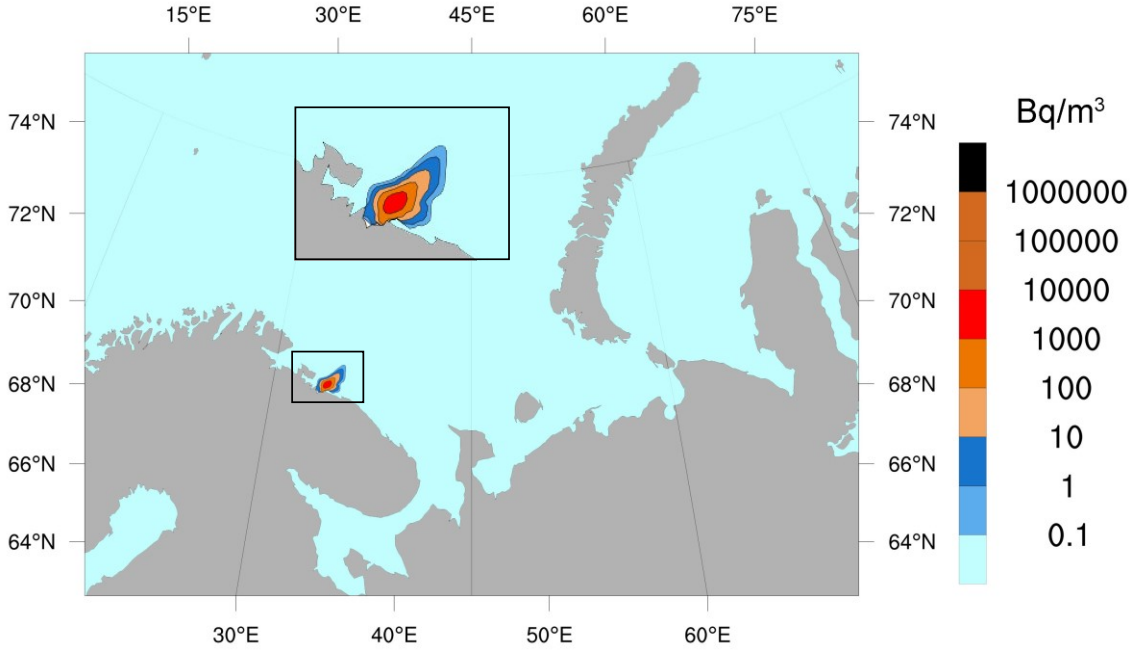

Figure 4.6a. Dispersion of radioactive contamination (^{137}Cs) following an emergency release of 50 TBq in early January from K-159 (surface position). Concentrations (Bq/m^3) at the horizon depth of 45 m, 5 days following the release.

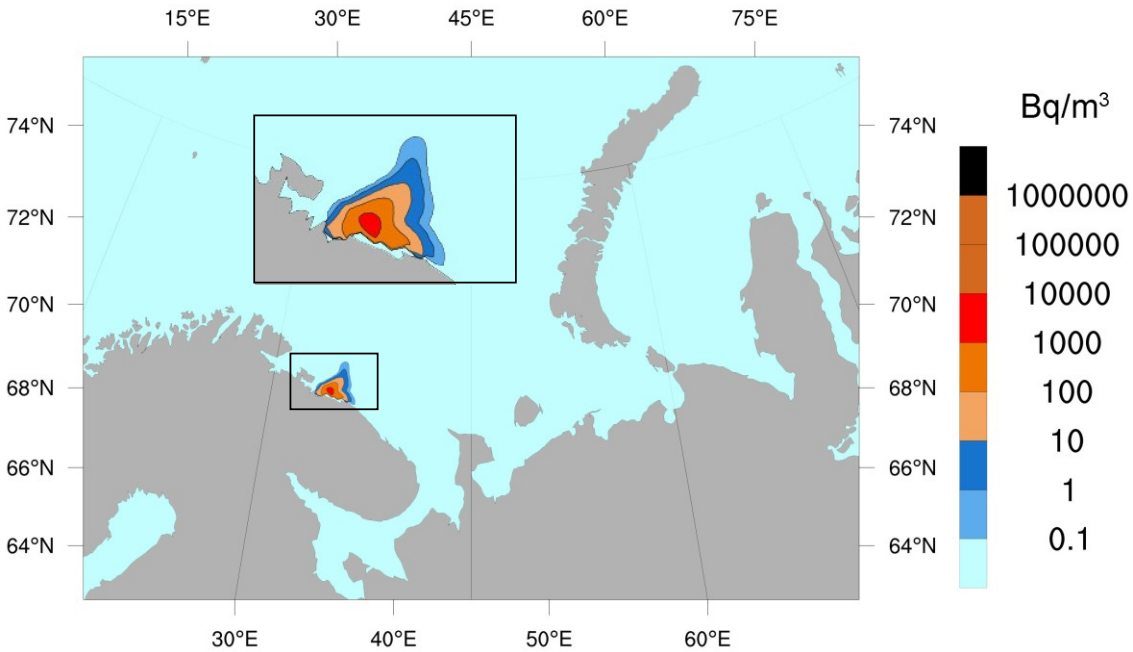

Figure 4.6b. Concentration (Bq/m^3) at the horizon depth of 45 m, 10 days following the release.

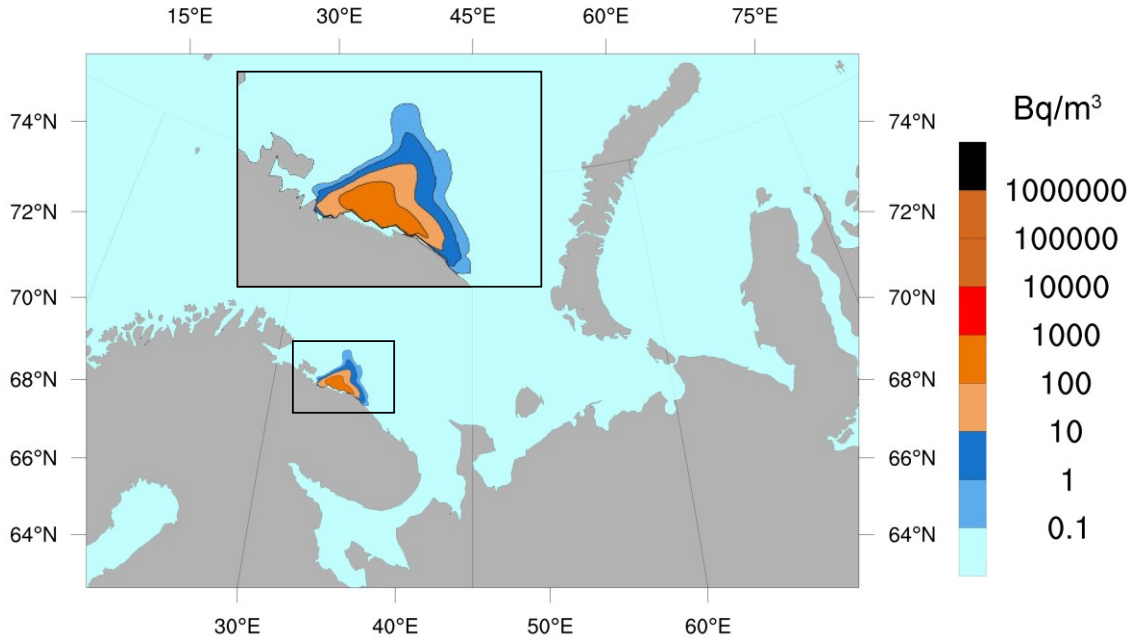

Figure 4.6c. Concentration (Bq/m^3) at the horizon depth of 45 m, 15 days following the release.

4.5.3 Bottom release at winter

A release occurring at 205 m depth in January. Cs-137 activity concentrations exceeding the MPL of 1 kBq/m^3 at the horizon depth of 205 m are observed within the first 20 days following the release. At overlying horizons, no concentrations above 1 kBq/m^3 are observed. Figure 4.7 displays the contaminant activity concentrations at the horizon depth of 205 m for 5, 20, and 360 days of the model time following the release.

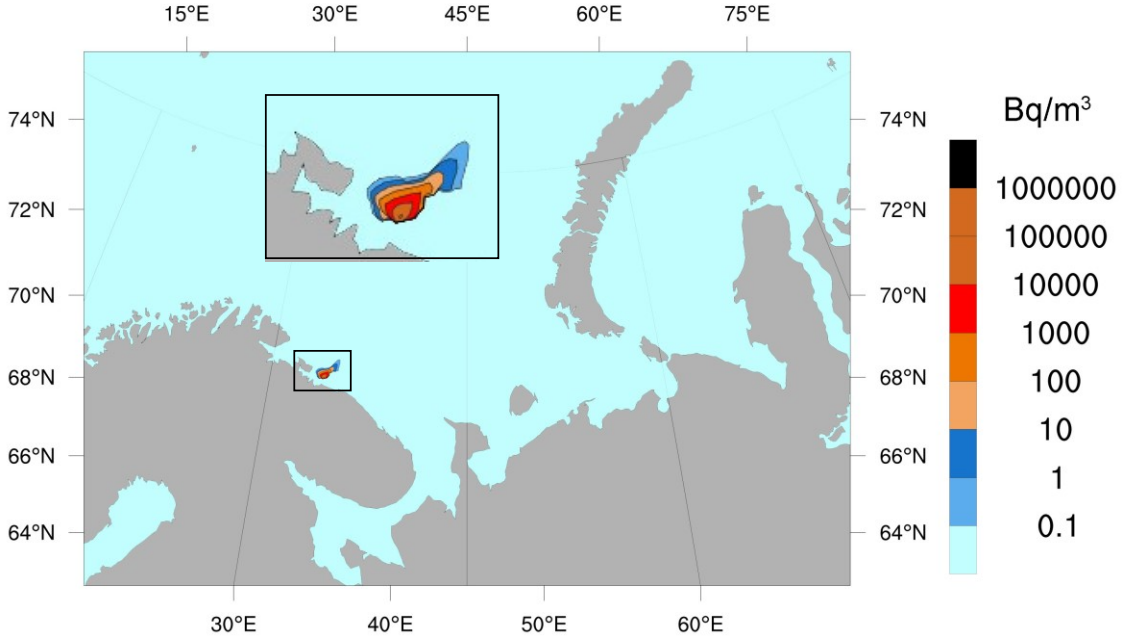

Figure 4.7a. Dispersion of radioactive contamination (^{137}Cs) following an emergency release of 50 TBq in early January from K-159 (bottom position). Concentrations (Bq/m^3) at the horizon depth of 205 m, 5 days following the release.

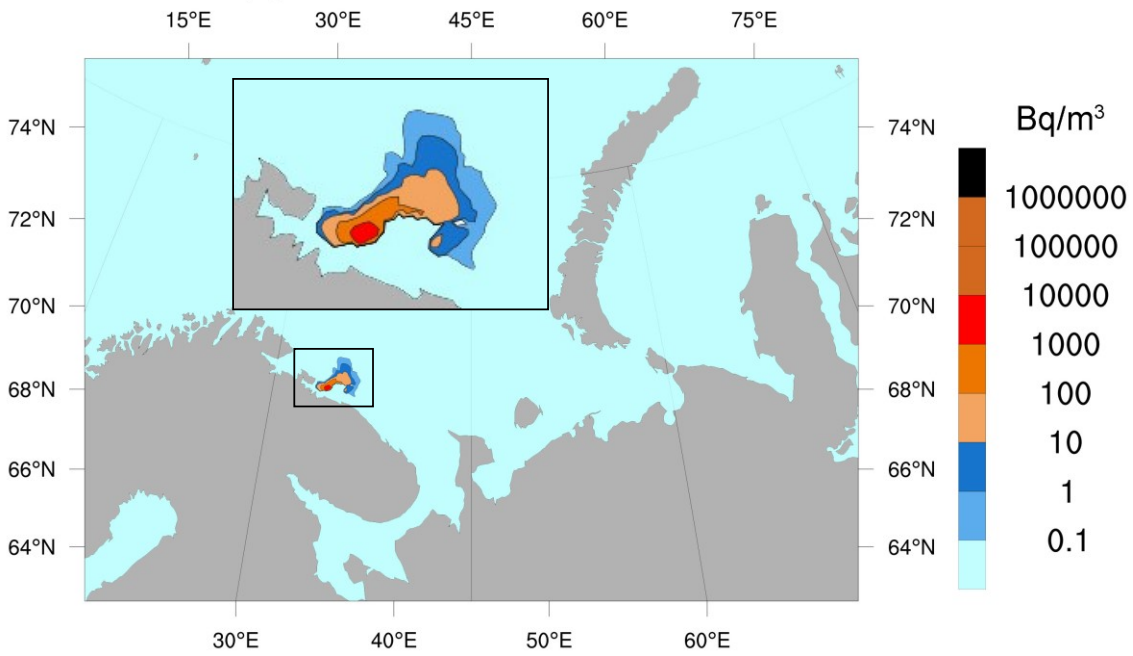

Figure 4.7b. Concentration (Bq/m^3) at the horizon depth of 205 m, 20 days following the release.

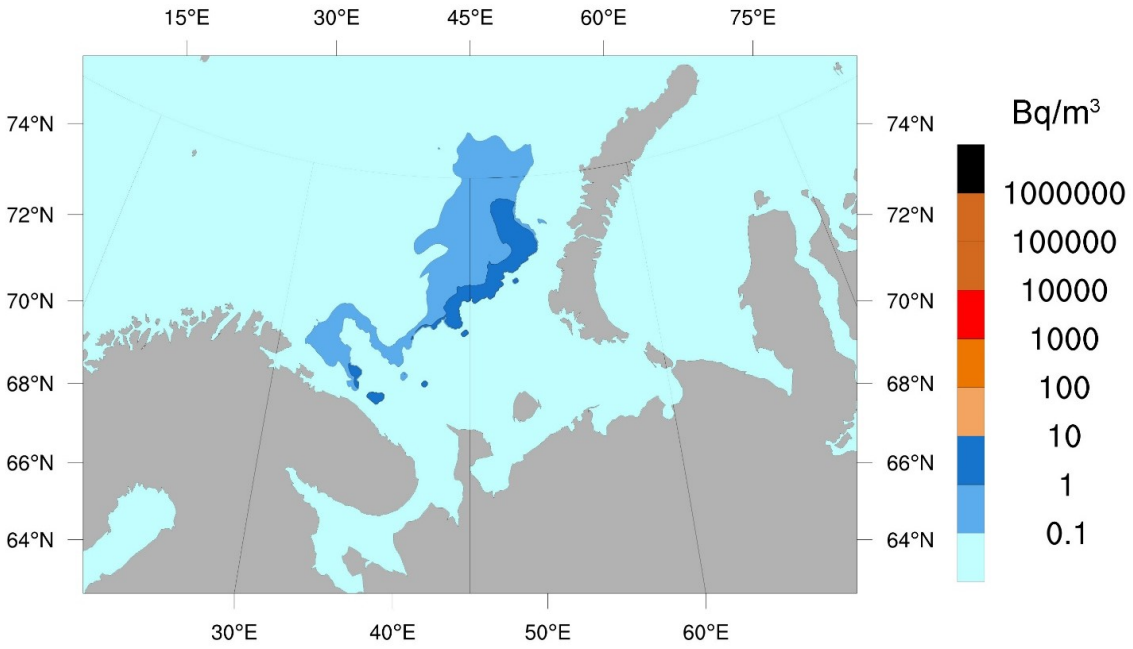

Figure 4.7c. Concentration (Bq/m^3) at the horizon depth of 205 m, 360 days following the release.

4.5.4 *Surface and bottom releases at summer*

These scenarios are concerned emergency releases occurring in early July. The qualitative picture of radionuclide dispersion does not change, though a slight increase in the period of contaminant activity concentrations exceeding the MPL from both the surface and the underwater release is observed. This is due to differences in the hydrophysical regime of the sea in winter and summer, namely, to the generation of a greater vertical stratification of seawater.

5 Atmospheric dispersion modelling

For the simulation of atmospheric dispersion of radionuclides, a model called SNAP (Severe Nuclear Accident Program) was used. SNAP is a Lagrangian particle model which was developed at the Norwegian Meteorological Institute, MET (Bartnicki et al., 2011) to simulate atmospheric dispersion of radioactive debris in an emergency situation.

The estimation of the atmospheric transport to and deposition over Norway has been performed in several steps, largely following the methodology used previously in analysis of the transport of radionuclides from the K-27 submarine (Bartnicki et al., 2016).

The SNAP model was run with a generic source term twice a day for a period between 1980 and 2012, using the meteorological database NORA10-EI (Reistad et al., 2011). This resulted in a database of depositions containing more than 24 000 deposition maps over northern Europe with a resolution of approx. 11 km.

From the obtained deposition maps, only those with deposition over the Norwegian main land were analyzed, and the cases with the largest total deposition to Norway have been selected for more in-depth investigation. For these calculations, the initial generic source term was amended to reflect the current state of K-159 and a possible accident scenario releasing 50 TBq of the current inventory to the atmosphere up to 100 m. The release was assumed to be short – one hour, in the form of radioactive particles. Based on these runs a worst case was identified and was further analysed for sensitivity to emission height and particle characteristics.

5.1 Construction of a deposition database

The ERA-Interim global meteorological database (Dee et al., 2011) from the European Medium Range Weather Forecast Centre (ECMWF) was used as a basis for a regional scale meteorological database, NORA10-EI (Reistad et al., 2011). Downscaling to regional scale was performed by dynamic downscaling with the regional HIRLAM numerical weather prediction model (Undén et al., 2002). The NORA10-EI has a horizontal resolution of approximately 11 km and a vertical resolution of 40 layers reaching up to 10 hPa[18]. The domain is on a rotated geographical grid, covering the area from Novaya Zemlya to the United Kingdom in north-south direction, and from Estonia to Iceland in an east-west direction. The domain with the position of the hypothetical release from K-159 at (69°22.64'N, 33°49.51'E) can be seen in Figure 5.1. The NORA10-EI database covers the period from 1980 to 2012, with forecast runs starting 4 times a day. The data for 6 and 9 hours forecasts after the analysis-time have then been used to build the hindcast meteorological database, storing these data for every 3rd hour.

[18] hectoPascal = 1 millibar

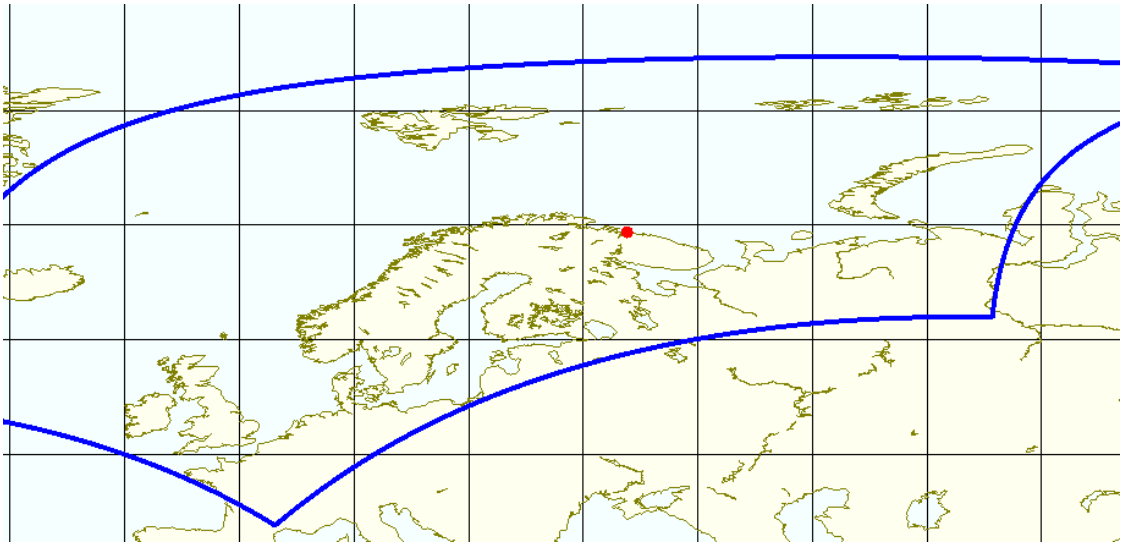

Figure 5.1. Position of K-159 submarine (red dot) in the NORA10-EI domain (blue frame).

To create the deposition database, the SNAP model was run twice each day from 1980 to 2012, starting at midnight and noon, using emissions lasting for 12 hours each time. The source term for the database used a unit-emission of activity of ^{137}Cs at a height between 0-800 m to cover a large range of emission scenarios. The unit-emission was distributed over 288000 model-particles for each run, and the SNAP model guarantees linear scaling to all activities. Each SNAP model-run was run for 96 hours, to ensure that most particles have settled out.

5.2 Worst case source term

For the release, only long-lived isotopes, i.e. ^{137}Cs and ^{90}Sr, were considered, as these are the main contributing radionuclides. Since both isotopes have similar and very long lifetimes (~ 30 years), compared to atmospheric transport times (96h), and both are transported as aerosols within the model, the worst-case source term for atmospheric transport considered to be 50 TBq ^{137}Cs, being the combined activity of ^{137}Cs and ^{90}Sr.

The selection of the worst case was an iterative process. The gridded depositions were first linearly scaled to the final inventory source term of 50 TBq. Then all grid-cells with depositions below a threshold of 10 Bq/m^2 were excluded. In order to avoid trivial deposition levels, which would result in trivial exposure level, this threshold of 10 Bq/m^2 ^{137}Cs was employed. In this way the focus of the analyses would be on areas where deposition was highest (See Appendix 3).

The gridded total depositions were then extracted for all Norwegian main-land territory and summed to give the total deposition of activity to Norway. These results were then sorted by magnitude and only the three largest cases used for further analysis.

The source term for the database used emissions lasting over 12h to cover the whole timespan between two model runs, while the final hypothetical case only utilised an emission of 1h duration. Therefore, the model was re-run 14 times for each of the three previously selected cases, this time with the vertical release range between 0 to 100 m. The same spatial selection procedure as for the

complete database has been used for these 3×14 runs and the result with the largest deposition to Norway selected as the final source term.

5.3 Concentrations in atmosphere and deposition

The atmospheric half-lives of aerosols are 5 to 26 days when distributed over the complete atmosphere (Kristiansen et al., 2016), but shorter in the initial phase of emissions, when the concentrations are highest close to the ground. For the initial source-term employed, on average 85(±13) % of the activity of ^{137}Cs was deposited to the model-domain after 96 h, whereof 65 % was attributable to wet and 20 % to dry deposition. In that time, on average 3(±5) % of activity remained in the atmosphere. Considering a mean time of 90 h after emissions, this results in atmospheric half-lives in the model domain of less than 18±24 h. About 12% of activity was transported so far that it left the model domain (see Figure 5.1).

5.3.1 Influence of thresholds and time on selection procedure

As a Lagrangian dispersion model with random-walk diffusion, single model-particle trajectories might reach a grid-cell without transporting much activity. The number of trajectories is for computational reasons limited and hence restricts areas that are affected by the transport. On the other hand, very small contributions might be well below detection limits or intervention limits. Results on probabilities of reaching Norway must, therefore, be robust against numerical model-limits. As can be seen in Figure 5.2, the 5% of model runs with largest depositions to Norway are not affected by a local (~120 km^2 grid cells) threshold of 10 Bq/m^2, while for low depositions, the probability to reach any single grid cell in Norway with a model-particle is above 70 %, whereas the probability to reach any grid-cell in Norway with model-particles contributing to more than 10 Bq/m2 in that cell is only 48 %.

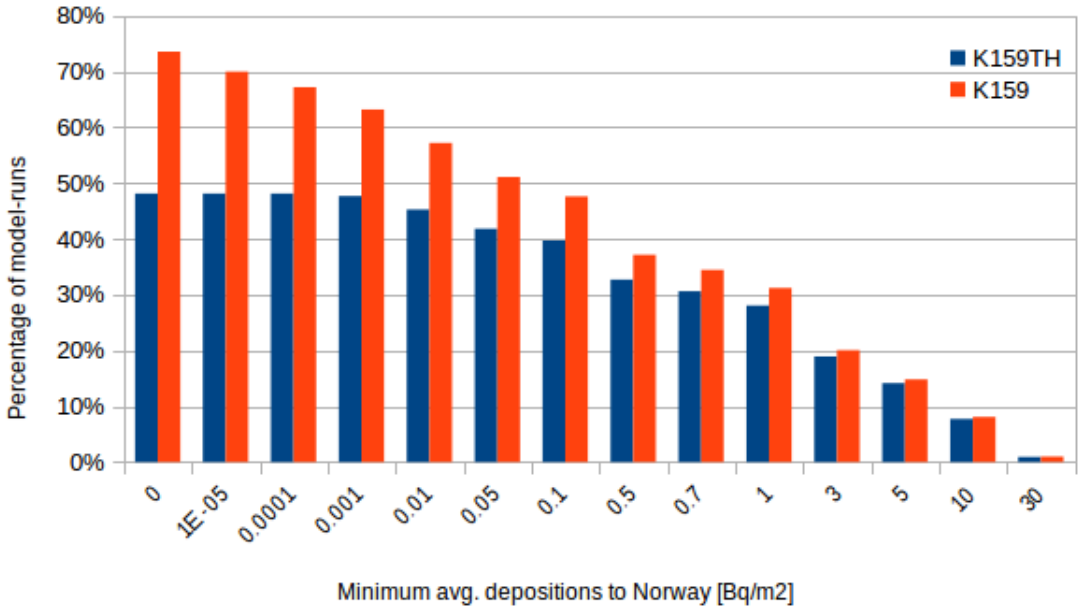

Figure 5.2. Percentages of model runs giving average total depositions to Norway above the value on the x-axis, both with a threshold per grid-cell of 10 Bq/m^2 (blue, K159TH) and without threshold (red).

An effect of the local threshold can be seen in Figure 5.3 showing the probability to reach a certain grid-cell. The probability to reach a grid-cell in Northern Norway is above 25% with the models

limitation of a restricted domain and 288000 model trajectories, while with a practical limit of 10 Bq/m^2, it is only 10%.

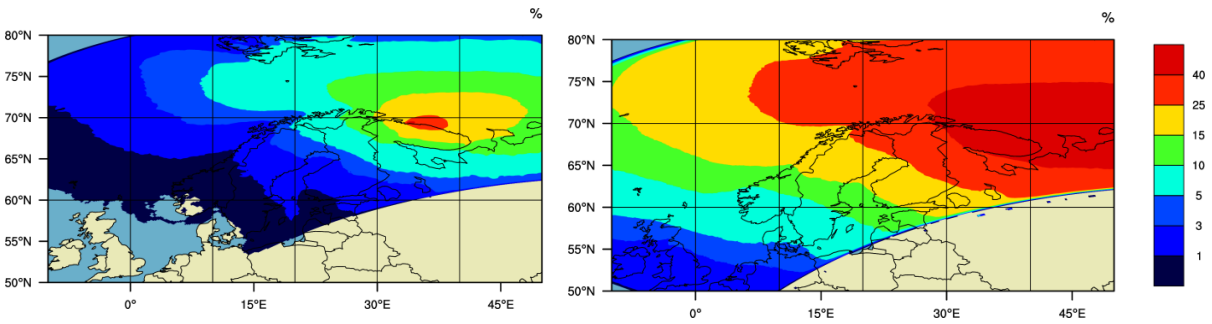

Figure 5.3. Probability to reach a grid-cell in Norway. Above threshold of 10 Bq/m^2 (left frame), without any threshold (right frame).

It can be concluded that the selection procedure of the worst case is not affected by the application of a local threshold. However, this is not the case for the probabilities of reaching Norway as these are affected by introducing a threshold. This indicates that the numerical limit of the SNAP model is lower than the selected threshold of 10 Bq/m^2.

5.3.2 Seasonal variation of air transport

The deposition database of 33 years allows the analysis of the risk to Norway on a monthly basis resulting from a possible accident involving K-159. In Figure 5.4, the monthly variation of deposition to Norway and probability to reach Norway with depositions above the 10 Bq/m^2 threshold are plotted. Both the depositions and the probabilities are averaged over all model-runs per month. During the summer months, May to July, the depositions are on average 3 times higher than in wintertime, i.e. December to February. In addition, the probability of reaching Norway increases from 40% in winter to 60% in the summer. However, the cold climate in the high latitudes allows only for handling of K-159 during summertime.

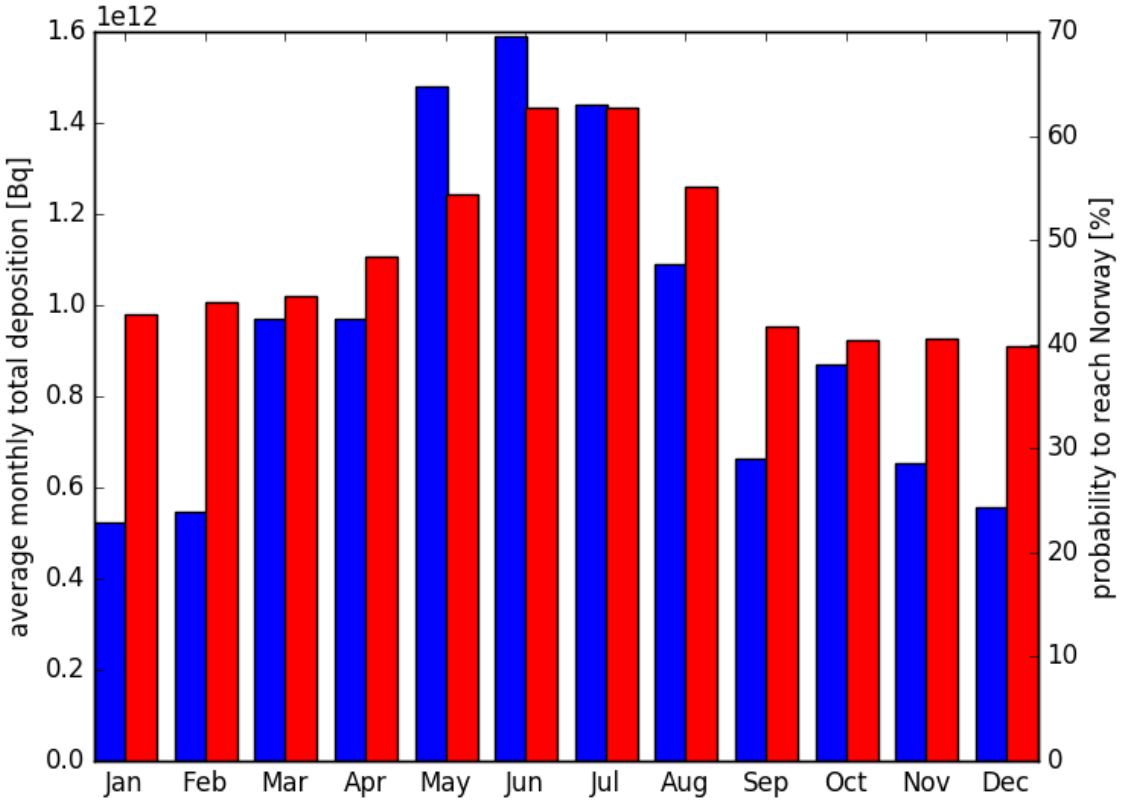

Figure 5.4. Seasonal variation of deposition in Norway (blue) and probability of transport to Norway (red).

5.4 Worst case run

The maximum total deposition to Norway for all 24100 model runs covering 33 years of bi-daily runs resulted in a ^{137}Cs deposition of 22 TBq. Even for the 100th worst case, the total deposition was still at 14 TBq. The three worst cases of the database runs were 1988-07-22 00UTC, 1999-06-23 12UTC and 2011-10-06 12UTC with 22.4, 22 and 21.3 TBq depositions to Norway, respectively.

Since the database model runs had 12 h rather than 1 h releases as assumed for the hypothetical accident, the three worst dates were run again for 14 times with hourly releases, starting 1 hour before the earliest of the previous 12 h continuous releases and ending 1 h after. The total amount of release for the 12 h and the 1 h releases were kept the same. Total deposition resulting from these runs can be seen in Figure 5.5. For all three dates, there exists at least one hourly release case which exceeds the 12 hourly release runs, even if the increase is not large. The absolutely worst case with respect to deposition over Norway can be found on 1988-07-22 with release between 06-07UTC, resulting in 26.9 TBq being deposited over Norway, which is 54% of the 50 TBq released.

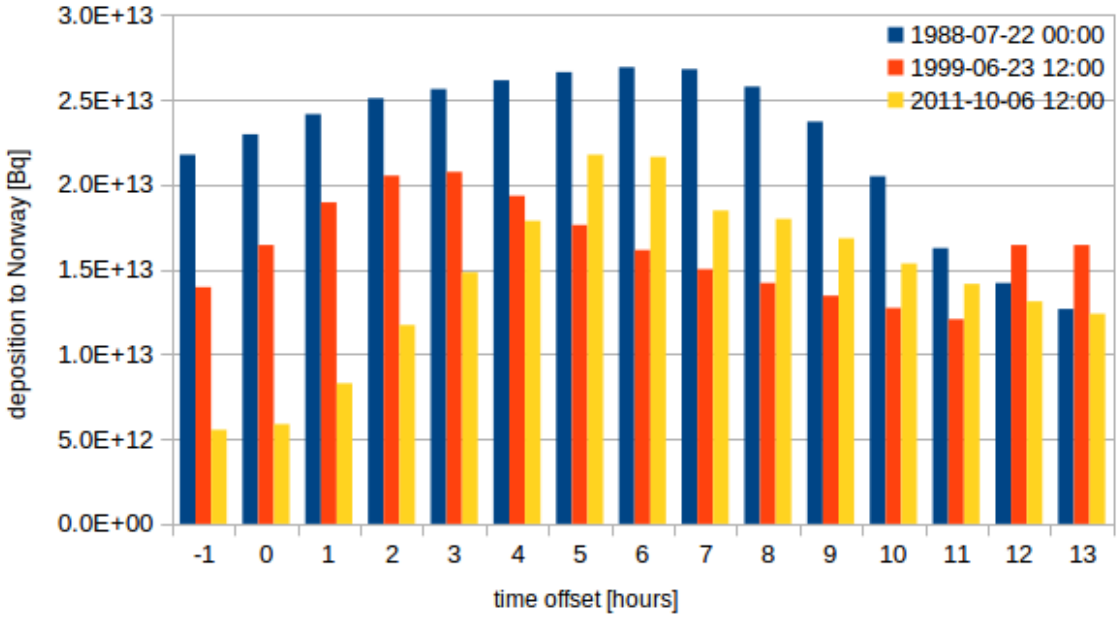

Figure 5.5. Estimation of worst time for releases of one hour duration for the 3 worst cases (see main text).

The deposition pattern of the worst case can be seen in

Figure 5.6. The weather situation consisted of strong winds from the east combined with heavy precipitation in Northern Norway, in particular in Finnmark where, over large areas, the deposition exceeds 1 kBq/m^2. The transport to Norway was fast, with surface trajectories reaching the Norwegian border in 6-9 hours.

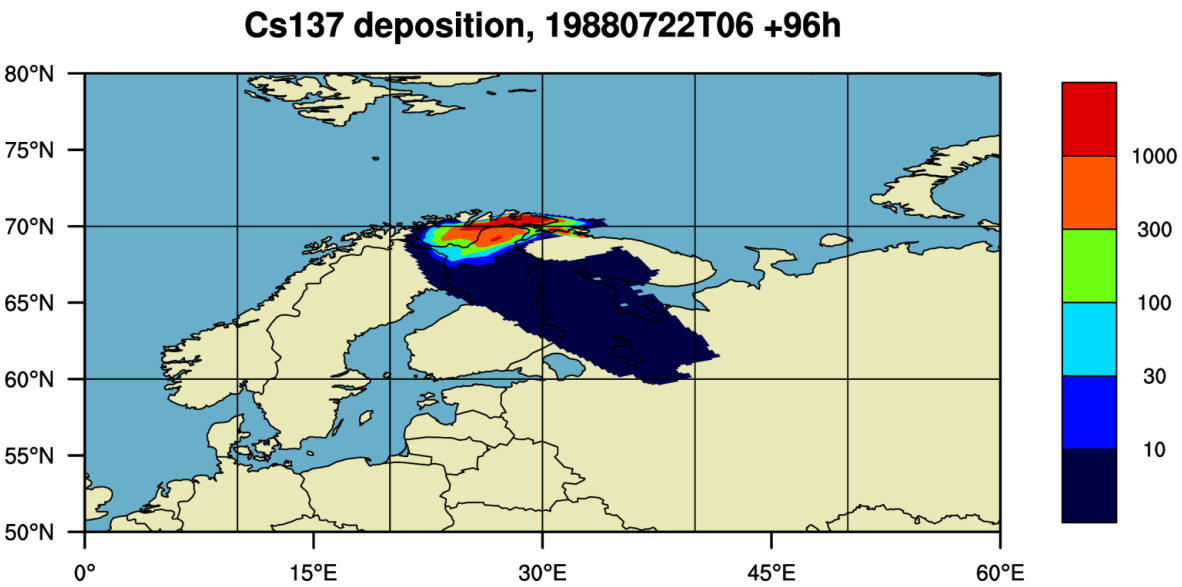

Figure 5.6. Deposition of ^{137}Cs (Bq/ m^2) after 96 h with emissions starting at 1988-07-22 06UTC.

5.5 Influence of release height and particle classes

The accident scenario had an emission height of 0 to 100 m. It is of interest to see if different emission height, i.e. resulting from larger explosions or hotter fires might increase or decrease the threat to Norway. Therefore, to determine the sensitivity to the emission height, the release height was varied in 100 m steps from 0-100 m to 1900-2000 m, with 100 m vertical release range. The results can be seen in Table 5.1. As can be seen, the total deposition to Norway can be increased by 20% by assuming a slightly increased emission height, 200m. For heights larger than 400 m the depositions will be lower than those from 0-100 m emissions.

Table 5.1. Depositions to Norway on 1988-07-22 6UTC as function of release elevation.

Release range (m)	Depositions (Bq)
0-100	2.69E+13
100-200	3.02E+13
200-300	2.84E+13
300-400	2.36E+13
400-500	2.08E+13
500-600	2.04E+13
600-700	2.19E+13
700-800	2.39E+13
800-900	2.45E+13
900-1000	2.32E+13
1000-1100	2.03E+13
1100-1200	1.69E+13
1200-1300	1.40E+13
1300-1400	1.20E+13
1400-1500	1.06E+13
1500-1600	9.59E+12
1600-1700	8.66E+12
1700-1800	7.68E+12
1800-1900	6.60E+12
1900-2000	5.43E+12

Radioactive particles of varying composition and properties have been released from nuclear sources more frequently than usually anticipated (Salbu, 2016). The characteristics of atmospheric transport with different particles types was therefore analyzed with particle sizes from 0.5 µm to 100 µm and particle densities of 1 g/cm^3, 2.1 g/cm^3 and 10.5 g/cm^3, corresponding to activity attached to UO_2-Be and to metal to cover a range of different particles which might be transported after an atmospheric release. The SNAP model was run for the worst case scenario with all activity attached to a particles class and the deposition to Norway calculated. In Figure 5.7 the total deposition to Norway is plotted as a function of various particle sizes and densities. The largest and heaviest particles do not reach Norway, while all particles with 5 µm and below have the same deposition characteristic. For a worst-case analysis of long-range transport, particles of larger sizes will decrease the deposition to remote areas. By not including particles, we might slightly over-estimate the deposition.

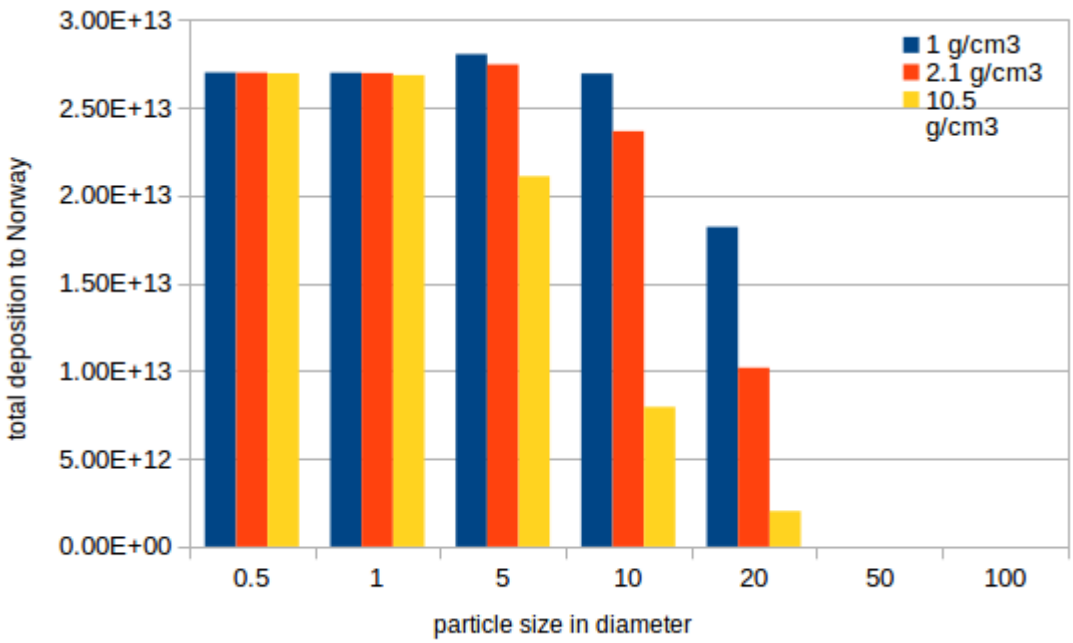

Figure 5.7. Particle size and density dependence of transport in the worst case. Larger and heavier particles will be deposited more locally and will not reach Norway.

6 Considerations regarding dose assessment methodology

6.1 Quantifying impacts to man and the environment

The initial part of this report deals with the processes of physical transport that lead to the advection and dispersion of contaminants in the atmosphere and marine environment following release. The output from these models, in the form of radionuclide activity concentrations in seawater and air (and concomitant deposition to land), provides the basis for subsequent quantifications of impact on humans and the environment.

The standard means of quantifying exposure and interpreting what the estimates mean in terms of an impact or risk of harm involves several steps:

- Analysis of potential exposure pathways
- Derivation of doses (effective doses for people, weighted absorbed doses for plants and animals)
- Contextualisation of the doses in terms of appropriate benchmarks

The ICRP advocate the use of several points of reference in moving from activity to exposure, exposure to dose and dose to effects (or risk of health detriment) for both humans and the environment. The Commission now recommends the use of the 'Representative Person' for the purpose of radiological protection of the public instead of the earlier critical group concept (ICRP, 2007). For protection of the environment the ICRP uses the related concept of Reference Animals and Plants (ICRP, 2008). Much effort has been expended on the selection of suitable representative organisms for Arctic ecosystems as described elsewhere (Brown et al., 2003a). For the methodology adopted here, a somewhat simplified approach was taken that, whilst considering previous analyses, also placed emphasis on there being a reasonable likelihood that kinetic transfer models could be developed for the selected organism(s) and/or the organism being a component of the human diet. The final list ended up as being for marine ecosystems : fish, seal, mollusk and crustacean and for terrestrial ecosystems: shrub/grass, small/burrowing mammal and large mammal.

With regards to exposure pathways for both human and environmental dose assessments there is an immediate requirement to simulate transfer of radionuclides through food-chains. There are commonly adopted standard methodologies used for implementing this based on the application of concentration ratios[19] (or factors), aggregated transfer factors (see IAEA, 2004, IAEA, 2010) but the applicability of such parameters is evidently more suited to either planned exposure situations or conditions existing some time following a release of radioactivity when steady state conditions

[19] The ratio of the radionuclide concentration in the receptor biota (fresh weight) from all exposure pathways (including water, sediment and ingestion/dietary pathways) to that in water/ soil.

are more prevalent. For conditions under which environmental activity concentrations are changing rapidly with time, models that account for the dynamics of the situation are more appropriate (Vives I Batlle et al, 2008). For this reason, marine and terrestrial food-chain models have been applied in the analyses presented in this report. There is a clear commonality in the approach in the sense that the assessment endpoints for the human and environmental assessment are often related. For example, for the environmental impact assessment with fish having been selected as a representative organism the food-chain model should be developed to provide activity concentrations associated with this organism group. As fish form a large component of the diet of some relatively highly exposed human groups, the same data might then be used to derive doses to humans through the application of appropriate dosimetric models. Similar considerations hold for the modelling undertaken for the terrestrial environment.

Clearly, in conducting an assessment, the selection of an appropriate point or region in geographical space is an issue requiring resolution. For humans, this might be the area covered by a fishery (as being a potential source of an ingestion dose) and for environment, this might relate to the location or region wherein a colony of the representative organisms is located at the selected time of year. The issue of spatial averaging has been raised earlier a critical feature relating to the spatial extent of various biota populations (Hosseini et al., 2010).

Information on activity concentrations in seawater have been extracted from the figures pertaining to the marine simulations explained earlier (Section 4.5) allowing estimates of radionuclide activity concentrations with time to be derived at a point or in relation to a defined area. Simulated activity concentration maps have been used along with simplifying assumptions in order to extract information on radionuclide levels in seawater. Highest activity concentrations in each simulated time point have been considered. As these max activities for different time points occur at various locations it was assumed that, the organism under discussion moves along the trajectory of the simulated plume and is thus always exposed to the highest activities. These kinds of assumptions introduce a high degree of conservativism into the resultant exposure estimates.

More details concerning the rationale for the selection of given locations or areas in the various assessment are provided within the more thorough descriptions given below (sections 6.3.1)

Both humans and plants and animals are exposed directly from radionuclides present in a contaminated environment (e.g. from radionuclides in water and soil) and appropriate dose conversion factors (themselves based on detailed dosimetric models) are available for the derivation of exposures from this pathway. Furthermore, for human (but not for environmental) assessments it is common practice to quantify explicitly the contribution of exposure pathways pertaining to inhalation of contaminated air and exposure from the passage of a contaminated plume in the period following an accidental release of radioactivity.

The models and parameters applied for various exposure pathways are outlined below. The radionuclides of interest are selected from knowledge of the source term, i.e. largest amounts released, and the radionuclides' radiological significance. For food-chain modelling, focus was placed upon ^{137}Cs for both terrestrial and marine systems. Earlier studies have shown the importance of ^{137}Cs in relation to ingestion exposure estimates (see Howard et al., 2004 in relation to releases from a hypothetical accident at the Kola nuclear power plant) although other radionuclides may also contribute substantially for given scenarios (NRPA, 2016; Brown et al., 2016a). The reader is referred to the earlier work of NRPA 2016, concerning hypothetical releases from the submarine K-27, where the food-chain transfer and exposures arising from ^{90}Sr for the

terrestrial environment were also considered. Although this previous study considers a different source term the work suggest that in certain cases, ingestion exposures from ^{90}Sr can be commensurate with those associated with ^{137}Cs.

6.2 Modelling transfer of radionuclides through food-chains

For the purpose of deriving activity concentrations in representative plants and animals and for human foodstuffs, food-chain models have been applied. For convenience these have been split into marine (Appendix 4-A) and terrestrial models (Appendix 4-B). The suite of equations describing the systems (as described below) has been constructed within the modelling platform software ECOLEGO-6. ECOLEGO is a simulation software tool that is used for creating dynamic models and performing deterministic and probabilistic simulations. Further details are reported in Avila et al. (2005). The approach follows closely the methodologies adopted in quantifying the impact of hypothetical releases arising from the dumped K-27 nuclear submarine the details of which can be found elsewhere (Brown et al., 2016a; NRPA 2016; Hosseini et al., 2017).

6.3 Modelling doses to humans and the environment

Once activity concentrations are derived models are required to derive dose estimates for both a representative person and representative plants and animals.

6.3.1 Models used for human dose assessment

Standard methodologies were used for the calculation of human exposures (see e.g. IAEA, 2015) from various exposure pathways. The pathways of exposure considered were:

- Ingestion from contaminated foodstuffs
- Inhalation of radionuclides
- Exposure arising from a passing plume of contamination – cloud shine
- Exposure from contaminated soil or shore sediments - ground shine

The total annual effective dose from the ingestion of food, $E_{ing,\ food,\ public}$ (in Sv/a), has been calculated using equation:

$$E_{ing,\ food,\ public} = \sum_k H_B(k) \sum_j \left(C_B(j,k)\, DC_{ing,j}(j)\right) \tag{1}$$

where:

$H_B(k)$ is the rate of human consumption of foodstuff k (in kg/a);
$DC_{ing}(j)$ is the dose coefficient for ingestion of radionuclide j (in Sv/Bq); these values were taken from ICRP publication (ICRP 1995a);
$C_B(j,k)$ is the concentration of radionuclide j in the edible fraction of foodstuff k (in Bq/kg, fresh weight).

The activity concentrations in foodstuffs (for either marine or terrestrial derived products) were obtained via the kinetic models (as described in Appendix 4) and where this was impracticable (e.g. parameters not available for a particular radionuclide) via the use of concentration ratios.

The (annual) effective dose (Sv) to an individual from inhalation of radionuclides from a passing plume, $E_{inh,\ pers}$ (in Sv/a), has been calculated using the equation:

$$E_{inh,pers} = \sum \left[C_{a,time-\mathrm{int}}(j)\, DF_a(j)\, BR_{pers} \right] \quad (2)$$

where:

$DF_a(j)$ is the dose coefficient for inhalation of radionuclide j (in Sv per Bq); from ICRP publication (ICRP 1995b);

$C_{a,\ time\text{-}int}(j)$ is the time integrated concentration of radionuclide j in air (in Bq h/m^3).

The exposure arising from cloud shine has been derived as follows:

$$E_{cs,pers} = \sum \left[C_{a,time-\mathrm{int}}(j)\, DF_{a,cs}(j) \right] \quad (3)$$

where:

$DF_{a,cs}(j)$ is the dose coefficient for cloud shine : (Sv h^{-1} Bq^{-1} m^3);

$C_{a,\ time\text{-}int}(j)$ is the time integrated concentration of radionuclide j in air (in Bq h/m^3).

Finally, the annual effective dose to people from external exposure to radionuclides deposited on soil or sediment/shore line, $E_{ext,\ public}$ (in Sv/a), was calculated using the equation

$$E_{ext,pers} = t_{pers} \sum \left[C_s(j)\, DF_{gr}(j) \right] \quad (4)$$

where:

t_{pers} is the time spent by person in contact with the contaminated soil/shore-sediment in a year (in h);

$DF_{gr}(j)$ is the dose coefficient for ground contamination of radionuclide j (in Sv/h per Bq/m^2);

$C_S(j)$ is the surface contamination of radionuclide j in the shore sediments/ on soil (in Bq/m^2).

6.3.1.1. Parametrisation of the human dose assessment models

The human dose assessment has been spilt into 2 main parts – the first relating to the local region in proximity to the K-159 sinking site and the second for Norwegian territory.

I. Kola Peninsula – representative person

It has been assumed that ingestion of marine products constitutes the dominant exposure pathway. In earlier work and in this regard, IASAP (International Arctic Seas Assessment Project) considered a representative of the average local Russian population (using local marine food products). This group was located on the Kola Peninsula. The dietary habits postulated for these populations were:

- Sea fish, 50 kg/a (assumed caught in the Barents Sea)
- Molluscs, 0.5 kg/a
- Crustaceans, 1 kg/a

The same dietary data has been used for the calculations presented in this report.

The activity concentrations of ^{137}Cs in marine biota have been derived using the marine food chain models described in Appendix 4-A using time series radionuclide activity concentrations in seawater as described above.

II. European/Norwegian assessment

II. a. Marine - representative person: high rate consumers of seafood

Standard calculation methods are used as presented above. The EFSA (European Food Safety Authority) Comprehensive European Food Consumption Database has been used as a source of dietary information.

It is still necessary to consider a representative person in Norway. Pragmatically this may be considered to be a high percentile (e.g. 99th percentile) consumer from the statistics based on the entire country. Consumption rates were provided for fish and seafood of 63 g/d and 250 g/d for an average person and person in the 99th percentile, respectively (Hosseini et al., 2017).

Since no differentiation is made between fish and seafood in the source data for the dietary information, the activity concentrations from the former category has been used in all dose calculations. The activity concentrations in seafood have been obtained via the kinetic models described in Appendix 4-A and where this was not possible (e.g. parameters not available for a particular radionuclide) via the use of concentration ratios.

In view of uncertainty regarding where the fish have been prior to capture, a conservative assumption was made that the fish caught were in a small area commensurate with the max concentration areas along the movement of the plume. The time series data for activity concentration in seawater for this area from 3 dimensional hydrodynamic modelling (see Section 4.5) has been taken as input to food-chain transfer models. The output from the modelling work is activity concentrations in fish with time. For the sake of conservatism the maximum value from this data series was used.

II. b. Terrestrial - representative person: consumers of natural products in high deposition areas in Finnmark exposed to initial plume and deposition

For the sake of conservatism the maximum values from model simulations (see Section 5.4) for the time integrated activity concentrations of radionuclides in air over Norwegian territory (in Finnmark) were used for inhalation and cloud shine dose estimates applying the equations given above (Equations 2 and 3).

Exposure from contaminated soil has been derived using the maximum deposition levels of radionuclides in Finnmark County. For this, it was conservatively assumed that a person is found in continual contact with contaminated soil over a 1 year period. The reality, even in the absence of orders to shelter or evacuate, would be that individuals are shielded from ground contamination for prolonged periods as people spend a great deal of time indoors.

Finally, ingestion doses for people have been derived using various assumptions concerning diet.

The kinetic model described in Appendix 4-B was used where possible to derive activity concentrations in various foodstuffs. The maximum deposition levels of radionuclides in Finnmark

County have been used as input to the model and appropriate activity concentration from the time series data generated in this process are then used for subsequent ingestion dose calculations.

Dietary surveys have been carried out in the Kautokeino area of Finnmark in 1999 and 2002 (Thørring et al., 2004). The survey included those foodstuffs that were believed to contribute the highest proportions to ^{137}Cs body burdens. The most recent (i.e. from 2002) ingestion rates for individual based questionnaires as oppose to household consumption data have been used because the former are believed to more closely reflect the actual amounts of food ingested by people. The information is summarized in Table 6.1. The average consumption rate has been selected as oppose to the 99th percentile (as adopted for the marine foodstuffs dose calculations) because the tabulated data already pertain to high rate consumers (or a critical group) and as such do not require the selection of an upper percentile ingestion value.

Table 6.1. Consumption of various foodstuffs per individual adult (g/d) (Thørring et al., 2004).

Foodstuff	**Average**	**Range**
Reindeer	89	1.1 – 330
Game meat	12	0 – 120
Berries	34	1.5 – 140

With regards to fruit from semi natural systems, harvesting will depend on the type of berry but for some species, such as Cloud berry (*Rubus chamaemorus*) harvesting can start as early as July. By the end of September, the main berry picking season will be over for most species. For the sake of the human ingestion dose assessment there is no requirement to model the change in activity concentration with time beyond that point. The input to the dose calculations was taken as the integrated (or strictly speaking, average) activity concentration in berries in the 2 months following the initial deposition event.

Finally, considerations for reindeer (*Rangifer tarandus*) were required. During the autumn season (September - December) in Finnmark, reindeer are slaughtered for sale and to some degree for domestic consumption. To avoid the requirement to develop a more sophisticated model to account for a change in the reindeers' diet as the seasons change, the simulation was truncated after 3 months. The activity concentration at 3 months (when the levels in reindeer meat attained a maximum) were selected as input for the human dose assessment. This might be considered a rather conservative approach in the sense that only the highest available values have been used but in fact such an evaluation is not entirely unambiguous. Following the Chernobyl accident, activity concentrations in reindeer in parts of Scandinavia were seen to increase in the winter months (Åhman, 2007), no doubt reflecting the change in diet of reindeer from one dominated by grass to one dominated by lichen. Although the simulation as set up will partly capture the influence of the ingestion of contaminated lichen on reindeer radiocaesium body burdens, there is no guarantee that the model prognoses will capture the extreme levels that could feasibly occur in the event of an accident.

6.3.2 Models used for environmental impact assessment

The methodology that was used in parallel for terrestrial and aquatic ecosystems was based around the ERICA Integrated Approach (Larsson, 2008).The approach was designed to provide guidance on

impacts of radioactivity on the environment to ensure that decisions on environmental issues give appropriate weight to the exposure, effects and risks from ionising radiation. Emphasis was placed on protecting the structure and function of ecosystems from radionuclides (Larsson, 2008), and supporting software (the ERICA Tool) was developed to serve this purpose (Brown et al., 2008).

Once activity concentrations in environmental media and biota have been collated and calculated, dose rates were derived through application of the ERICA Tool.

The basic underlying equations (Equations 5 and 6) utilise activity concentration data in order to derive internal (D_{int}) and external (D_{ext}) absorbed dose rates (in units of µGy h^{-1}). The total absorbed dose rate is the sum of these components, through the application of dose conversion coefficients (DCCs).

$$\dot{D}^{b}_{\text{int}} = \sum_{i} C^{b}_{i} * DCC^{b}_{\text{int},i} \qquad (5)$$

where:

C^{b}_{i} is the average concentration of radionuclide *i* in the reference organism *b* (Bq kg^{-1} fresh weight),

$\mathrm{DCC}^{\mathrm{b}}_{\mathrm{int},i}$ is the radionuclide-specific dose conversion coefficient (DCC) for internal exposure defined as the ratio between the average activity concentration of radionuclide *i* in the organism *j* and the dose rate to the organism b (µGy h^{-1} per Bq kg^{-1} fresh weight).

$$\dot{D}^{b}_{ext} = \sum_{z} v_{z} \sum_{i} C^{ref}_{zi} * DCC^{b}_{ext,zi} \qquad (6)$$

where:

v_z is the occupancy factor, i.e. fraction of the time that the organism *b* spends at a specified position *z* in its habitat.

C_{zi}^{ref} is the average concentration of radionuclide *i* in the reference media of a given location *z* (Bq kg^{-1} fresh weight or dry weight (soil or sediment) or Bq l^{-1} (water)),

$DCC^{j}_{ext,zi}$ is the dose conversion coefficient for external exposure defined as the ratio between the average activity concentration of radionuclide *i* in the reference media corresponding to the location *z* and the dose rate to organism *b* (µGy h^{-1} per Bq kg^{-1} fresh weight or Bq l^{-1}).

The DCCs used correspond to those reported in ICRP (2008). Occupancy factors for organisms have been selected such that they might characterise a simplified yet realistic exposure geometry (Table 6.2).

Table 6.2. Summarised source target exposure geometry for selected organisms

Organism	**Exposure geometry assumption**
Rat/burrowing mammal	In soil, volumetric source
Deer/herbivorous mammal	On soil, volumetric source

Weighted total dose rates (in µGy h^{-1}) are derived through the application of weighting factors (dimensionless) for alpha, low beta and high beta-gamma radiation (Equations 7 and 8).

$$DCC_{int} = wf_{low\beta} \cdot DCC_{int,low\beta} + wf_{\beta+\gamma} \cdot DCC_{int\beta+\gamma} + wf_{\alpha} \cdot DCC_{int,\alpha} \quad (7)$$

$$DCC_{ext} = wf_{low\beta} \cdot DCC_{ext,low\beta} + wf_{\beta+\gamma} \cdot DCC_{ext,\beta+\gamma} \quad (8)$$

where:

wf = weighting factors for various components of radiation (low β, β + γ and α)

DCC = dose conversion coefficients in μGyh^{-1} per Bq l^{-1} or Bq kg^{-1}

Default radiation weighting factors of 10 for alpha radiation and 1 for beta and gamma radiation are applied in this assessment in line with those applied in UNSCEAR (2008).

The dosimetric calculation underpinning the derivation of DCCs is dealt with in detail elsewhere (Ulanovsky and Pröhl, 2006; Ulavnovsky et al., 2008). Radioactive progeny are included in the DCCs of their parent if their half-lives are shorter than 10 days. DCCs for internal exposure were derived assuming a homogeneous distribution of the radionuclide in the organism; the error introduced by this assumption is, in view of the assessment goals, considered to be of minor significance (Gómez-Ros et al., 2008).

No specific information was required with regards to detailed parametrisation of the environmental dose models applied, i.e. no bespoke geometries or occupancy factors were applied with reliance placed only on default dosimetric parameters available in the ERICA Tool (Brown et al., 2016b). For the terrestrial food-chain models the locations of maximum deposition were selected as input for the subsequent dose calculations.

For the marine system, activity concentrations of ^{137}Cs in seawater (both at the bottom and the surface) and biota were selected for an area encompassing the most elevated levels associated with the main plume of contamination for the release scenarios.

6.4 Contextualising impacts to humans and the environment

6.4.1 Humans

One way of contextualizing potential impact to humans is through direct comparison of predicted activity concentrations in foodstuffs with corresponding levels derived from various pertinent, e.g. radiological, criteria. For example, in a study exploring the potential impact of releases from the sunken submarine K-159 and the Komsomolets in Arctic seas, Heldal et al. (2013) used the intervention level of 600 Bq/kg fw, as currently applied by Norwegian authorities, to contextualize activity concentration data derived for commercial fish species.

By considering cod and capelin abundance data, the authors were also able to define the % of a given population (in the Barents Sea) which exceeded a level of 0.2 Bq/kg ^{137}Cs commensurate with the current contamination level in cod in the Norwegian and Barents Seas. In a conceptually similar approach, Thørring et al. (2010) considered impacts to the Norwegian environment following a hypothetical release to air from the Sellafield plant in the UK by utilising information from atmospheric advection-dispersion and deposition models and linking this with data on transfer to the food chains and statistics on production and hunting to assess the 'consequences for foodstuffs'. Through comparison with food intervention levels as applied by Norwegian authorities

it was then possible to identify areas for animal production where intervention would then be necessary accounting for a range in (empirically derived) transfer factors. Although these aforementioned approaches have clear practical merit and as such might have been suitably adopted for the current analysis, a decision was made not to focus on criteria based on foodstuffs as a sole indication of radiological significance. The reasons for this decision are elaborated elsewhere (see NRPA 2016).

Kocher (1987) introduced the concept of a *de minimis* dose defining a level below which control of radiation exposures would be deliberately and specifically curtailed. Such a dose would need to be set well below established limits on acceptable dose from all sources of exposure and, furthermore, be below any established dose limit for specific practices. In the context of setting criteria to allow or forbid the dumping of radioactive material at sea, the IAEA (1999, 2015) have used a *de minimis* dose of 10 µSv per annum. This effective dose (in tandem with a defined collective effective dose) to a representative person would allow a practice to be exempted from further regulatory consideration. Although not strictly applicable because of its development specifically for the London Convention, the *de minimis* level specified above provides a robust indication of what might be widely considered to be a trivial radiation dose and as such provides an appropriate benchmark with which the doses calculated in this assessment might be compared.

For emergency (and existing) exposure situations, the source-related restriction recommended by the ICRP is termed a “reference level” (ICRP, 2007). The concept of a reference level is used in the process of optimisation of protection to assist in ensuring that all exposures are kept as low as reasonably achievable, societal and economic factors being taken into account.

The ICRP are quick to emphasise that reference levels do not represent a demarcation between ‘safe’ and ‘dangerous’ or reflect a step change in the associated health risk for individuals. Nonetheless, the recommended levels may be used in the current assessment as (essentially an upper-bound) benchmark with which to contextualize calculated committed effective doses to humans.

In emergency or existing controllable exposure situations, the reference levels represent the level of dose or risk, above which it is judged to be inappropriate to plan to allow exposures to occur, and for which therefore protective actions should be planned and optimised. At doses higher than 100 mSv, there is an increased likelihood of deterministic effects and a significant risk of cancer. For these reasons, the ICRP considers that the maximum value for a reference level is 100 mSv incurred either acutely or in a year. The ICRP set a reference level band of 20 to 100 mSv set for the highest planned residual dose from a radiological emergency.

6.4.2 Environment

Although in a strict sense there are activity concentration based criteria available with which to contextualize the impact of given levels of radionuclides in seawater or soil, in the form of Environmental Media concentration Limits (see Brown et al., 2008), the standard methodology for making inferences about potential environmental effects involves the application of dose-based criteria.

The ICRP (ICRP, 2008) recommend the application of a set of derived consideration reference levels (DCRLs) for particular categories of Reference Plants and animals (Figure 6.1). These are defined

(see ICRP, 2009) as "A band of dose rate within which there is likely to be some chance of deleterious effects of ionising radiation occurring to individuals of that type of Reference Animal or Plant (derived from a knowledge of defined expected biological effects for that type of organism) that, when considered together with other relevant information, can be used as a point of reference to optimise the level of effort expended on environmental protection, dependent upon the overall management objectives and the relevant exposure situation."

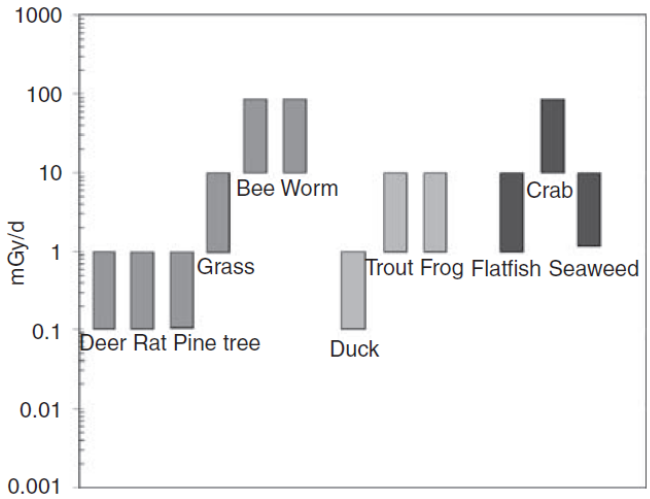

Figure 6.1. Derived Consideration Reference Levels (DCRLs) for environmental protection for each Reference Animal or Plant (RAP), the RAPs being grouped according to their terrestrial, freshwater, or marine habitat. Reproduced from ICRP (2014).

In the recent report ICRP-124 (ICRP, 2014), the Commission has begun to elaborate on the application of these criteria under cases other than planned exposure situations (for which the original criteria were developed). For existing emergency exposure situations where control of the source has not been obtained, if the dose rates are above the relevant DCRL band, the ICRP recommends that the aim should be to reduce exposures to levels that are within the DCRL bands for the relevant populations, with full consideration of the radiological and non-radiological consequences of so doing. If dose rates are within the bands, the ICRP recommends that consideration should be given to reduce exposures, assuming that the costs and benefits are such that further efforts are warranted.

7 Estimated activity concentrations and doses

It is important to note that the ^{137}Cs activity concentrations in plants and animals derived for the given scenarios would be in addition to the levels already present in the environment from various historical sources of contamination. For the locations of interest in these studies, the primary sources of "background" ^{137}Cs contamination can be attributed to the global fallout arising from atmospheric weapons testing (primarily in the 1950s and early 1960s), the Chernobyl accident (to a much lesser extent) and, for the marine environment, releases from western European reprocessing plants (AMAP, 1998).

As already mentioned (see section 3.2.2) in case of an accident, there will be two main radionuclides that contribute to contamination of the environment in the longer term, i.e. years following a hypothetical accident, these being ^{137}Cs and ^{90}Sr. In the following, only ^{137}Cs will be discussed. However, ^{90}Sr has been considered elsewhere in the context of releases from a related source (the dumped submarine K-27) as described by NRPA 2016. The results from that work provide insights into the fate and deposition of ^{90}Sr, to terrestrial systems, for selected hypothetical releases from Gremikha that in turn offer insights into the relative importance of this radionuclide, in terms of impacts, pertinent for the current analysis.

7.1 Terrestrial ecosystem

The dynamics of ^{137}Cs activity concentrations in terrestrial biota (Shrubs, small mammal and deer), at the location of maximum deposition in Finnmark, following releases from the "docking" accident scenario, are presented in Figure 7.1.

Activity concentrations in vegetation (shrubs and grass) are simulated to fall quite rapidly from levels exceeding 2000 Bq kg^{-1} f.w. ^{137}Cs in the initial days after deposition to levels below 10 Bq kg^{-1} f.w. ^{137}Cs when the time elapsed approaches 100 days. This period would correspond to mid-November by which time many areas in Finnmark could conceivably be covered in snow and temperatures could be sub-zero. The dynamic model has not been parameterised for these conditions. Nonetheless, processes dominated by the rapid loss of radionuclides, reflecting substantial wash-off of contaminants from shrubs and grass, is expected to transition towards processes characterised by steady-state but lower transfer to vegetation in the long term. This occurs as root uptake and translocation become more dominant processes, months and years after the fallout event, than interception and surficial retention.

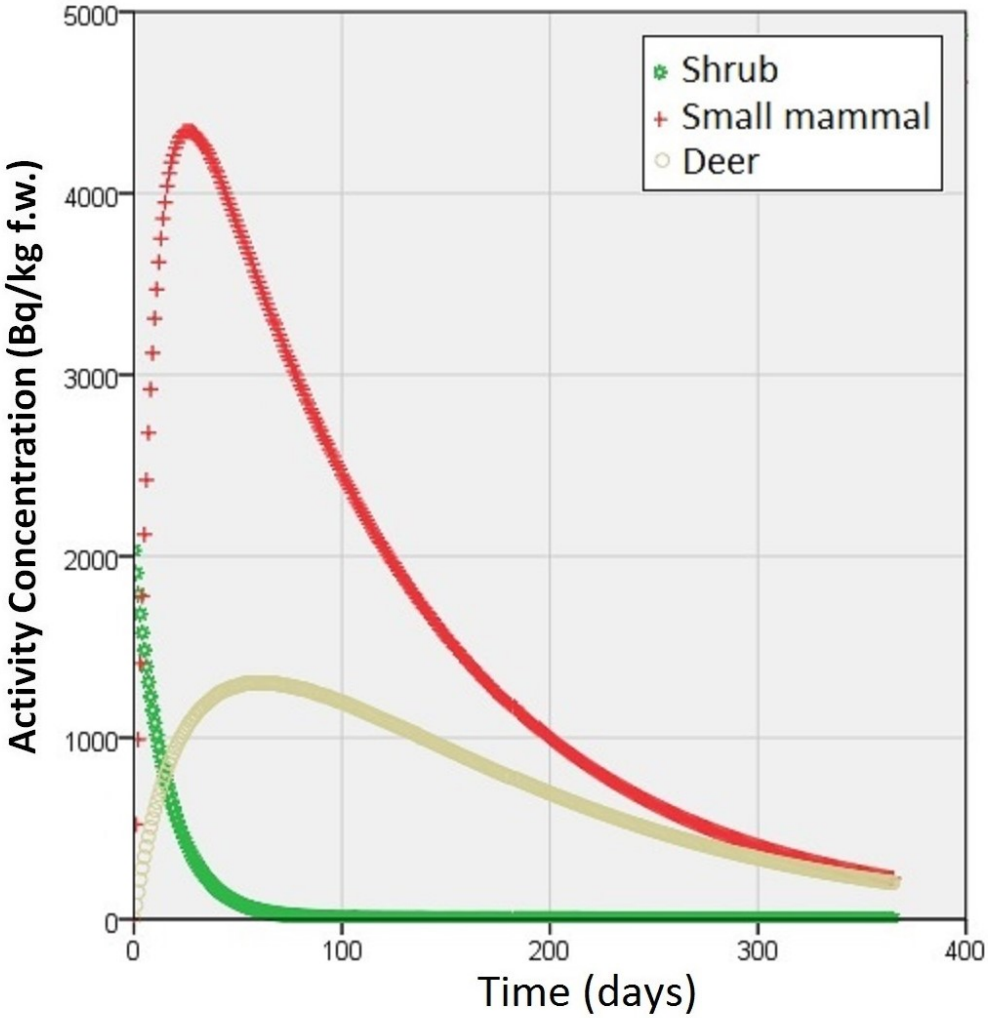

Figure 7.1. Activity concentrations (Bq/kg f.w.) of ^{137}Cs in shrub (including Vaccinium spp.), small burrowing mammal (including game animals) and Deer (as exemplified by Reindeer) for the area of maximum deposition in Finnmark for the "docking" scenario.

As considered for vegetation, the output ^{137}Cs activity in small (burrowing) mammals (taken to include game animals), post 2-3 months, needs to be appraised with due caution because the model was not configured to account for changing environmental conditions (such as snowfall) with the seasons. However, the prognoses for the first months are considered to be robust in the sense of providing reasonable conservatism. The activity concentrations of ^{137}Cs are simulated to increase following the initial deposition event with ^{137}Cs attaining a maximum activity concentration of ca. 4340 Bq kg^{-1} f.w. towards the end of the first month following deposition before falling moderately rapidly to a level slightly in excess of 2450 Bq kg^{-1} f.w. by 100 days.

The kinetics of ^{137}Cs in deer-reindeer, unsurprisingly, follow a similar pattern to those observed for small mammals with regards to an observed build up of activity with time following the initial deposition event. However, the biological half-lives characterising the retention of ^{137}Cs in the whole body of deer are protracted compared to the much smaller burrowing mammal. This simply reflects the employment of allometric relationships in the derivation of biological half-lives for model parameterisation – the larger the animal, the longer the biological half-life. The activity concentration of ^{137}Cs in deer attain a maximum of ca. 1300 Bq kg^{-1} f.w. some 2 months following

the initial fallout event. In the case of reindeer, the diet and the biological half-lives (for radiocaesium and by proxy conceivably for other radionuclides) are known to vary throughout the year (Åhman, 2007) but these considerations are not accounted for in the model. Further consideration regarding this point are provided in NRPA 2016 where comparisons between the model of (Åhman, 2007) and the model applied in the present study, for the same release levels (but pertaining to a different source, i.e. K-27) have demonstrated reasonable congruence in output for the initial (several months) period following deposition. An interesting feature of Åhman's model is the closeness with which the observed high amplitude sinusoidal form of ^{137}Cs levels in reindeer can be simulated by accounting for factors such as the animal's changing diet and metabolism over the season. Although ^{137}Cs activity concentrations might be expected to fall quite rapidly after the initial peak, as predicted in the simplified model applied in the current study, it is quite evident that new peak activities, coinciding with subsequent winter periods, might be expected as discussed by NRPA 2016. These subsequent peaks with quite elevated activity concentrations, for the first few years at least, might also be expected to fall at levels that are not dramatically lower than the initial maximum.

The activity levels for small burrowing mammals and deer can be compared to the current relevant Norwegian intervention level of 3000 Bq kg^{-1} f.w for radiocaesium applicable to, *inter alia*, reindeer and game (Thørring et al., 2010). Clearly the maximum ^{137}Cs activity concentrations in game are in excess and those for reindeer are of the same order of magnitude as the intervention level. The introduction of restrictions on the consumption of such foodstuffs would therefore be likely, potentially involving various measures such as the dissemination of dietary advice and, for reindeer at least, the use of live monitoring before slaughtering. Although the simulations suggest a fairly rapid decline in ^{137}Cs activity concentrations within the first year, the uncertainty associated with the longer term predictions would precipitate the need for careful monitoring of the situation. In other words, model prognoses of this type could not be used in isolation to predict for how long any introduced restrictions would need to be retained. Similarly for shrubs (used as a proxy for berries) restrictions on fruit consumption might foreseeably need to be introduced, at least in the first harvesting season. The highest predicted levels are substantially above the Norwegian intervention level for basic foodstuffs of 600 Bq kg^{-1} f.w for radiocaesium (Liland et al.,2009; Thørring et al., 2010).

As noted in a general sense above, the predicted ^{137}Cs activity concentrations in reindeer in Finnmark, for the given scenario, would occur in addition to elevated levels that continue to persist from global fallout. As of 2005, average activity concentrations of ^{137}Cs were still in the region of 100 Bq kg^{-1} (Thørring and Skuterud, 2012). Even accounting for (the long-term component) of an effective half-life of approximately 11 years for Kautokeino reindeer meat (IAEA, 2010), this would mean the "background activity" would still be at a level of ca. 50 Bq kg^{-1}. The additional ^{137}Cs activity concentration arising from inputs attributable to the hypothetical scenario would therefore be very distinctive, dwarfing any signal from historical contamination events.

7.2 Marine ecosystem

Surface activity concentrations of ^{137}Cs in seawater, fish, seal and seabird are presented in Figure 7.2 for an area encompassing the most elevated levels associated with the main plume of contamination for the "lifting" accidental release scenario.

The pulsed nature of activity concentrations of ^{137}Cs in seawater are quite evident with maximum activity concentration of ca. 100 Bq/l occurring within the first 5 days of simulation. The levels are then predicted to decrease rapidly to levels around 10 Bq/l once a period of 10 days has elapsed and around 1 Bq/l once a period of 20 days has elapsed. For sake of comparison, Heldal et al. (2013), using a 3D numerical ocean model, predicted maximum (essentially depth averaged) levels of around 0.5 Bq/l ^{137}Cs in seawater for a 5.2 PBq instantaneous input (compared to our input of 50 TBq) from the K-159 submarine. Nonetheless, it is important to note that the maximum reported by Heldal et al. (2013) appears to pertain to a time point some 6 months following the initial release that may largely explain the substantial differences in model predictions. The seawater ^{137}Cs activity concentrations for the selected area used in our analyses have fallen substantially below 1 Bq/l by this time.

Maximum activity concentrations simulated to occur in fish, seal and seabird, in contrast to those for seawater, build up slowly with maximum ^{137}Cs levels attained at approximately 20 days for fish, 70 days for seal and 60 days for seabirds (Figure 7.2). The maximum ^{137}Cs activity concentrations in biota were ca. 440, 850 and 2490 Bq kg^{-1} (f.w.) for fish, seal and seabird respectively. These levels are above, in the case of seal and seabird, and only slightly below, in the case of fish, the intervention level of 600 Bq kg^{-1} applied for basic foodstuffs in Norway (Liland et al., 2009). Furthermore, the predicted ^{137}Cs activity concentrations in fish, are substantially above the Japanese regulation value of 100 Bq kg^{-1} (fresh weight) for sale and human consumption that was applied following the accident at Fukushima Daiichi (Buesseler, 2012). The potential requirement for restrictions on the consumption of sea products cannot be dismissed. In line with the Antipov et al. (2015), restrictions, at least in the short term, could plausibly be required. These might involve, for example, the introduction of fishing bans over certain marine areas.

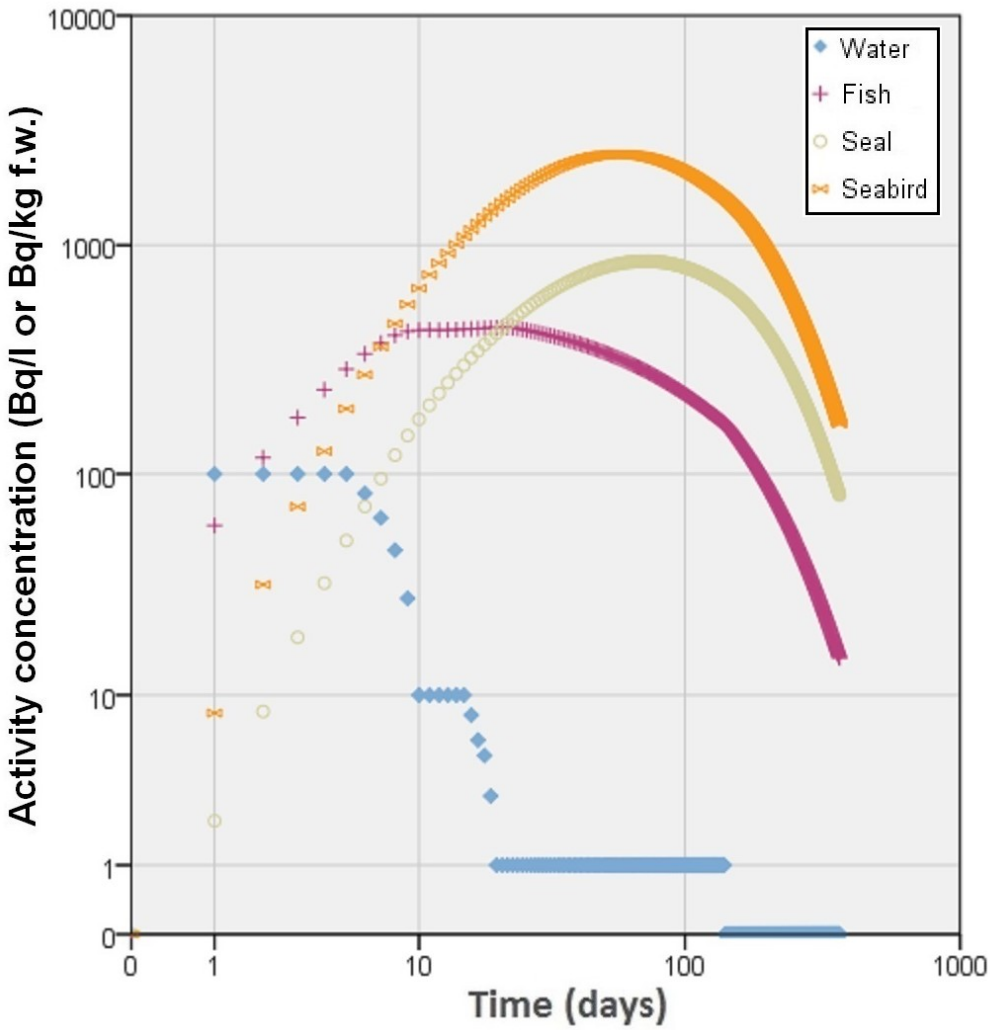

Figure 7.2. Surface activity concentrations of ^{137}Cs in sea water (Bq/l), fish, seal and seabird (Bq kg^{-1} f.w.) based on releases to the marine environment for the "lifting" scenario.

For releases related to the 'in situ' scenario, i.e. as a result of degradation of fuel integrity, releases at the bottom of the seawater column have been considered. As such releases could hypothetically occur at any time, we have looked at releases both in summer and in winter. Through comparison of activities in biota, it was found that releases occurring in summer would result in slightly higher activities in biota. To be in line with our conservative approach, decision was made to use activities in water for releases at the sea bottom in the summer time. Resulting radionuclide activities in bottom water, fish, molluscs and crustaceans are shown in. Figure 7.3.

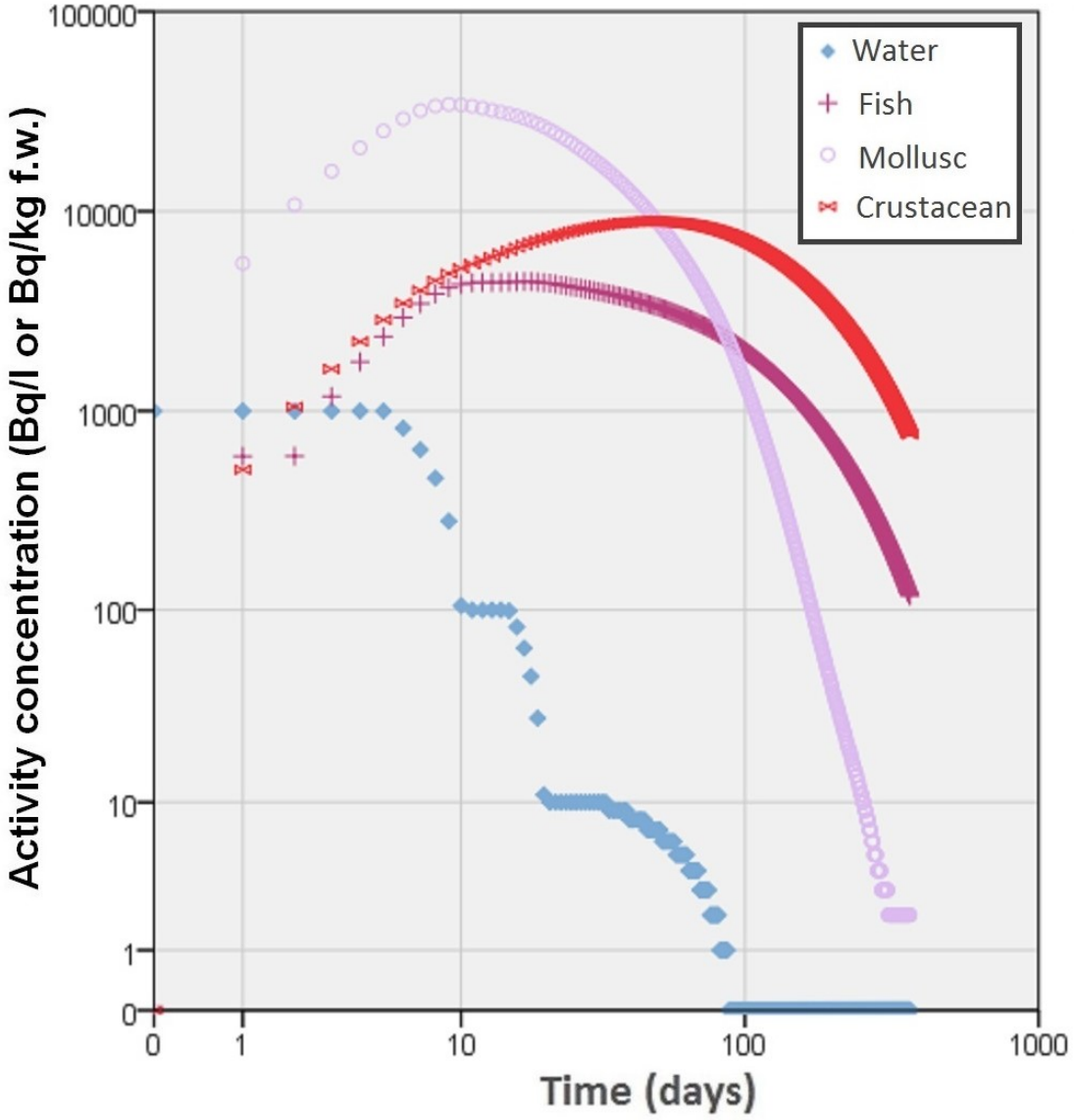

Figure 7.3. Activity concentrations of ^{137}Cs in bottom sea water (Bq/l), fish, mollusc and crustacean (Bq kg^{-1} f.w.) based on releases to the marine environment for the "in situ" scenario.

Maximum activity concentrations in biota actually occur in mollusc attaining levels exceeding 34 kBq kg^{-1} ^{137}Cs within the first 10 days following the release. By comparison, maximum activity concentrations of ^{137}Cs are predicted to be 8.9 kBq kg^{-1} in crustaceans (at around 50 days) and 4.4 kBq kg^{-1} in fish (at around 18 days). The levels of ^{137}Cs fall quite substantially with time for all biota categories although activity concentration are predicted to remain above 1 kBq kg^{-1} in crustaceans even following an elapsed time of 300 days. The relatively elevated levels in benthic biota compared to the lifting scenario involving surface releases leads to the potential for many hypothetical marine foodstuffs to be above the relevant national intervention level for extended periods. There seems no doubts that restrictions (on fishing/harvesting of shellfish etc,) would need to be applied should radionuclide releases of the magnitude considered in the 'in situ' scenario occur.

7.3 Human dose estimates

The estimated annual effective doses for individuals in identified population group in Norway who could be affected by releases following a potential accident at the Nerpa Shipyard are shown in Table 7.1. The table also includes annual effective dose estimate for the average local Russian population living on the Kola Peninsula.

Table 7.1. Estimated effective doses to human for various pathways based on releases to atmosphere and the marine environment at Barents Sea.

Release type	***Pathway***	***Effective dose (mSv)***	***Comments***
Atmospheric	Inhalation	1.4E-04	Individuals in identified population group in Norway
	Cloud shine	2.9E-06	
	Ground shine	3.3E-02*	
	Ingestion (*terrestrial food*)	8.9E-01*	
Surface release	Ingestion of fish	5.2E-01*	Individuals in identified population group in Norway, high rate consumers of fish
Bottom release	Ingestion of seafood	3.2E+00*	Average local Russian population sited on the Kola Peninsula

** Annual effective dose.*

Two representative groups can be considered in Table 7.1, one being a group living inland (assumed to be exposed via inhalation, cloud shine, ground shine and ingestion of local terrestrial foods) exposure pathways and the other constituted by a group of high rate consumers of fish. The high rate fish consumers, of course, might hypothetically be exposed via other pathways, but the assumption is made that the relative exposure levels would be small compared to the terrestrial group.

The doses to a representative person in Finnmark, Norway would be dominated by the ingestion pathway. This is congruent with the findings of the analysis performed for the K-27 submarine following a salvaging operation where a scenario at Gremhika involving fire led to the conclusion that in the longer term (over the first year), ingestion from foodstuffs would constitute the dominant exposure pathway. Internal doses from terrestrial food products are somewhat higher than the internal doses associated with a high rate fish consumer living in Norway. The doses are far above the *de minimus* level and would therefore certainly not be categorized as being trivial.

The hypothetical doses calculated for critical groups in Norway are only slightly below 1 mSv but would not constitute a level of exposure where concerns would be extreme[20]. The doses fall within the ICRP's reference band below 1 mSv where a requirement for significant intervention would not be deemed appropriate. There is a distinct contrast with Russian 'critical group' populations on the Kola Peninsula where hypothetical doses could exceed 3 mSv. The doses fall within the ICRP's reference band below 1-20 mSv where a requirement for general information should be made available to enable individuals to reduce their doses.

As described above (Sections 7.1 and 7.2)**,** interventions in the form of food restrictions would be plausibly driven by activity concentration based intervention levels. The predicted activity concentrations for foodstuffs in both the terrestrial and marine environments are at such a level that restrictions would need to be introduced over at least the short term. Nonetheless, this rather pessimistic prediction should be tempered by the consideration that the prognoses being made here are highly conservative. Efforts have been made to err undoubtedly on the side of caution in making the hypothetical predictions given above.

7.4 Dose estimation for non-human biota

7.4.1 Terrestrial

Dose rates to vegetation (shrub and grass), small burrowing mammals (considered to also characterise game animals harvested by hunting) and deer/reindeer are presented in Figure 7.4 for the 'docking' release scenario. The highest exposures were calculated for small mammals with maximum dose rates in excess of 0.7 µGy/h and accumulated doses for a 90 days period of 1.3 mGy. The dose rates fall substantially over the simulation period of one year reflecting the rapid fall of radiocaesium in the small mammals assumed diet and the short biological half-life of ^{137}Cs- in the animal. External irradiation of the animal from ground deposition of ^{137}Cs is small in comparison to the dose arising from internal contamination. The dose-rates predicted for deer/reindeer in the earliest period of the accident are lower than those for small mammals with maximum dose rates slightly below 0.5 µGy/h and accumulated doses for a 90-day period of approximately 0.8 mGy. The maximum dose rates for deer/reindeer occur slightly later, at around 60 days, than those simulated for small mammals.

The dose-rates for shrub decrease rapidly from a dose rate slightly in excess of 0.3 µGy/h, coinciding with the initial deposition event, to less than 0.1 µGy/h within the first 20 days of simulation. The accumulated dose in the first month following the hypothetical release is a relatively low 0.1 mGy.

[20] According to the Nordic Flag Book (NFB, 2014), the dose criteria for operational intervention level for an internal dose via inhalation is a projected dose of 10 mSv in two days.

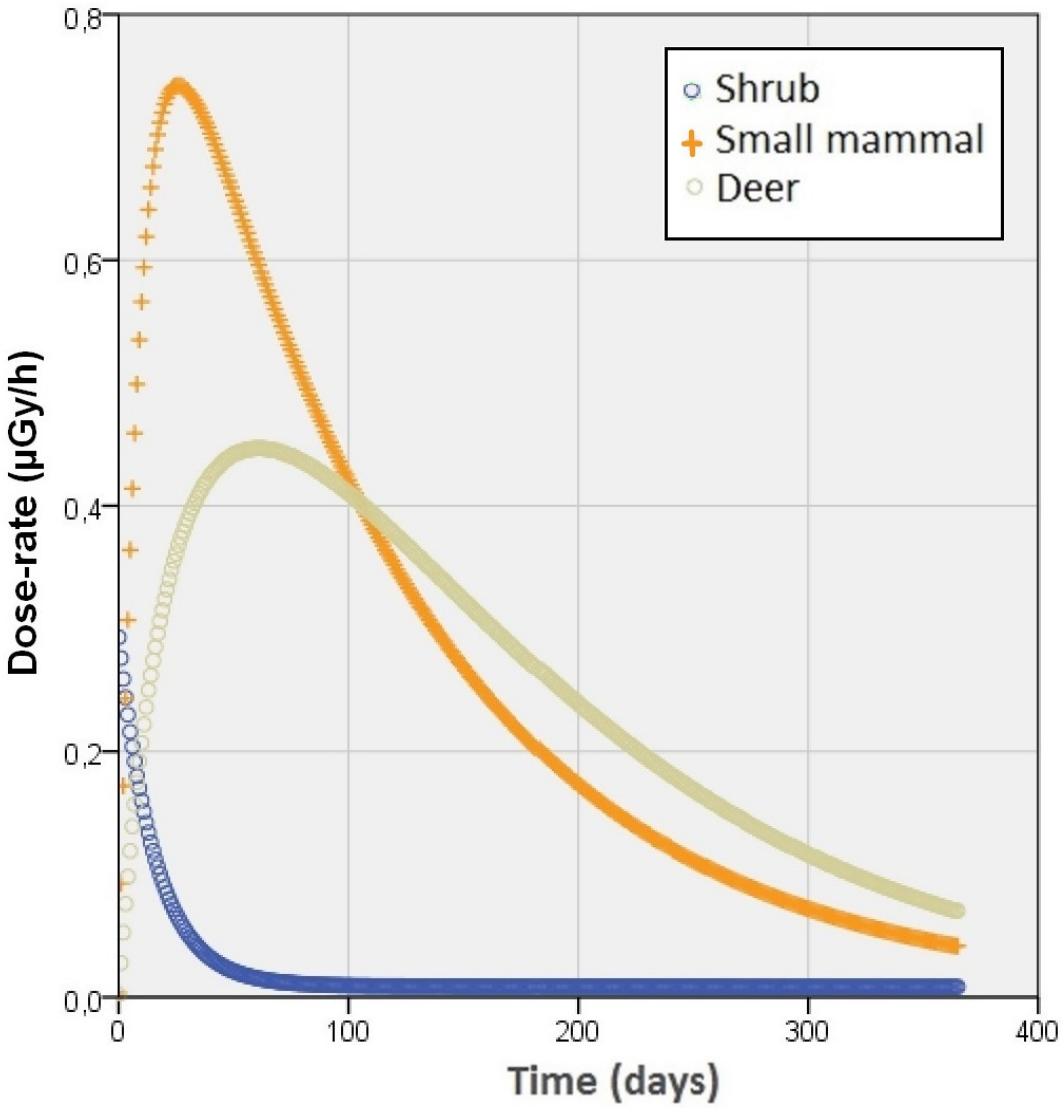

Figure 7.4. Dose-rate (µGy/h) for Shrub (and other vegetation such as grass), small (burrowing) mammal, and Deer (as exemplified by Reindeer) for the area of maximum deposition in Finnmark for the docking release scenario.

To place the exposures into some kind of context, typical background dose rates (from terrestrial primordial radionuclides and excluding inhalation doses from ^{222}Rn) for terrestrial organisms have been reported in the range 0.07 to 0.6 µGy/h (Beresford et al., 2008a).

Dose rates were far below the levels where even sub-lethal effects such as impairment of reproductive capacity or scoreable cytogenetic damage might be observed. Although strictly speaking accumulated doses are more appropriate to consider in the aftermath of an accident (see Strand et al., 2014), for sake of comparison, the lower end of DCRL bands are attributed by the ICRP (ICRP, 2008) to 0.1 mGy/d (or ca. 4µGy/h) for (Pine) tree, and the mammals - Deer and Rat. At dose rates below this level, the likelihood of observing radiation-induced effects would be considered to be vanishingly small. The dose-rates generated for the given scenarios fell, even at maximum exposure levels, substantially below this benchmark and would, therefore, be considered insignificant in terms of their potential impacts on wild organisms.

7.4.2 *Marine*

The dose rates for fish and seal predicted to arise from the lifting release scenario using surface activity concentration in seawater are presented in Figure 7.5. The total dose rates essentially reflect the activity concentrations of ^{137}Cs in the organisms, per se, as oppose to ambient seawater concentrations with >99 % dose-rate attributable to internal body burdens of radioaceasium at times after 1 month. The maximum dose rates calculated were slightly below 0.1 µGy/h for fish, slightly below 0.3 µGy/h for seal and slightly below 0.5 µGy/h for seabird. These values are commensurate with the unweighted absorbed dose rates derived as being characteristic of marine reference animals and plants (flatfish, crab and seaweed) exposed to naturally occurring primordial radionuclides (Hosseini et al., 2010). The accumulated doses (90 days) of slightly above 0.1, slightly below 0.5 and ca. 0.8 mGy have been derived for fish, seal and seabird respectively. These are low doses falling substantially below levels where any types of effect on organisms might be expected.

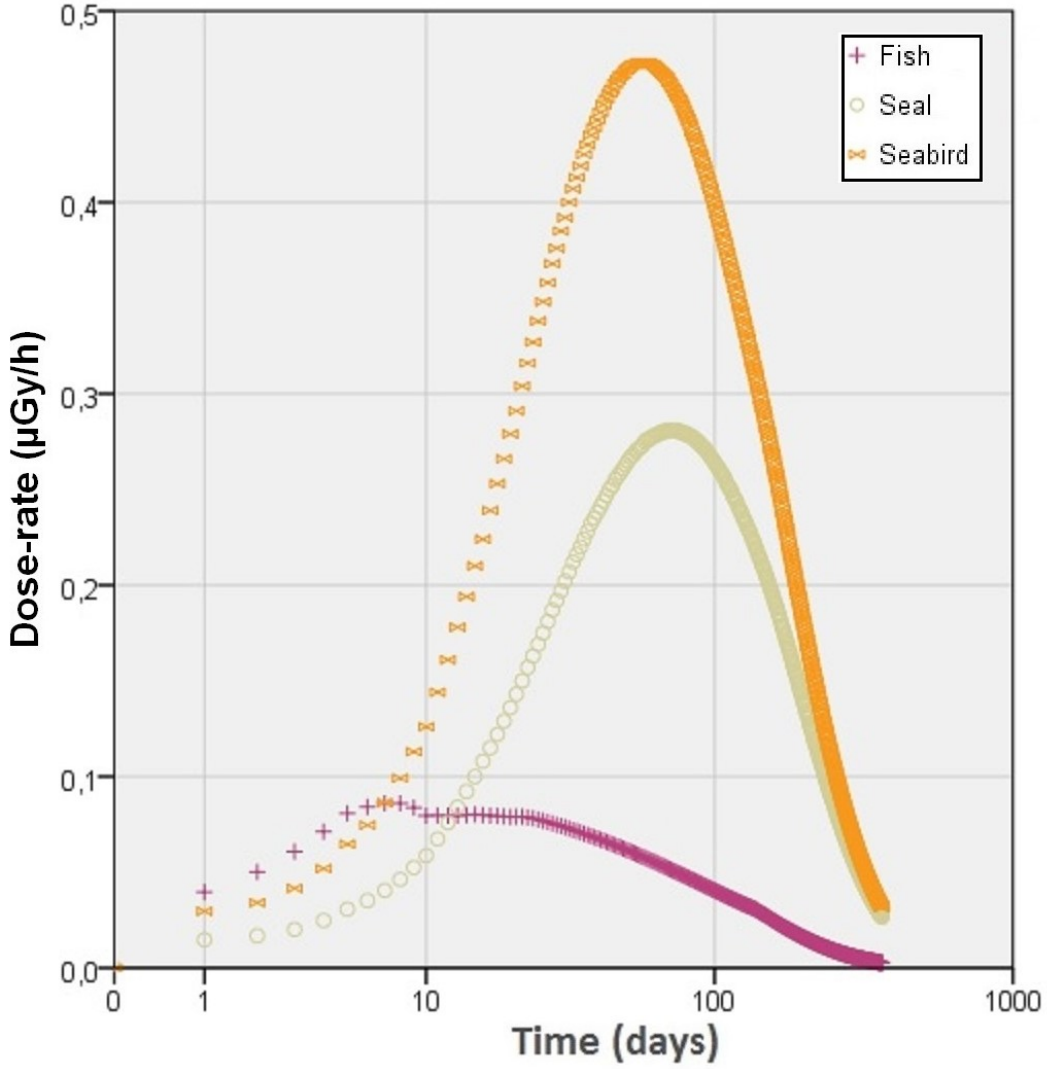

Figure 7.5. Dose-rate (µGy/h) for fish, seal and seabird for the lifting scenario derived from at surface activity concentrations of ^{137}Cs in sea water.

The maximum dose-rates of ca. 7 µGy/day for seals are orders of magnitude below the 0.1-1 mGy/d DCRL band recommended for application to mammals (strictly speaking Reference Deer and Rat but mammals are known to exhibit similar radiosensitivity) by the ICRP (2008). This band is considered to correspond to dose-rates where the probability of radiation-induced effects occurring is very low. The above-mentioned dose-rates might furthermore be contextualized through consideration that the maximum (total including radionuclides in addition to ^{137}Cs) for fish in proximity to the main release point from the Fukushima Daiichi accident were (at an early stage post-accident) ca. 140 µGy/h whereas dose rates determined at a later stage further offshore were in the range 0.10 to 0.17 µGy h^{-1} (benthic fish, crustaceans and molluscs) (Vives i Batlle et al., 2014). The dose rates determined for the aforementioned Fukushima study were not considered to be at a level that might cause substantial impacts on populations of wild organisms.

8 Dealing with uncertainty

It is apparent that any assessment of risk (to both humans and the environment) requires the specification and inclusion of many elements. In our case, these elements comprise of problem formulation, models, scenarios, assumptions, data, expert judgement and the various tools employed. In dealing with any of these components, we eventually have to face situations of inadequate information and uncertainty (Van der Sluijs, 2007). However, uncertainty may not simply reflect a lack of knowledge, it can also arise due to variability inherent to the system under discussion. The distinction between these two types of uncertainty is often of great importance (Frey, 1992).

Walker et al. (2003) defined uncertainty as a three dimensional concept. They argued that in discussing the uncertainty related to model-based studies, we have to distinguish between three dimensions of uncertainty: location, level and nature. The first dimension refers to relevant locations where uncertainty can manifest itself e.g. context, model structure, inputs, parameters, and model outcome (result). The second dimension represent what we know and ranges from perfect knowledge to total ignorance. Finally, the third dimension describes whether the uncertainty is due to the lack of knowledge or due to inherent variability of the phenomena being studied.

Hence, a thorough characterisation of uncertainty requires a critical analysis of all the components comprising the assessment (e.g. models, scenarios, underlying assumptions, underpinning data). Such a detailed analysis of uncertainty would require the allocation of considerable resources and effort and was considered beyond the scope of the present work.

We have to bear in mind that for the case of K-159 (or any other dumped or sunken object for which salvage is an option) there are factors which add extra layers to the existing uncertainty. Such factors might include, for example, the time and circumstances of lifting and the characteristics of the scenarios considered. When in the future a salvage operation would take place and which technology would be used has an impact on the applicability of the results arising from any concomitant impact assessment (NES, 2013). We cannot foresee the future but to indicate what might happen, we make use of scenarios. The latter implies making assumptions that often cannot be verified. Uncertainties of this kind most probably mask much of the efforts in characterising other types of uncertainties that could be described statistically. Conscious of these sources of great uncertainty, spending resources to characterise model and parameter uncertainties, measurement and sampling errors and other location relevant uncertainties would not be fully justified.

Hence, a resource efficient and pragmatic approach to deal with uncertainty and consequently lend credibility to the outcomes of a study of the kind we have conducted would be to apply conservative assumptions, consider extreme accident scenarios and employ high-end input values (IPCS 2014). We have adopted such an approach in this study. Application of a sensitivity analysis in order to identify the most important parameters/ factors (e.g. Avila et al., 2004) as well as

determining their influence on the outputs would also be of a great use. However, this was considered as being beyond the scope of the current analysis.

Conservatism has been introduced at various points in the assessment. This has been done by looking for the worst case scenarios which represent extreme situations (e.g. worst metrological cases), considering various accident scenarios (accident under water, at the surface and on the land), employing conservative parameters and assumptions (spontaneous release of total inventory, highest possible SCR), focusing on higher end input values (considering critical groups, using 95th percentiles). In addition, to reduce uncertainty, further attempts have been made to use best available knowledge/ information through consulting the most relevant sources and employing state of the art models.

9 Summary and concluding remarks

Dumped and sunken radioactive waste contributes the greatest proportion to the total activity found in the Arctic Seas, followed by inputs from European nuclear reprocessing facilities and global fallout from the nuclear weapons testing period (Sarkisov et al., 2009). Of the dumped and sunken objects present within the Arctic, those containing Spent Nuclear Fuel (SNF) are of special importance given the nature of such materials. With regards to potential impacts on Norway (both economically and environmental), the sunken Russian nuclear submarine K-159 is of great concern. The submarine currently lies at a depth of 246 meters in the Barents Sea, less than 130 km from the border with Norway. In addition to its proximity to Norway, the K-159 submarine lies close to fishing areas of the Barents Sea. It also represents the single largest potential source of radioactive contamination to the Arctic marine environment (NRPA, 2014).

Now, 14 years after its sinking, more detailed information regarding potential source terms and possible recovery operations have come to light. This, in conjunction with the availability of more sophisticated modelling tools, renders a detailed assessment timely and more robust than assessments conducted earlier. To provide a better foundation for the evaluation of possible radiological impact, especially in the case of a potential recovery of the submarine, a new health and environmental impact assessment has been undertaken. The study has been based on the derivation of a number of hypothetical accident scenarios and the evaluation of possible consequences for humans and the environment as a result of these hypothetical scenarios.

The existing SNF onboard of K-159 represents a potential source of contamination of the Arctic. According to estimates made for this study, the inventory of the submarine is of the order of 2.6E+03 TBq, being mostly (> 90 %) comprised of ^{90}Sr and ^{137}Cs. Considering various release scenarios, it was estimated that the expected maximum activity of radionuclides released from the submarine to the environment may reach 45 TBq. However, this value was rounded up to 50 TBq and was used as a starting point for all considered accident scenarios.

In general, three categories of accident scenarios were considered: in situ, lifting and docking. While the location for the first two accident scenarios would be the current site of the submarine, the docking accident occurs at a different location, i.e. a shipyard which would receive the submarine after being raised. In all these scenarios, the main focus was directed to situations under which a spontaneous chain reaction (SCR) can take place. It is worth noting that the considered SCR accident scenarios are purely hypothetical and the probability of their occurrence is (in a qualitative sense) considered to be extremely low. Even in the worst case involving corrosion and degradation of materials, when the complete inventory of spent fuel sloughs down to the reactor bottom, the SCR might only appear in some part of the reactor volume where certain relatively stable configurations of fuel fragments and water forms a local critical mass. Any attempt to assess the probability of occurrence for such a configuration and the magnitude of the resulting SCR (in a quantitative sense) is, however, impracticable owing to a large number of undefinable system parameters.

Nonetheless, for the present assessment, a simplifying and conservative assumption was to presuppose that while all releases from both 'in situ' and 'lifting' accident scenarios would end up in the sea, the releases associated with the 'docking' scenario would only be to the atmosphere. Concerning potential consequences for Norway, the latter scenario was considered as the worst case.

To elucidate the transport, distribution and fate of relevant radionuclides in aquatic and terrestrial ecosystems following hypothetical accidents, use was made of state of the art 3-dimensional hydrodynamic and atmospheric dispersion models.

To evaluate the marine dispersion of potentially released radionuclides, a series of scenarios was simulated and analyzed for the cases of the submarine surface and underwater positions in summer and winter. Spatial distributions of ^{137}Cs in seawater during the first month (every 5 days) and within a year (every 3 months) were analyzed for characteristic depths of 0, 50, 100 and 200 meters. Cs-137 activity concentrations exceeding 1 Bq/l were observed during the first 15-20 days following the release at horizons of the source location within a very limited area (maximum 10-20 km in diameter). After 30 days, ^{137}Cs activity concentration did not reach values above 0.1 Bq/l in most cases.

Some key data pertaining to activity concentrations in marine biota are given in Table 9.1.

Table 9.1. Simulated maximum activity concentration in water and marine biota along with the mean values. Accident location is at the submarine site in the Barents Sea.

Release location	***Maximum activity concentration, ^{137}Cs***			***Mean values***
	Water (Bq/l)	Biota (Bq/kg f.w.)		(Bq/kg f.w.)
Surface	100	Fish	4.4E+02	1.5E+02
	(3)*	Seal	8.5E+02	4.4E+02
		Seabird	2.5E+03	1.1E+03
Bottom	1000	Fish	4.4E+03	1.3E+03
	(26)*	Molluscs	3.4E+04	3.4E+03
		Crustaceans	8.9E+03	4.2E+03

*Mean values

To place the simulated and predicted activity levels (both in seawater and in biota) into context, the measured ^{137}Cs activity concentrations within the areas of interest are summarized in Table 9.2.

Table 9.2. Measured activity concentrations of 137Cs in seawater and fish based on samples collected in the Barents Sea and Norwegian Sea in recent years.

Location	***Measured activity concentration, ^{137}Cs***			Reference
	Water (Bq/l)	*Biota (Bq/kg f.w.)*		
Barents Sea	1.6E-03 – 2.0E-03	Fish	<0.3	Gwynn et al. 2012
Norwegian Sea	1.1E-03 – 5.9E-03	Fish*	<0.5	NRPA (2011) & NRPA (2015)

* Caught within the coastal waters of Finnmark and Troms.

For regional level atmospheric dispersion involving long range transport of radionuclides, the Norwegian Meteorological Institute's SNAP (Severe Nuclear Accident Program) model was employed using a source term based upon the "docking" accident scenario, where 50 TBq of activity would be released into the atmosphere. Table 9.3 shows the modelled activities in terrestrial biota along with the resultant dose rates following release upon an accident during the docking of the submarine.

Table 9.3. Simulated maximum activity concentration in terrestrial biota as a result of an accident during the docking of the submarine along with the estimated associated dose rates for biota.

Accident location	***Maximum activity, Bq/kg (f.w.)***		***Maximum dose rate (µGy/h)***
	Biota	***^{137}Cs***	
Nerpa shipyard	Vegetation	5.4E+02	2.9E-01
	Small mammals	3.4E+03	7.4E-01
	Deer	1.3E+03	4.5E-01

The output data (see Tables 9.1 and 9.3) from the various models employed were used as inputs to ingestion dose calculations along with other exposure pathways for humans (e.g. cloud shine, ground shine and inhalation). The contribution from these latter exposure pathways, in turn, were calculated via outputs (radionuclide air concentration and deposition levels) from atmospheric dispersion models. Doses to both humans and biota were then derived (see Tables 9.3 -9.5). Because of the uncertainties involved in modelling work of this type, a degree of conservatism was introduced at various points in the assessment. Bearing such conservatism in mind, it remains apparent that serious impacts on either human health or environmental integrity, as a result of releases from the hypothetical scenarios studied, would not be expected. The hypothetical terrestrial-based dose calculated to a critical group in Finnmark was estimated to be close to 1 mSv and, as such, would not constitute a level of exposure where concerns would be extreme (see Table 9.4). Nonetheless, the doses are non-trivial and there would conceivably be attempts made to reduce doses as far as possible with due regard to social and economic considerations.

Table 9.4. Estimated effective doses to human for various pathways based on releases related to the "docking" accident scenario..

Accident location	***Pathway***	***Effective dose(mSv)***	***Comments***
Barents Sea	Inhalation	1.4E-04	Individuals in identified population group in Norway
	Cloud shine	2.9E-06	
	Ground shine	3.3E-02*	
	Ingestion (*terrestrial food*)	8.9E-01*	
	Total	**9.23E-01**	

** Annual effective dose.*

With regards human individuals in Norway, the dose for a high rate consumer of fish, derived for the ingestion of contaminated fish (see Table 9.5) is about half of the potential dose rate from ingestion of contaminated terrestrial foodstuffs (see Table 9.4). While the former would be a possible consequence in case of "in situ" and "lifting" accident scenarios, the latter would be envisaged occurring under the "docking" accident scenario. The doses derived for the consumption of marine products in Norway were not values that would likely cause extreme concern from a regulatory perspective but, in practice, regulatory action for Norwegian and Kola Peninsula populations would be driven by considerations regarding activity concentrations in foodstuffs.

Table 9.5. Estimated annual effective doses to human for ingestion pathway based on releases to the Barents Sea ("In situ" and "Lifting" accident scenarios).

Accident location	***Pathway***	***Annual effective dose (mSv)***	***Comments***
Barents Sea	Ingestion of seafood	3.2E+00	Average person in Kola Peninsula
Barents Sea	Ingestion of fish	5.2E-01	Individuals in identified population group in Norway, high rate consumers of fish

It has been shown that, should radionuclide releases of the magnitude considered in the accident scenarios occur, the predicted activity concentrations for foodstuffs in both the terrestrial and marine environments would be at such a level that restrictions would need to be introduced over at least the short term. In the case of terrestrial ecosystems, the introduction of restrictions on the consumption of foodstuffs, such as game and reindeer, would therefore be likely, potentially involving various measures such as the dissemination of dietary advice and, for reindeer at least, the use of live monitoring before slaughtering. In line with the Antipov et al. (2015), restrictions, at least in the short term, could plausibly be required for sea areas in proximity to K-159. The relatively elevated levels in benthic biota for the 'in situ' scenario leads to the potential for many

hypothetical marine foodstuffs to be above the relevant national intervention level for extended periods. There seems no doubts that restrictions (on fishing/harvesting of shellfish etc.) would need to be applied should radionuclide releases of the magnitude considered in the scenario occur.

Nonetheless, these rather pessimistic predictions should be tempered by the consideration that the prognoses being made here are highly conservative.

10 Acknowledgments

This work was financed with funding from the Norwegian government's Nuclear Action Plan with allocation from the Ministry of Foreign Affairs. We also highly appreciate the support provided by the Research Council of Norway through its Centre's of Excellence funding scheme, project number 223268/F50.

Appendix 1: Mathematical Formulation of the INM-IO Ocean Model

Circulation of ocean waters in a basin of arbitrary geometry is described by 3D thermohydraulic equations. The water-air interface is free, and spatial variability of the sea surface topography and variability of the mean sea level are simulated. Interactions between the atmosphere and the sea are described by the fluxes of momentum, heat and moisture. When favorable conditions are created for ice formation, the ice model is activated that describes thermodynamic processes in the ice (temperature variations, freezing and melting) as well as dynamic processes (motion, hummocking *etc.*). In that case the water mass, heat, salt and momentum fluxes through the atmosphere-water boundary are replaced by those across the atmosphere-ice and ice-water interfaces.

The ocean model explicitly describes water flows and its properties (salinity, heat) via lateral boundaries (river runoff and water exchange through straits) and the air-water interface (evaporation, precipitation). At the open boundaries the adaptive conditions based on the wave equation are set (Marchesiello et al., 2001). This method allows the waves to freely go out of the internal area through the open boundaries, independent of the direction of advective transport, and to transmit information (large-scale characteristics) from the external (with respect to the given domain) area into the inner domain.

The thermohyrdaulic state of the ocean is described by 3D functions of temperature, salinity and sea-current velocity components as well as by a 2D function of the height of the ocean-level surface. As a detailed mathematical description of the ocean model is not the purpose of this Report, only a general formulation of the modeling approach and references to original papers are provided below.

The ocean thermohyrdaulic model includes complete 3D equations of geophysical thermo-hydrodynamics (Bryan, 1969; Sarkisyan, 1966; 1977; 1991; Marchuk and Sarkisyan, 1988; Marchuk et al. 1984). The equations of the model are formulated in the Cartesian coordinate system. The dynamics of the upper ocean boundary, taking into account the mass flux (atmospheric precipitation, evaporation and ice melting), is described by a free ocean-surface equation. Horizontal turbulent viscosity and diffusion of heat and salt are accounted for and are described by appropriate operators.

The system of equations contains a spectrum of motions with a large range of characteristic velocities: the velocities of currents and baroclinic gravitation waves are 1-3 *m/s*; and the velocities of barotropic gravitation waves are 30-200 *m/s*. The choice of approximation equations is driven by two arguments, namely, the importance of describing evolution of particular processes and the applicability of the domain decomposition method for the following parallelization of the code.

The application of a time-explicit approximation method when solving the equations requires using rather small time steps in order to satisfy the Courant–Friedrichs–Lewy (CFL) condition[21] for the whole range of waves described by the system of equations including barotropic gravitation waves. The most important processes (at the present level of knowledge) for climatic phenomena in the ocean are determined by currents and baroclinic waves. Splitting the solution of the system into relatively slow baroclinic motions and fast barotropic motions is a way to override rigid constraints on the time step. Except for the processes of vertical diffusion, an explicit time approximation is preferable.

Another requirement for the approximation of equations is the applicability of the decomposition method. For example, the assumed maximum size of the computational grid (close to spherical one) in the World Ocean model is 10^4 x 10^4 x 10^2 nodes. The domain decomposition method is one of efficient solvers of the equations on multiprocessor computers with distributed memory. For grids of such dimensions, application of the decomposition method based on two horizontal coordinates is reasonable. A decomposition of 100 vertical nodes into subdomains is inefficient. Maximum efficiency of the domain decomposition method is attained when explicit methods of equation approximations are used. Thus, to apply the decomposition method using two horizontal coordinates, explicit methods of equation approximations with respect to horizontal space operators of the problem are appropriate. The use of an implicit method when solving the vertical diffusion operator does not restrict the decomposition based on two horizontal coordinates.

[21] CFL condition provides good convergence of the iteration series in numerical solution of Partial Differential Equation (PDE), in particular, hyperbolic PDE.

A. Approximation of spatial operators

As stated above, solution of the dynamic subsystem of equations is divided into two parts: solving 3D equations for baroclinic motions; and solving 2D shallow-water equations for barotropic motions. In a case of implicit time approximation, the system of equations for barotropic motions is reduced to an elliptic sea-level equation (Ibrayev, 2001 and 2008). In the present work, an explicit time approximation is applied to solve the system of shallow-water equations considered in Killworth et al., 1991.

B. Application of the model

The 'INM-IO' ocean model is described in (Ibrayev, 2001, Sarkisyan et al., 2010). A fast algorithm for solving shallow-water equations on computers with distributed memory is provided in Kalmykov and Ibrayev, 2013.

The 'INM-IO' model was applied when studying water circulation as well as seasonal and year-by-year variability of the thermo-hydrodynamic regime in various seas: the Caspian Sea (Ibrayev 2008; Knysh et al. 2008, Ibrayev et al. 2010; Ibrayev and Kurdyumov, 2003) and the Black Sea (Ibrayev 2001, Ibrayev et al. 2001). The model was also used to simulate fields of currents in open areas of the World Ocean - the Hawaiian Islands area (Bondur et al. 2008).

In most recent studies, the World Ocean water circulation is studied using a high-resolution model (Ibrayev et al. 2011 and 2012). A review of models of the global atmosphere and the World Ocean, algorithms and supercomputer computational technologies are considered in (Tolstykh et al. 2013).

Appendix 2: Marine dispersion modelling - assumptions and resultant concentration maps

This appendix contains concentration maps displaying modeled activity concentrations of ^{137}Cs in water following an instantaneous release of 50 TBq at different depths and times assuming passive contaminant transport by sea currents. Radionuclide activity concentrations are measured in Bq/m^3.

For the time of release two dates have been assumed, one in winter (from 00h 00'00''/0006.01.01 to 12h 00'00''/0006.01.01) and the other in summer (from 00h 00'00''/0006.07.01 to 12h 00'00''/0006.07.01).

Each map has a title of the following format: exp: p##, func: P###, time: date – hour.

Exp stands for the name of experiment which is either p63 or p71:

p63 — a winter release

p71 — a summer release

Of the three digits following P, the first one indicating the considered palce of the source which is:

P1 — the source is at a depth of 3 meters,

P2 — the source is at a depth of 205 meters.

The last 2 digits indicating the depth/ horizon at which the concentration has been modeled for:

01 — Horizon No 1 corresponding to 3 m;

06 — Horizon No 6 corresponding to 45 m;

11 — Horizon No 11 corresponding to 105 m;

17 — Horizon No 17 corresponding to 205 m;

For example, the title “exp: p71, func: P101, time 05.07.6 – 00:00:00” showing the simulated concentration at horizon nr. 01 for a release in summer (p71), at surface (P1), 5 days after the release.

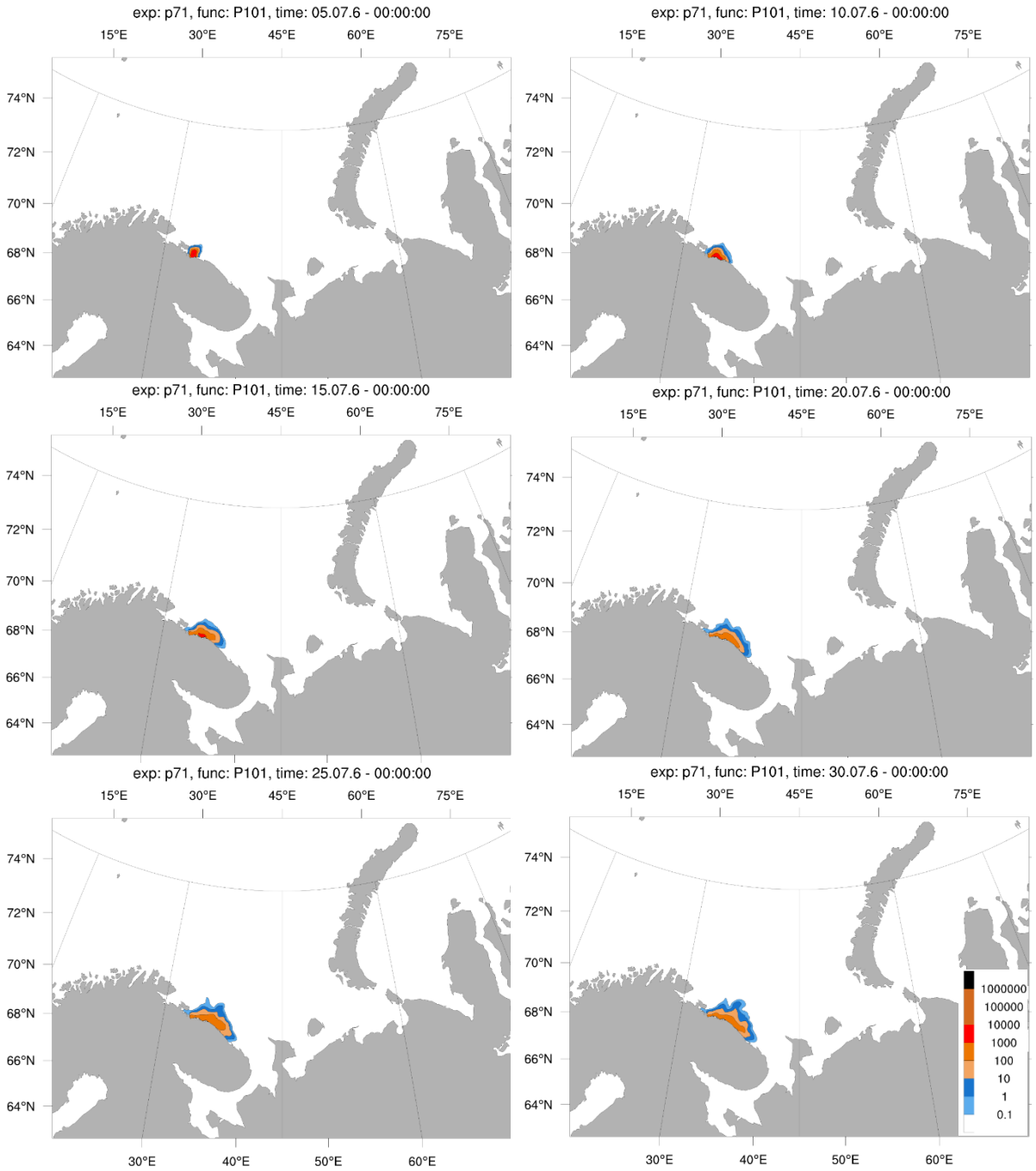

A2.1a. Concentration of ^{137}Cs (Bq/m^3) following an instantaneous release of 50 TBq at surface in summer. Maps show distribution of the contamination at 5, 10, 15, 20, 25 and 30 days after the release.

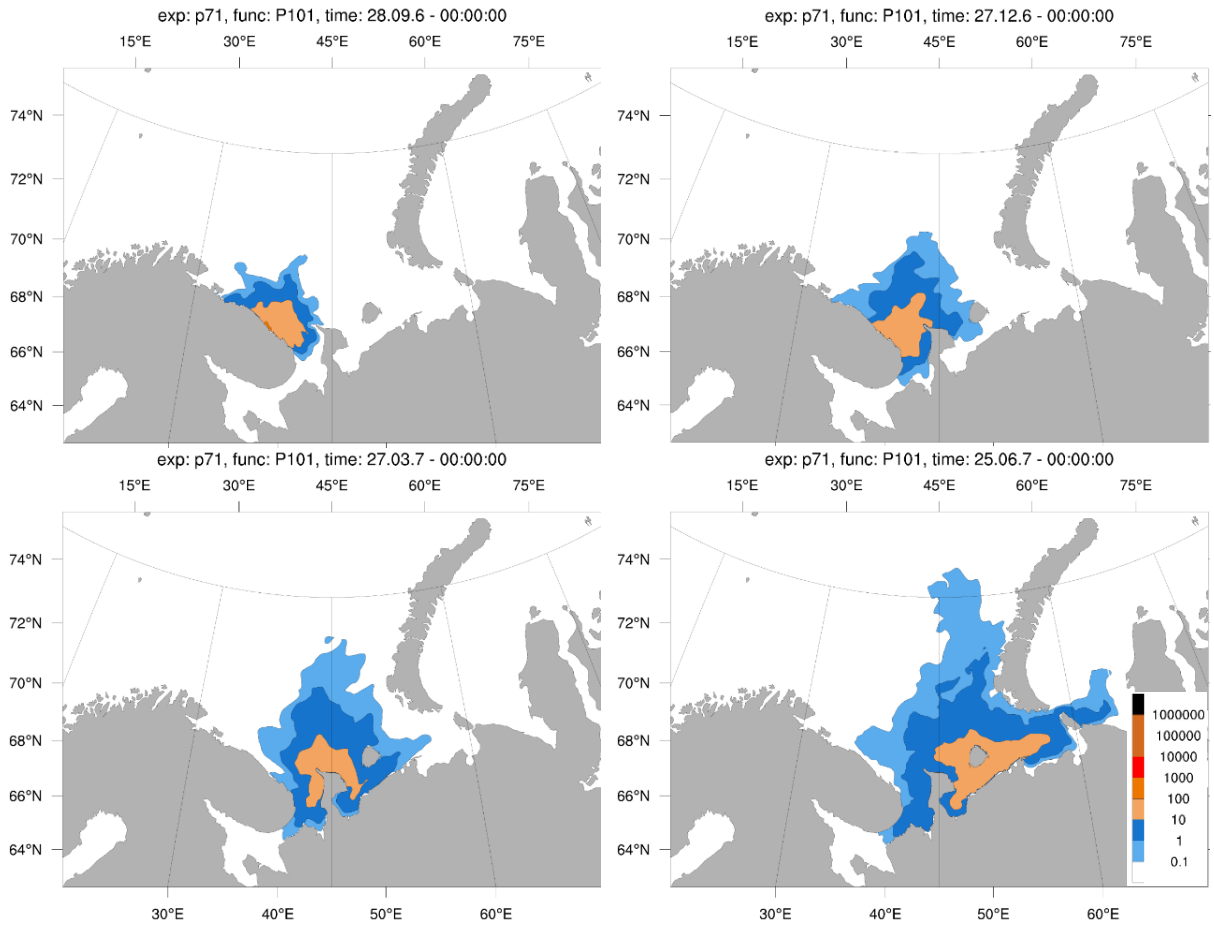

A2.1b. Concentration of ^{137}Cs (Bq/m^3) following an instantaneous release of 50 TBq at surface in summer. Maps show distribution of the contamination at 3, 6, 9 and 12 months after the release.

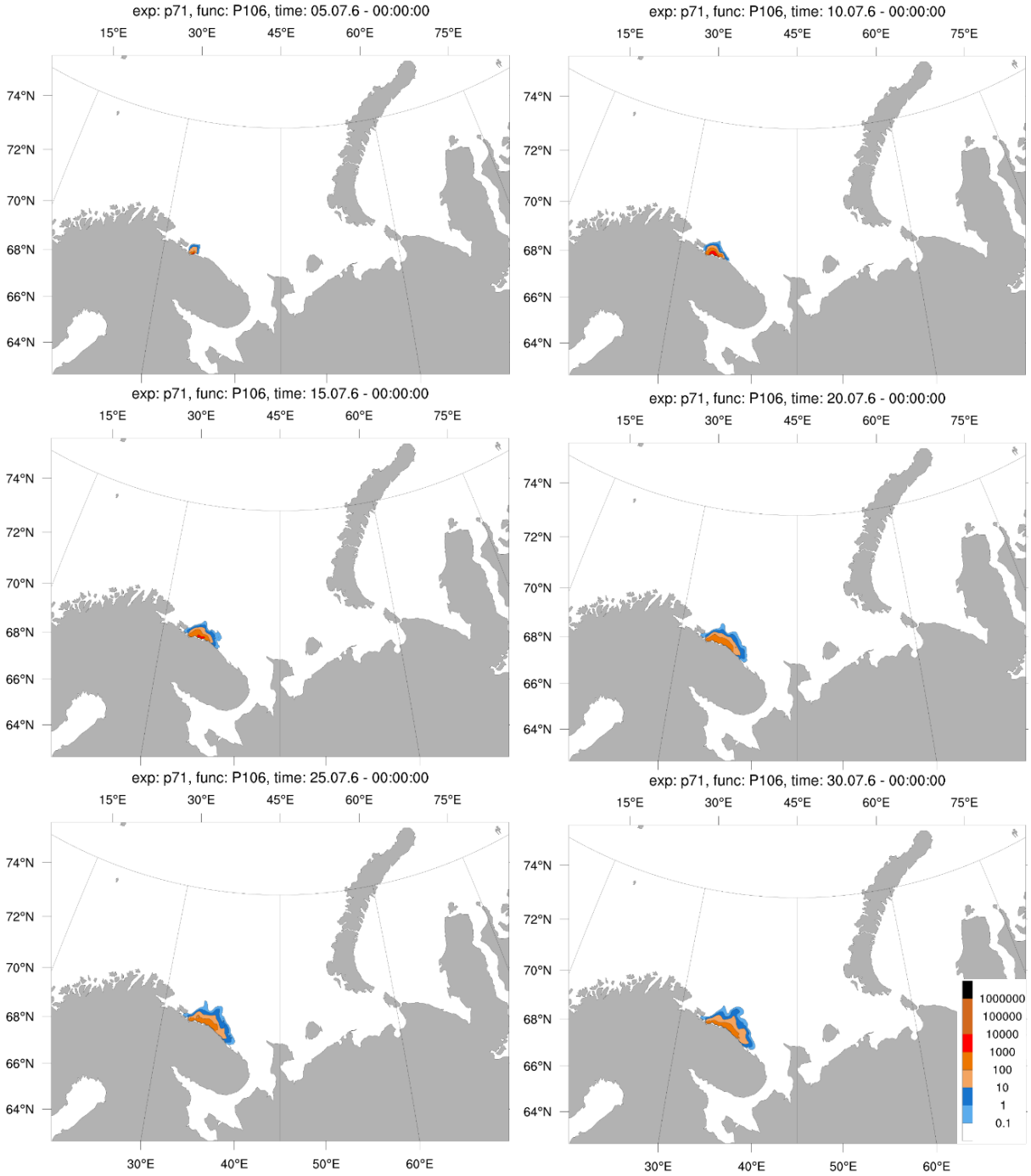

A2.2a. Concentration of ^{137}Cs (Bq/m^3) at a depth of 45 m following an instantaneous release of 50 TBq at surface in summer. Maps show distribution of the contamination at 5, 10, 15, 20, 25 and 30 days after the release.

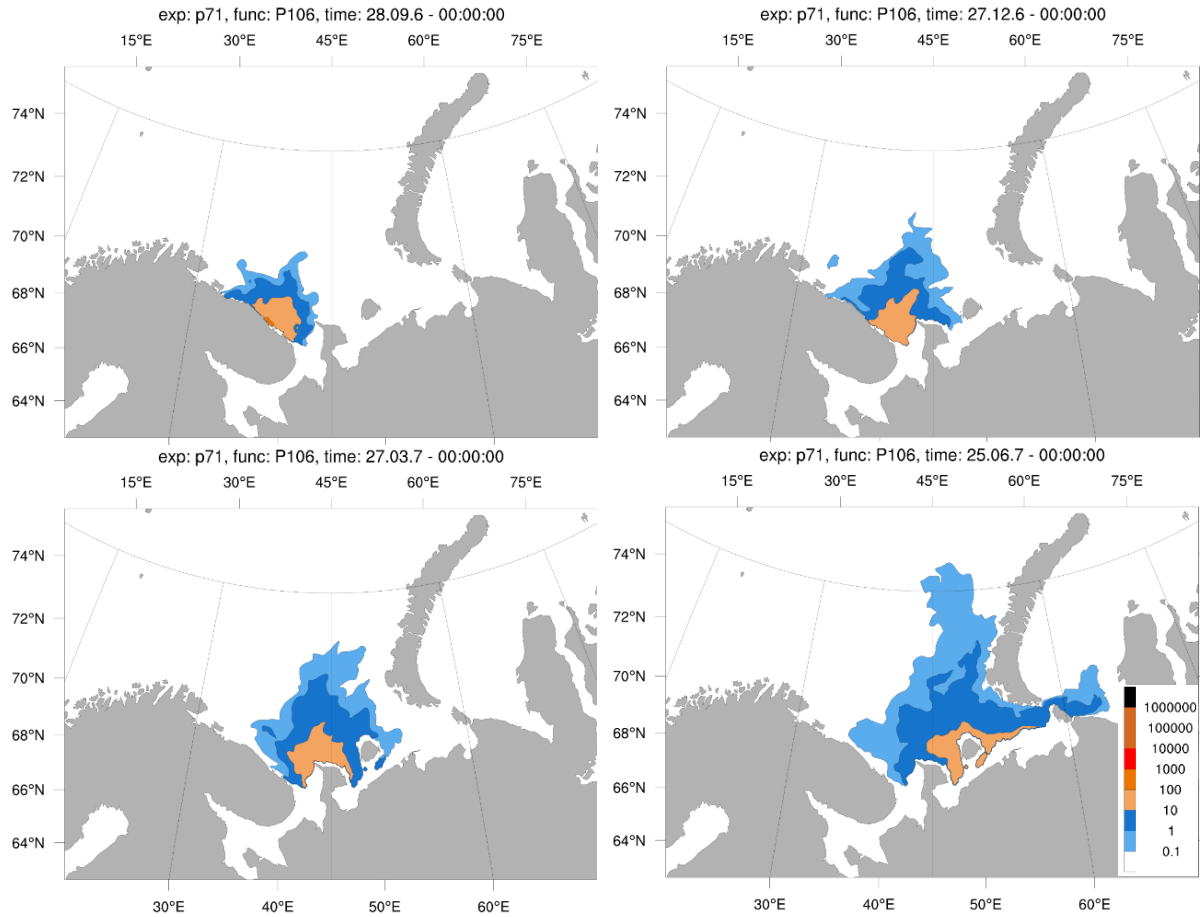

A2.2b. Concentration of ^{137}Cs (Bq/m^3) at a depth of 45 m, following an instantaneous release of 50 TBq at surface in summer. Maps show distribution of the contamination at 3, 6, 9 and 12 months after the release.

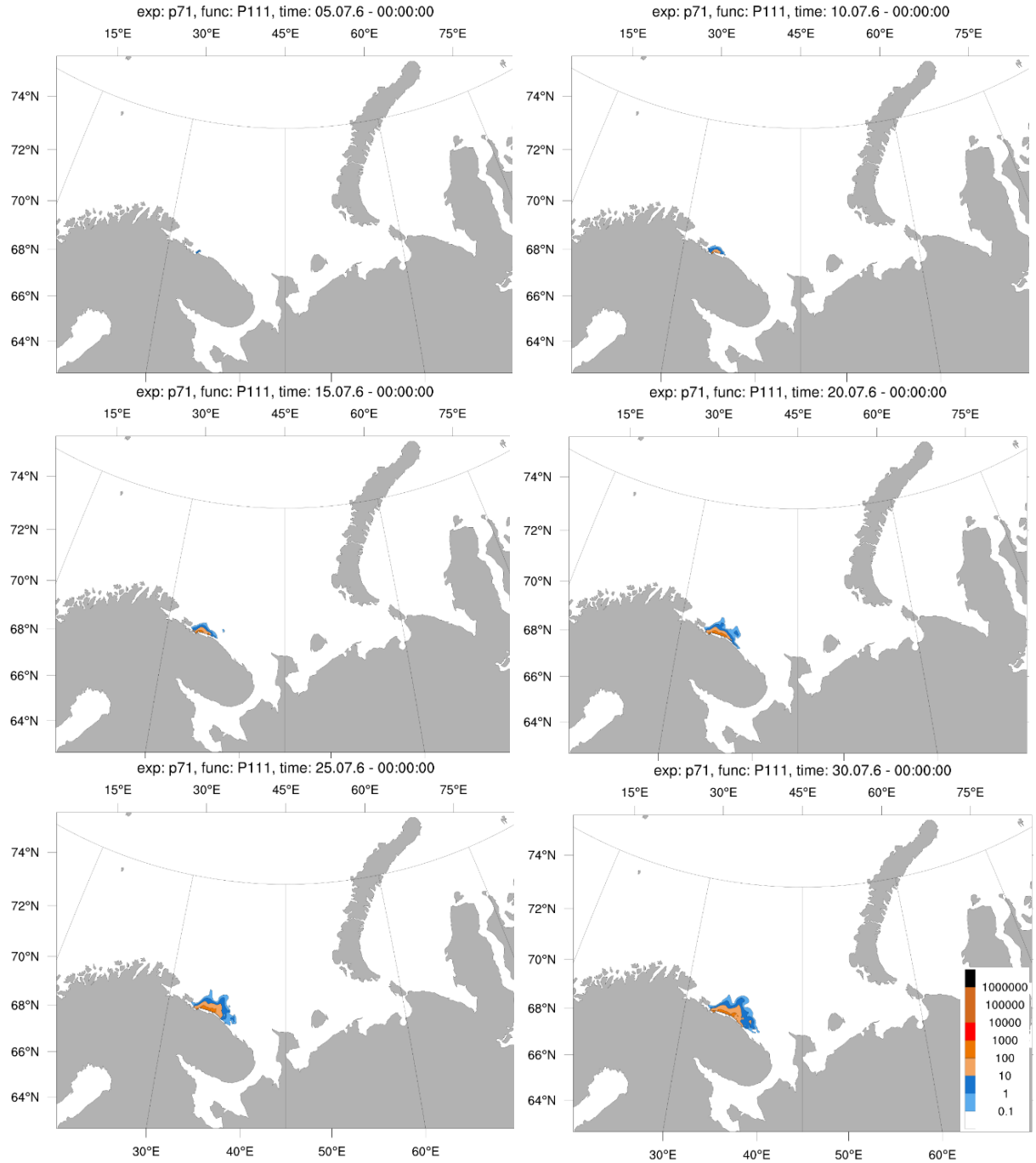

A2.3a. Concentration of ^{137}Cs (Bq/m^3) at a depth of 105 m following an instantaneous release of 50 TBq at surface in summer. Maps show distribution of the contamination at 5, 10, 15, 20, 25 and 30 days after the release.

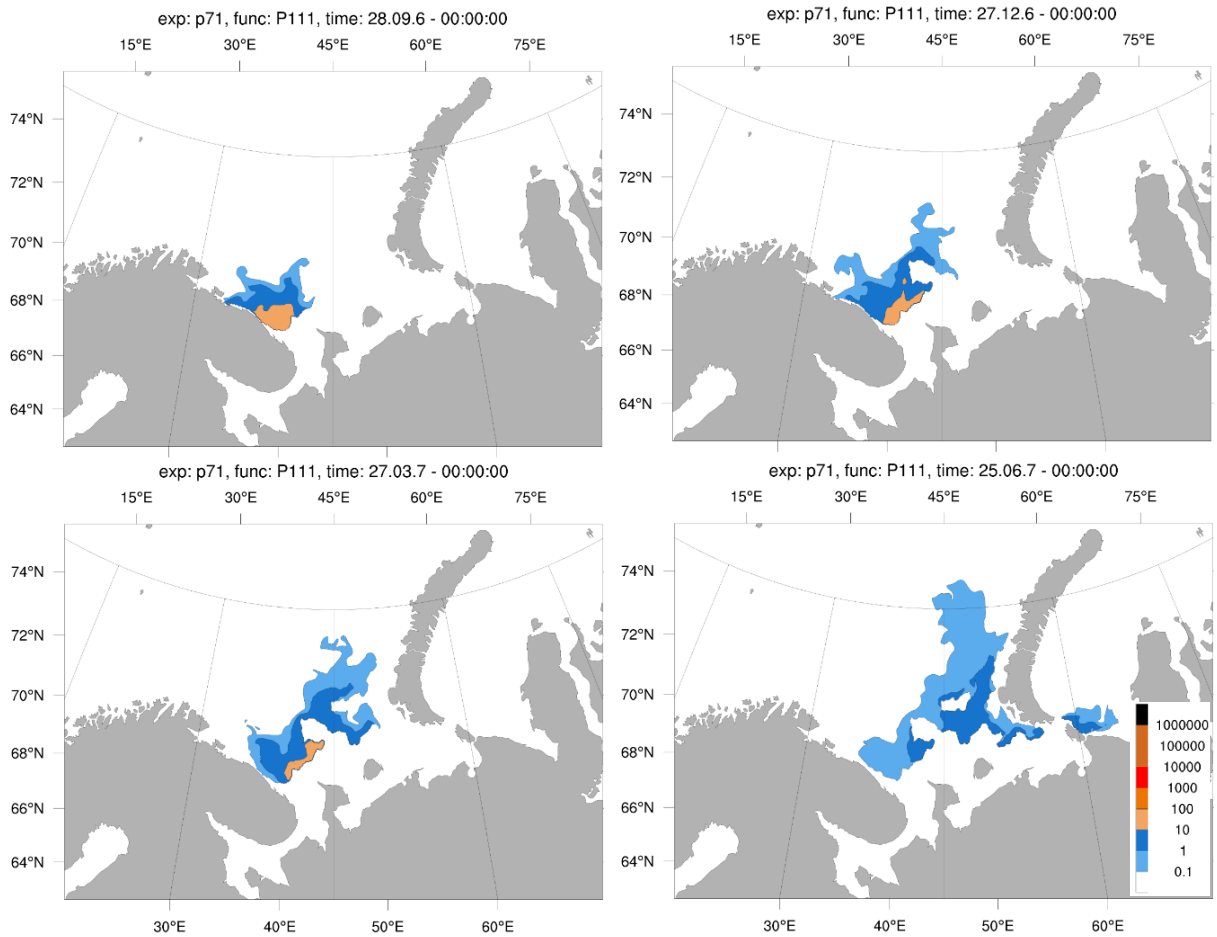

A2.3b. Concentration of ^{137}Cs (Bq/m^3) at a depth of 105 m, following an instantaneous release of 50 TBq at surface in summer. Maps show distribution of the contamination at 3, 6, 9 and 12 months after the release.

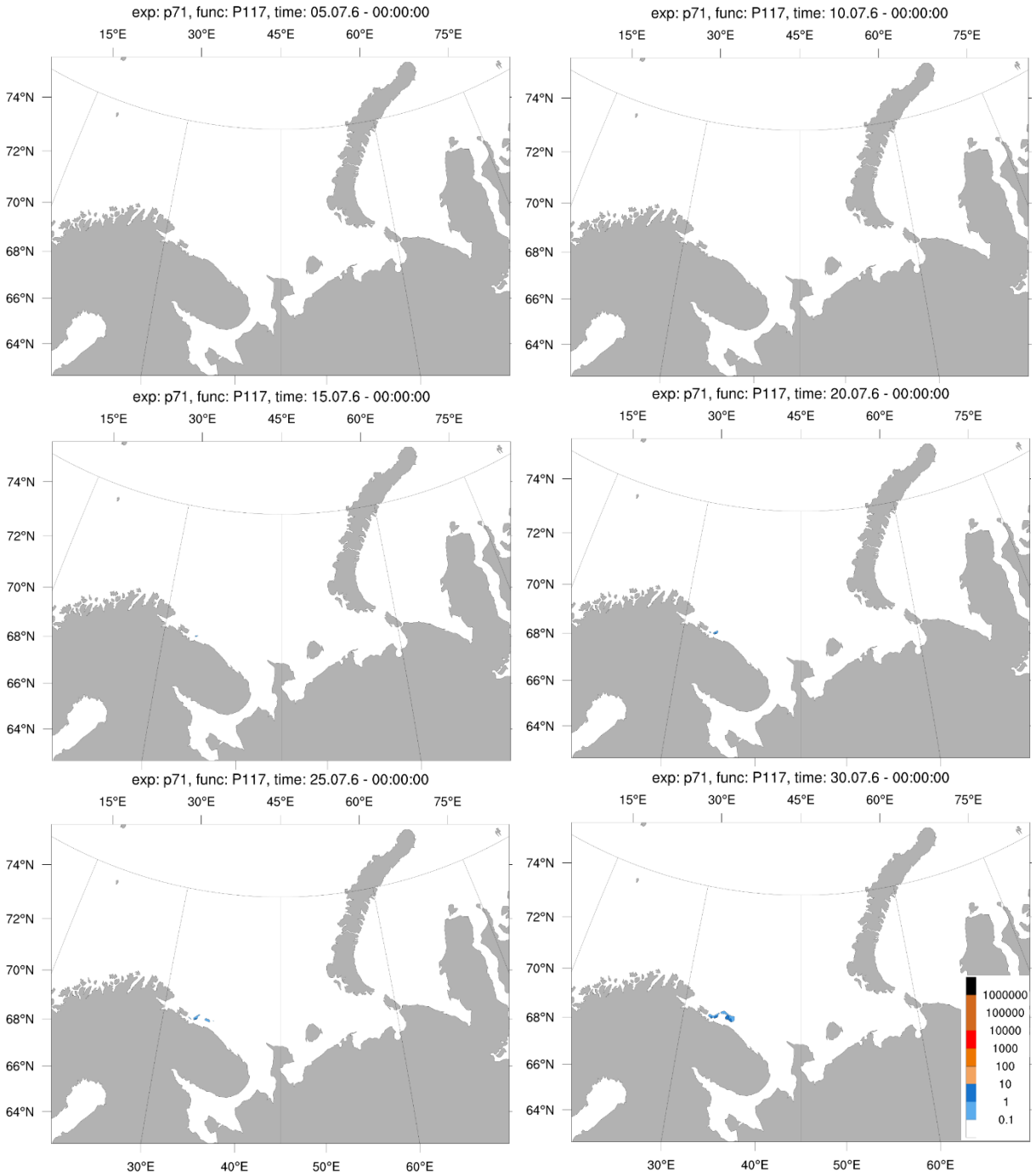

A2.4a. Concentration of ^{137}Cs (Bq/m^3) at a depth of 205 m following an instantaneous release of 50 TBq at surface in summer. Maps show distribution of the contamination at 5, 10, 15, 20, 25 and 30 days after the release.

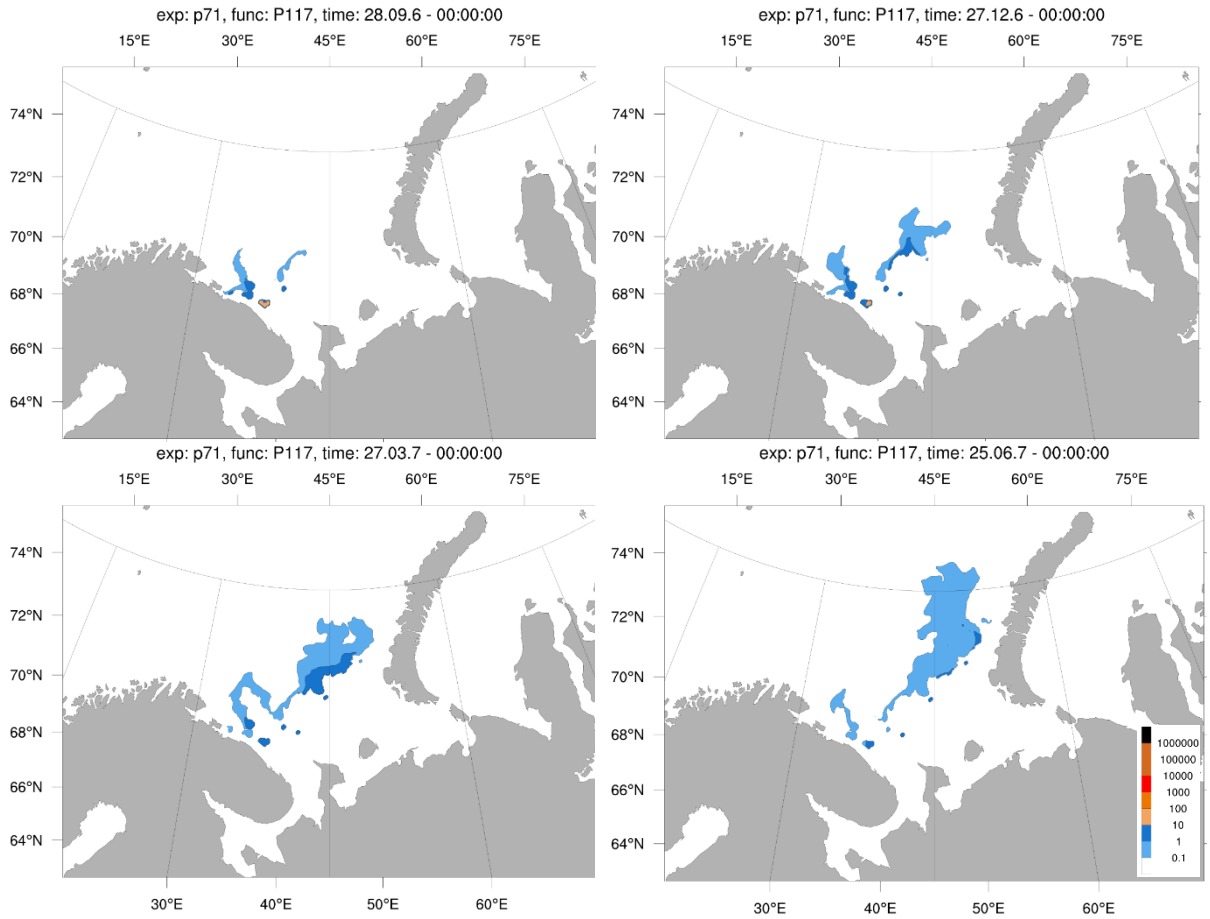

A2.4b. Concentration of ^{137}Cs (Bq/m^3) at a depth of 205 m, following an instantaneous release of 50 TBq at surface in summer. Maps show distribution of the contamination at 3, 6, 9 and 12 months after the release.

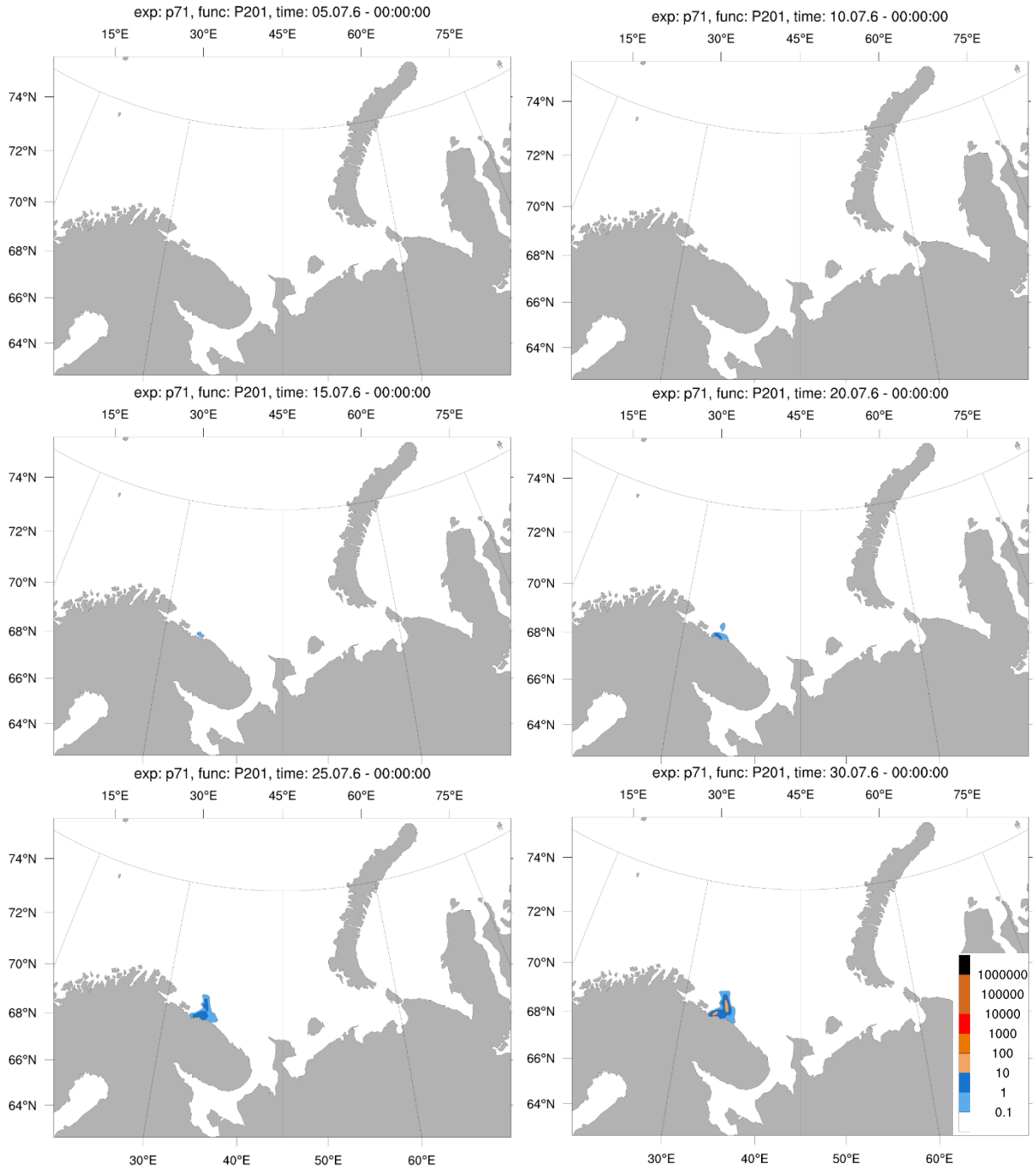

A2.5a. Concentration of ^{137}Cs (Bq/m^3) at the surface following an instantaneous release of 50 TBq at a depth of 205 m in summer. Maps show distribution of the contamination at 5, 10, 15, 20, 25 and 30 days after the release.

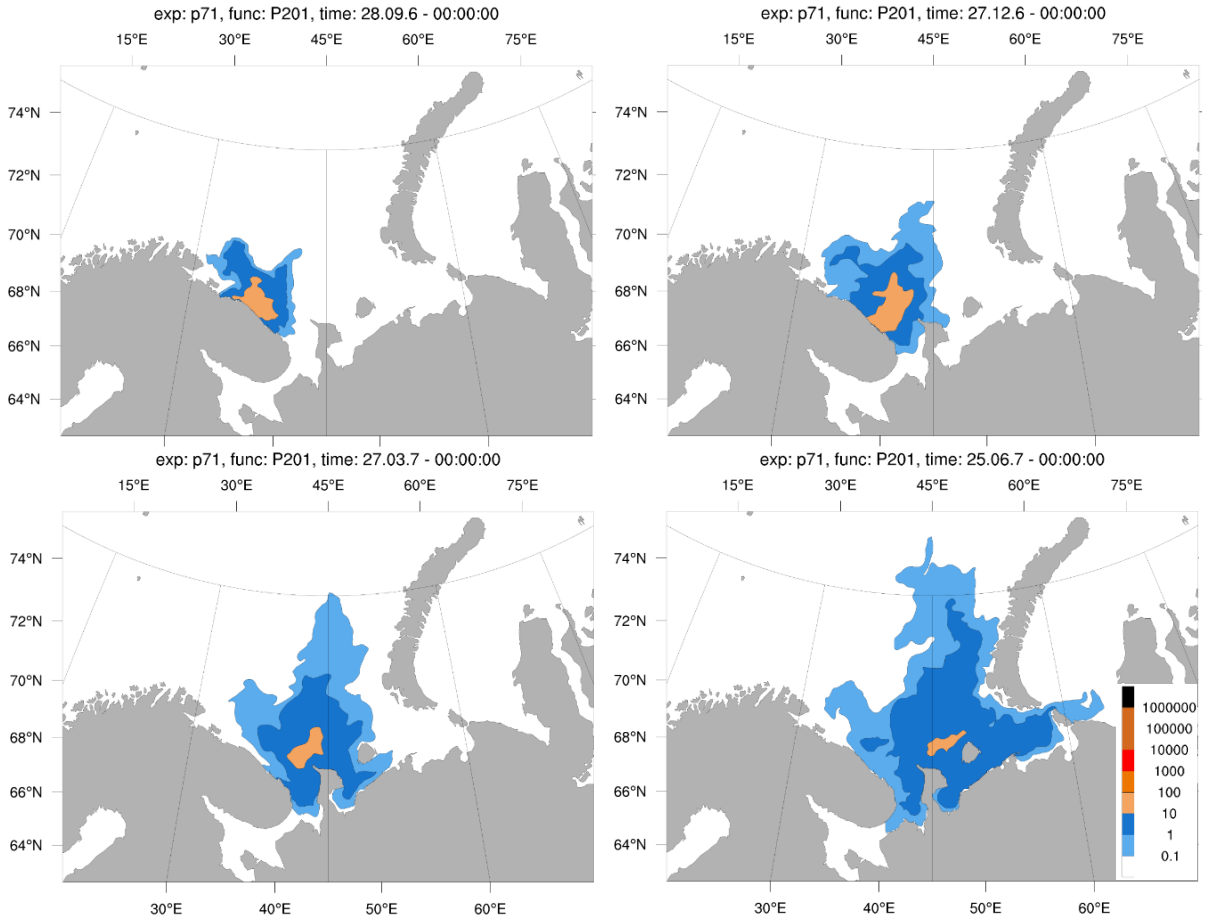

A2.5b. Concentration of ^{137}Cs (Bq/m^3) at the surface following an instantaneous release of 50 TBq at a depth of 205 m in summer. Maps show distribution of the contamination at 3, 6, 9 and 12 months after the release.

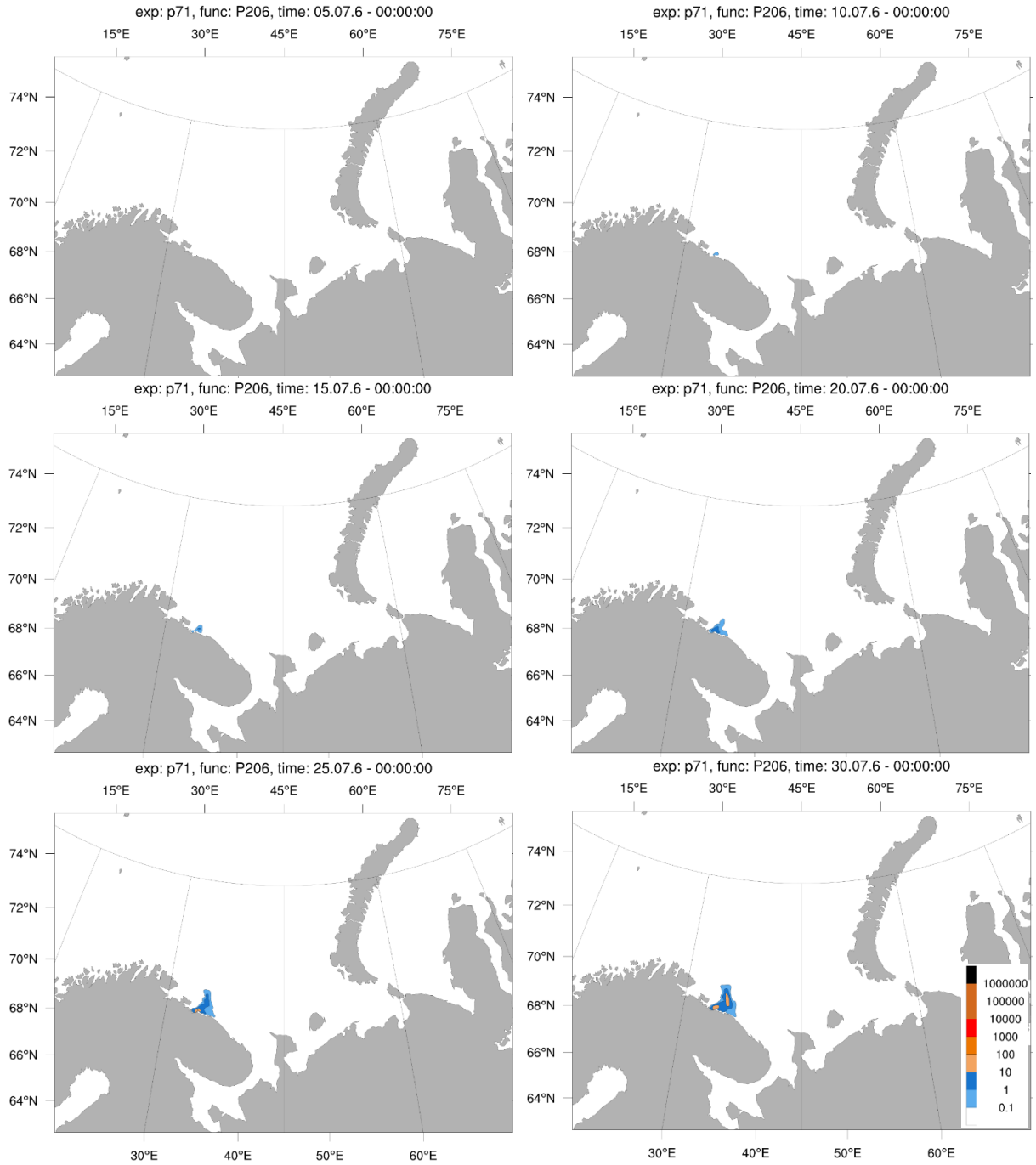

A2.6a. Concentration of ^{137}Cs (Bq/m^3) at a depth of 45 m following an instantaneous release of 50 TBq at a depth of 205 m in summer. Maps show distribution of the contamination at 5, 10, 15, 20, 25 and 30 days after the release.

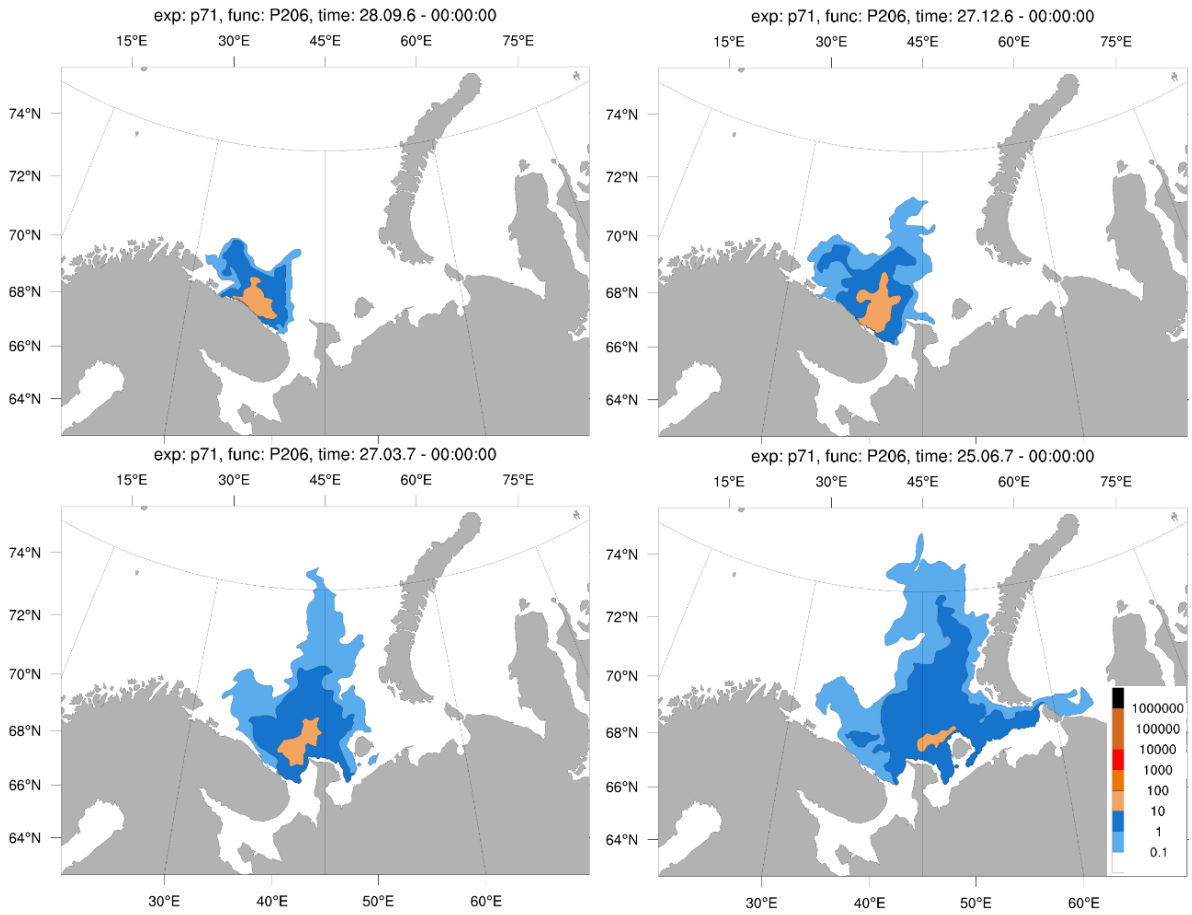

A2.6b. Concentration of ^{137}Cs (Bq/m^3) at a depth of 45 m following an instantaneous release of 50 TBq at a depth of 205 m in summer. Maps show distribution of the contamination at 3, 6, 9 and 12 months after the release.

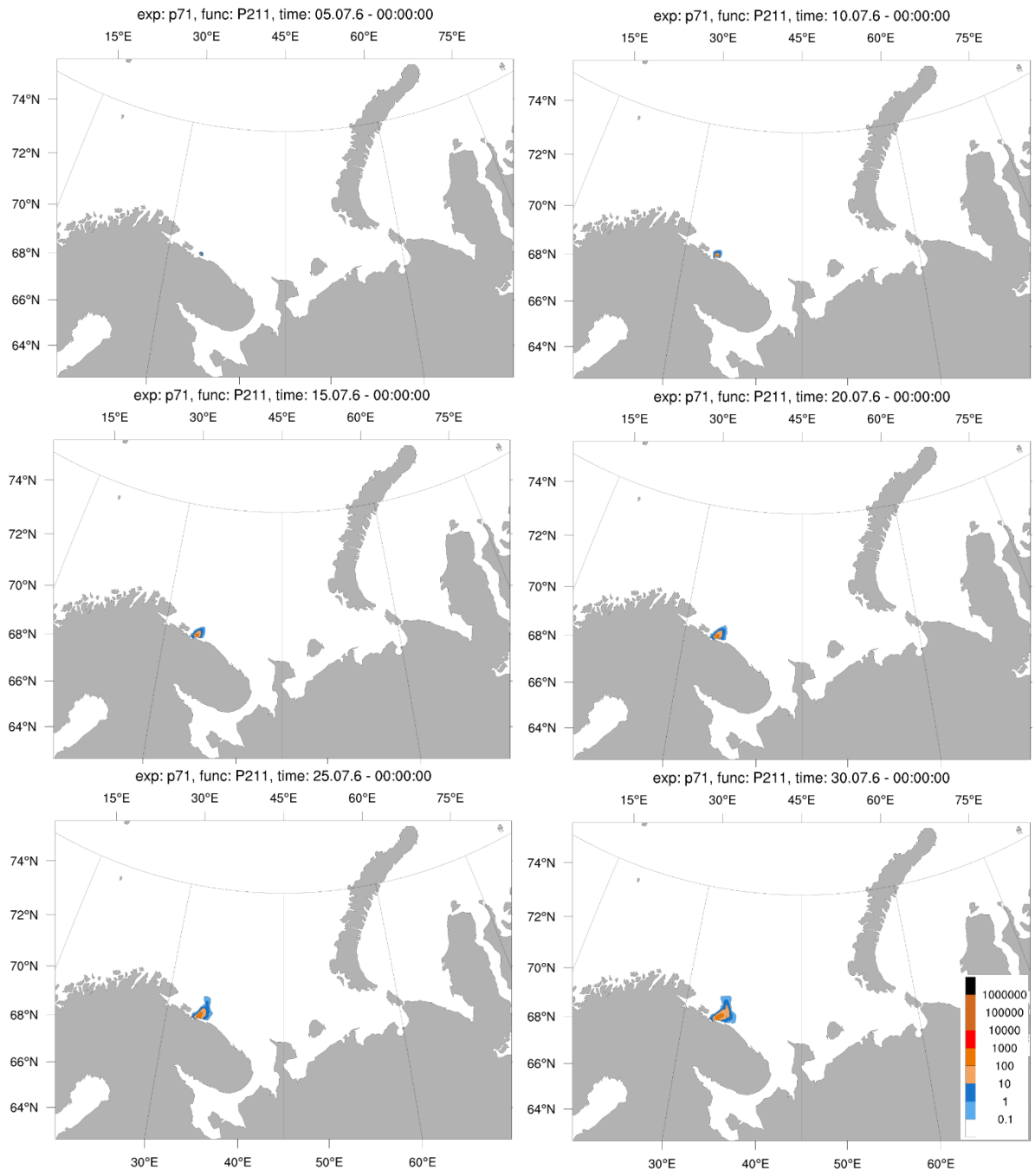

A2.7a. Concentration of ^{137}Cs (Bq/m^3) at a depth of 105 m following an instantaneous release of 50 TBq at a depth of 205 m in summer. Maps show distribution of the contamination at 5, 10, 15, 20, 25 and 30 days after the release.

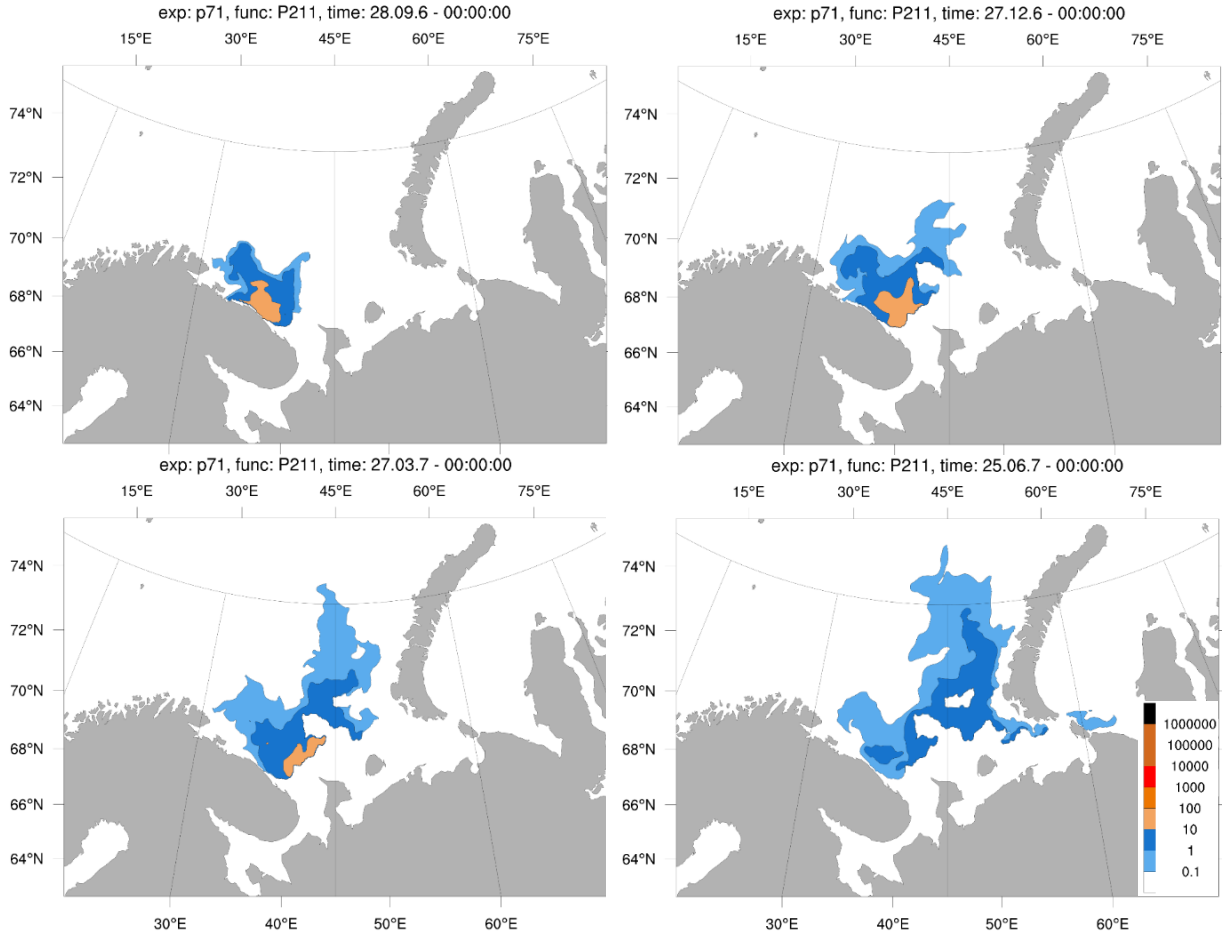

A2.7b. Concentration of ^{137}Cs (Bq/m^3) at a depth of 105 m, following an instantaneous release of 50 TBq at a depth of 205 m in summer. Maps show distribution of the contamination at 3, 6, 9 and 12 months after the release.

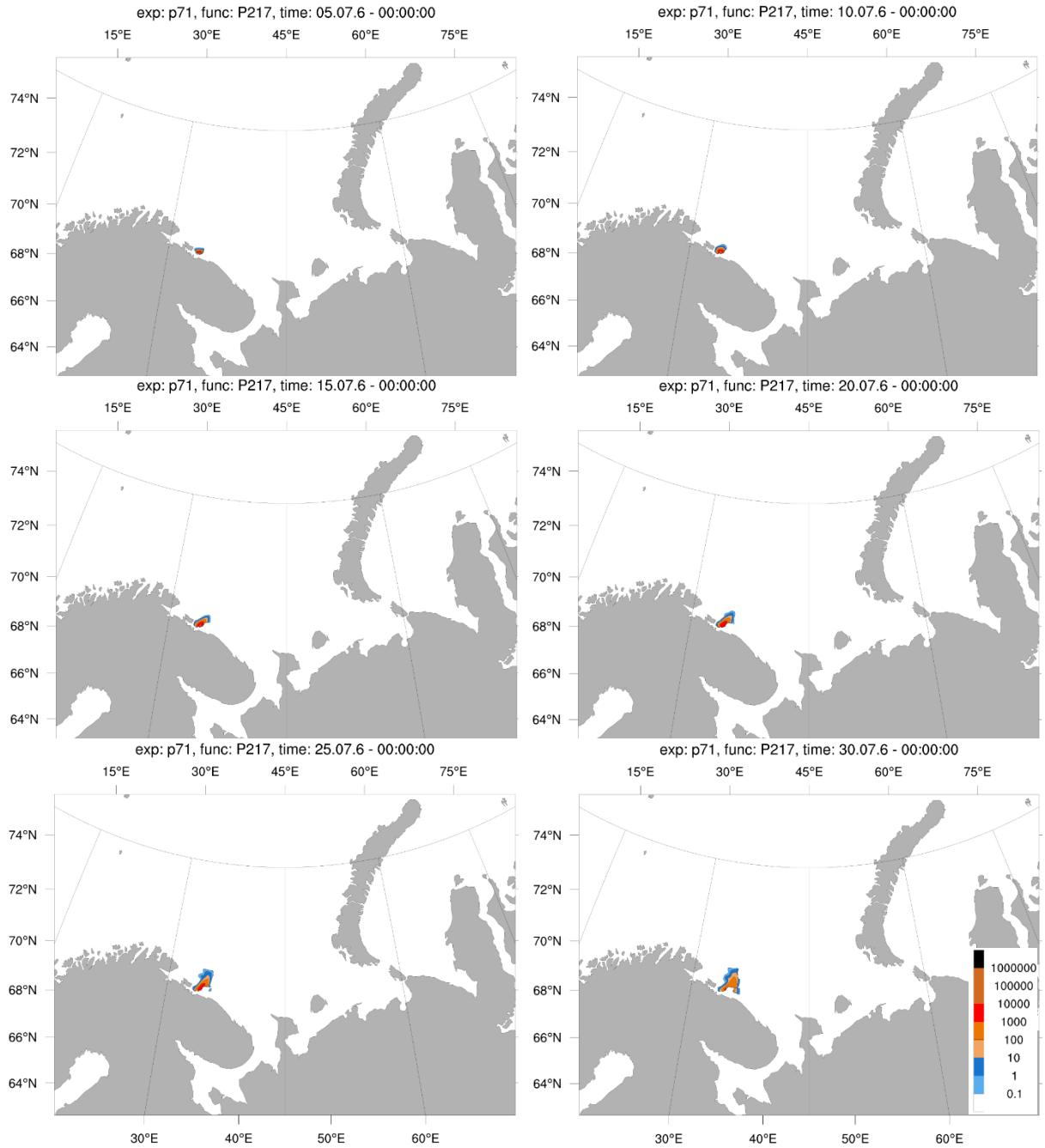

A2.8a. Concentration of ^{137}Cs (Bq/m^3) at a depth of 205 m following an instantaneous release of 50 TBq at a depth of 205 m in summer. Maps show distribution of the contamination at 5, 10, 15, 20, 25 and 30 days after the release.

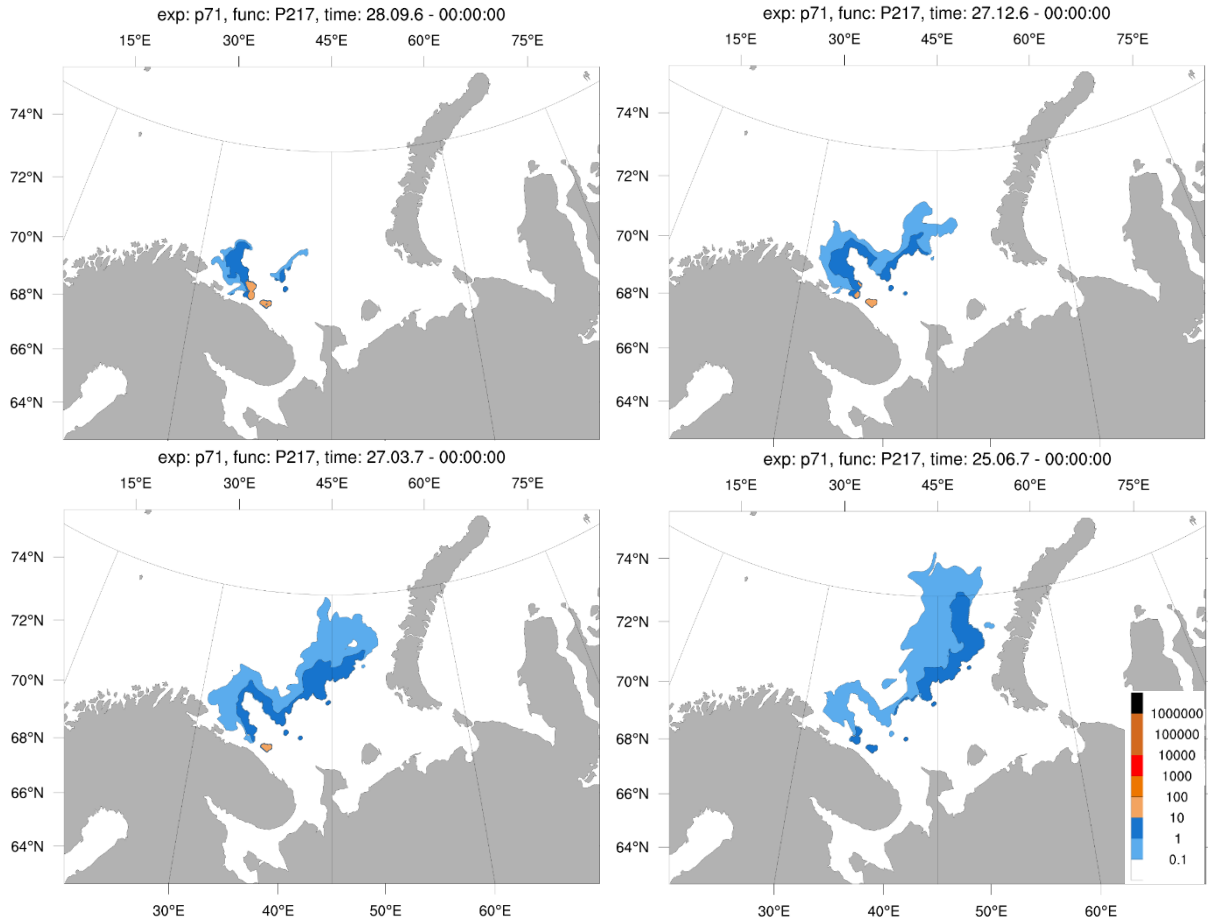

A2.8b. Concentration of ^{137}Cs (Bq/m^3) at a depth of 205 m, following an instantaneous release of 50 TBq at a depth of 205 m in summer. Maps show distribution of the contamination at 3, 6, 9 and 12 months after the release.

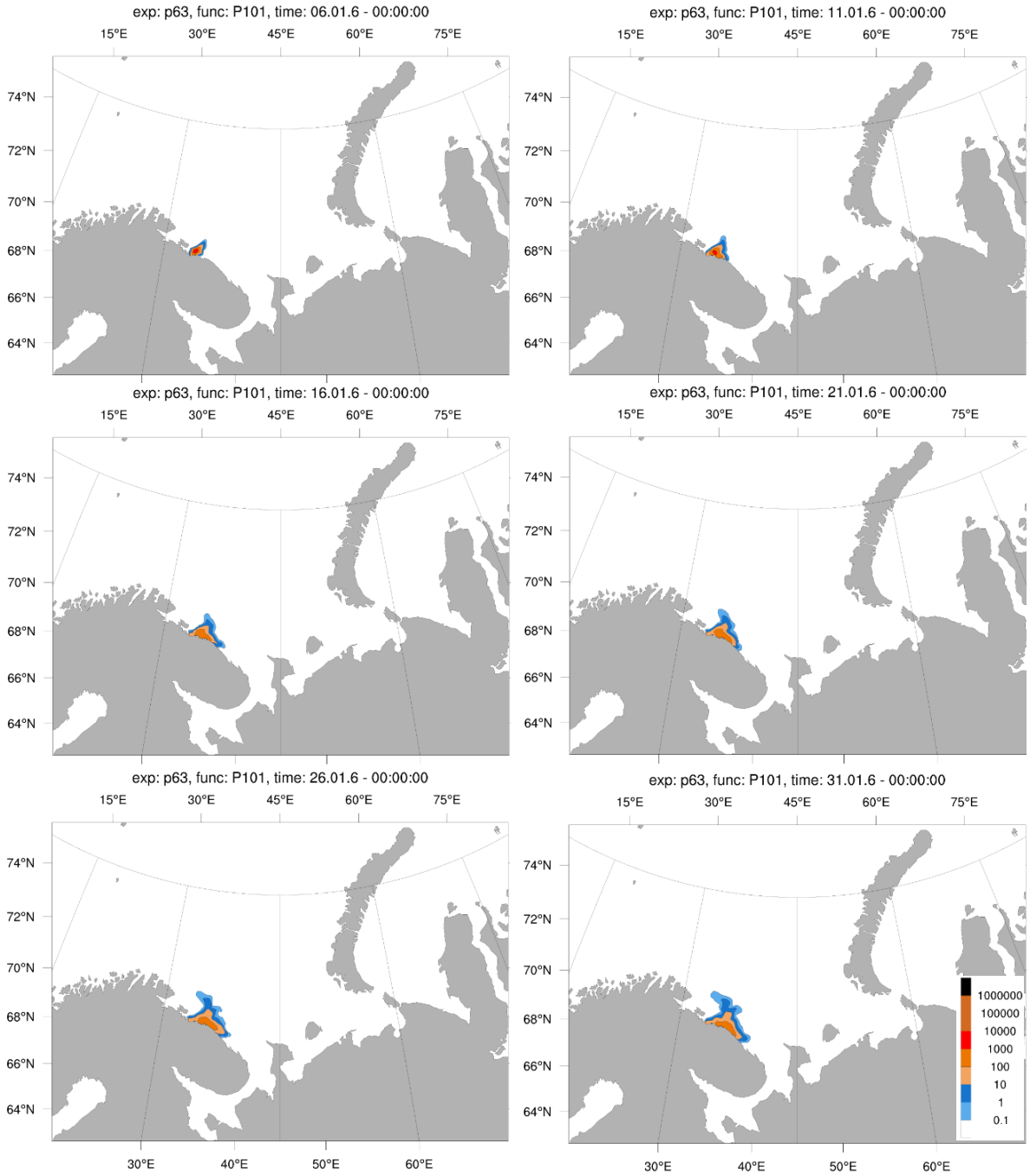

A2.9a. Concentration of ^{137}Cs (Bq/m^3) following an instantaneous release of 50 TBq at surface in winter. Maps show distribution of the contamination at 5, 10, 15, 20, 25 and 30 days after the release.

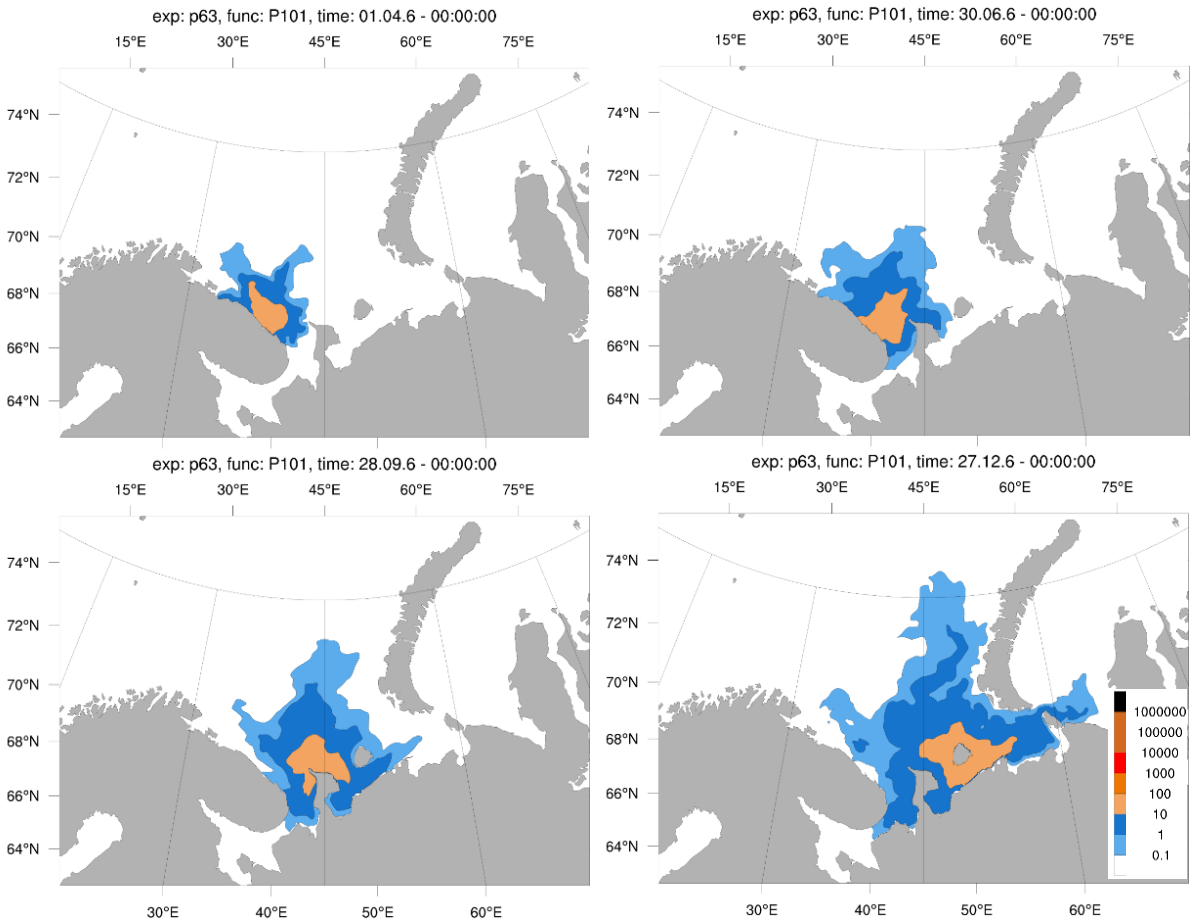

A2.9b. Concentration of ^{137}Cs (Bq/m^3) following an instantaneous release of 50 TBq at surface in winter. Maps show distribution of the contamination at 3, 6, 9 and 12 months after the release.

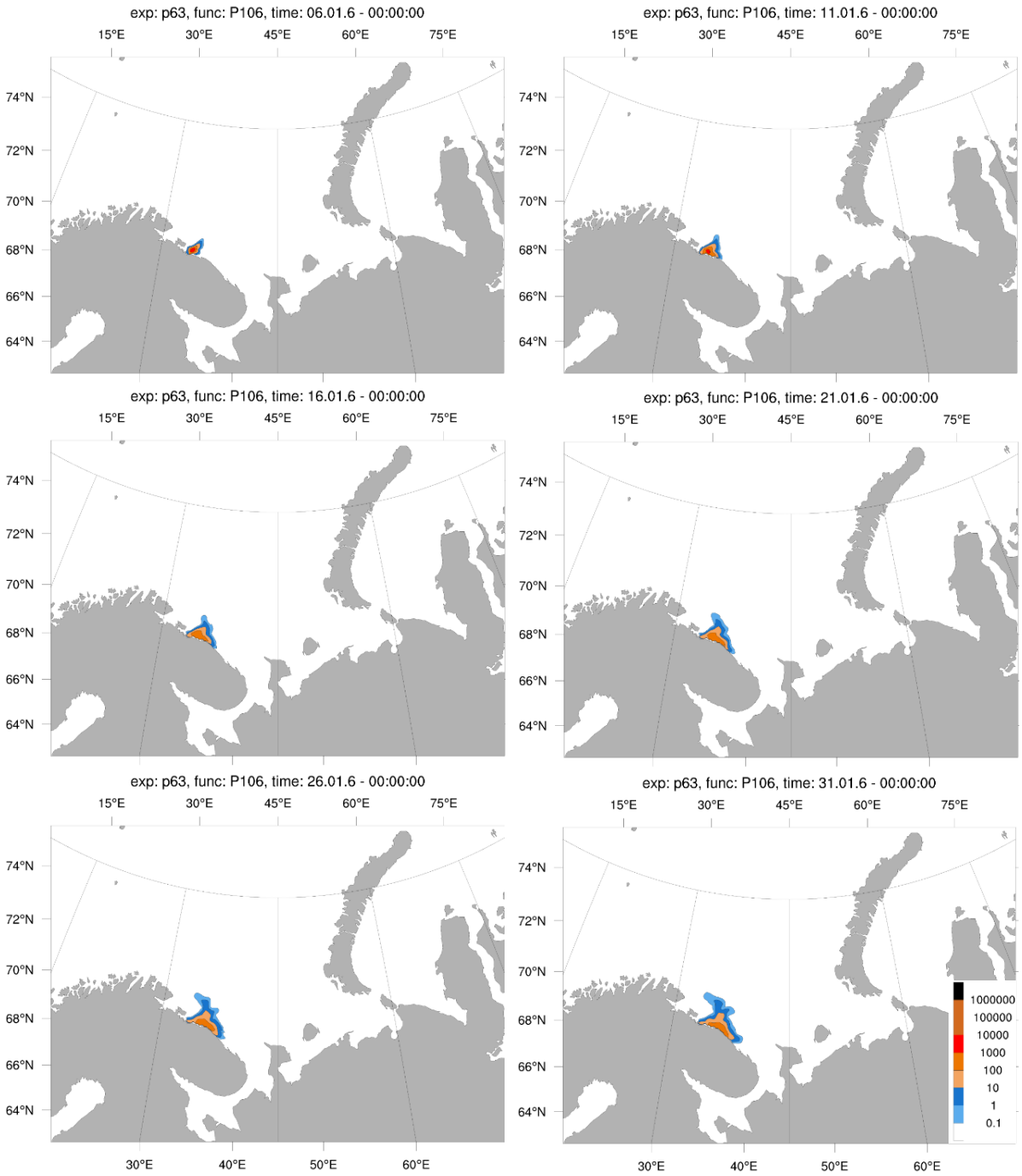

A2.10a. Concentration of ^{137}Cs (Bq/m^3) at the depth of 45 m following an instantaneous release of 50 TBq at surface in winter. Maps show distribution of the contamination at 5, 10, 15, 20, 25 and 30 days after the release.

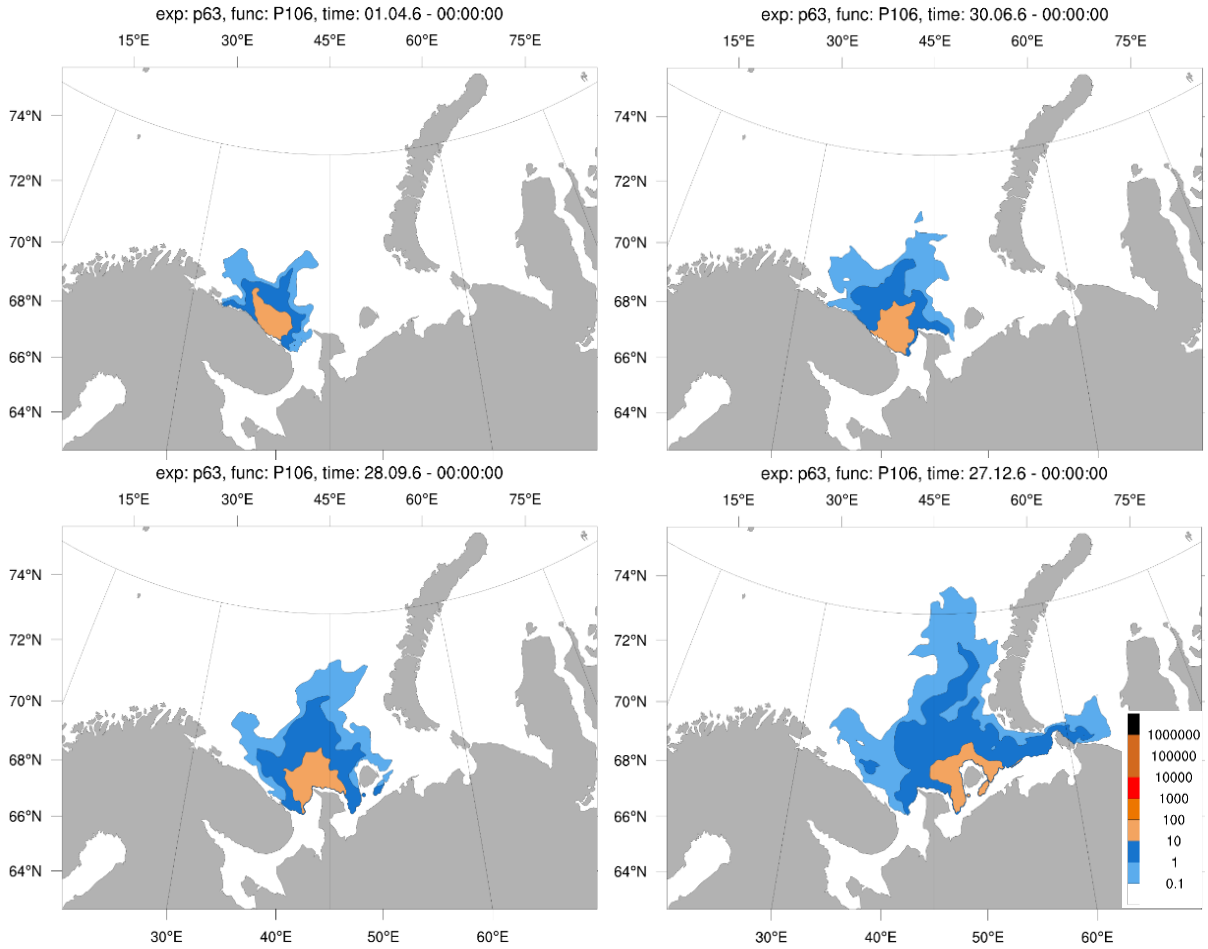

A2.10b. Concentration of ^{137}Cs (Bq/m^3) at a depth of 45 m, following an instantaneous release of 50 TBq at surface in winter. Maps show distribution of the contamination at 3, 6, 9 and 12 months after the release.

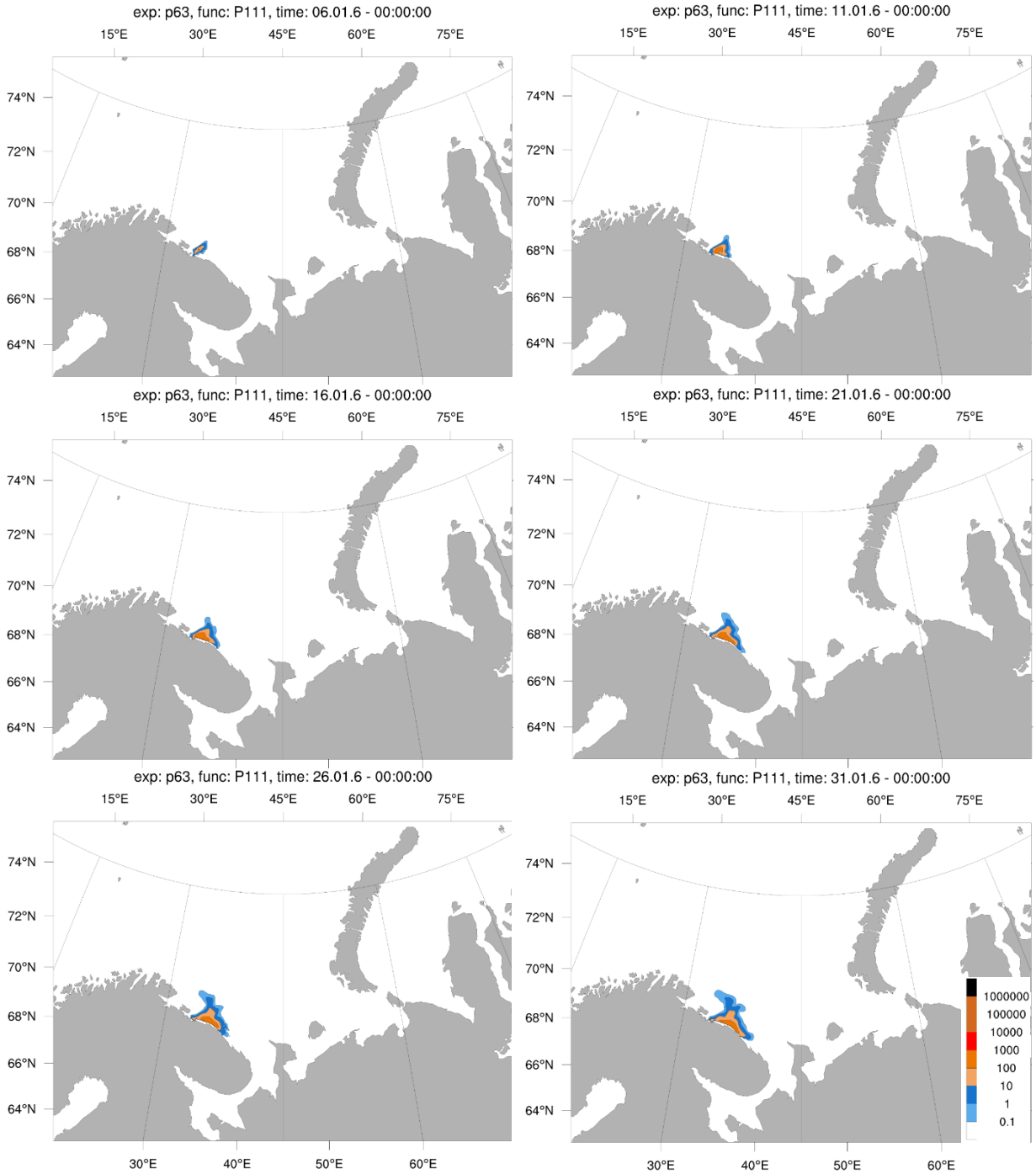

A2.11a. Concentration of ^{137}Cs (Bq/m^3) at a depth of 105 m, following an instantaneous release of 50 TBq at surface in winter. Maps show distribution of the contamination at 5, 10, 15, 20, 25 and 30 days after the release.

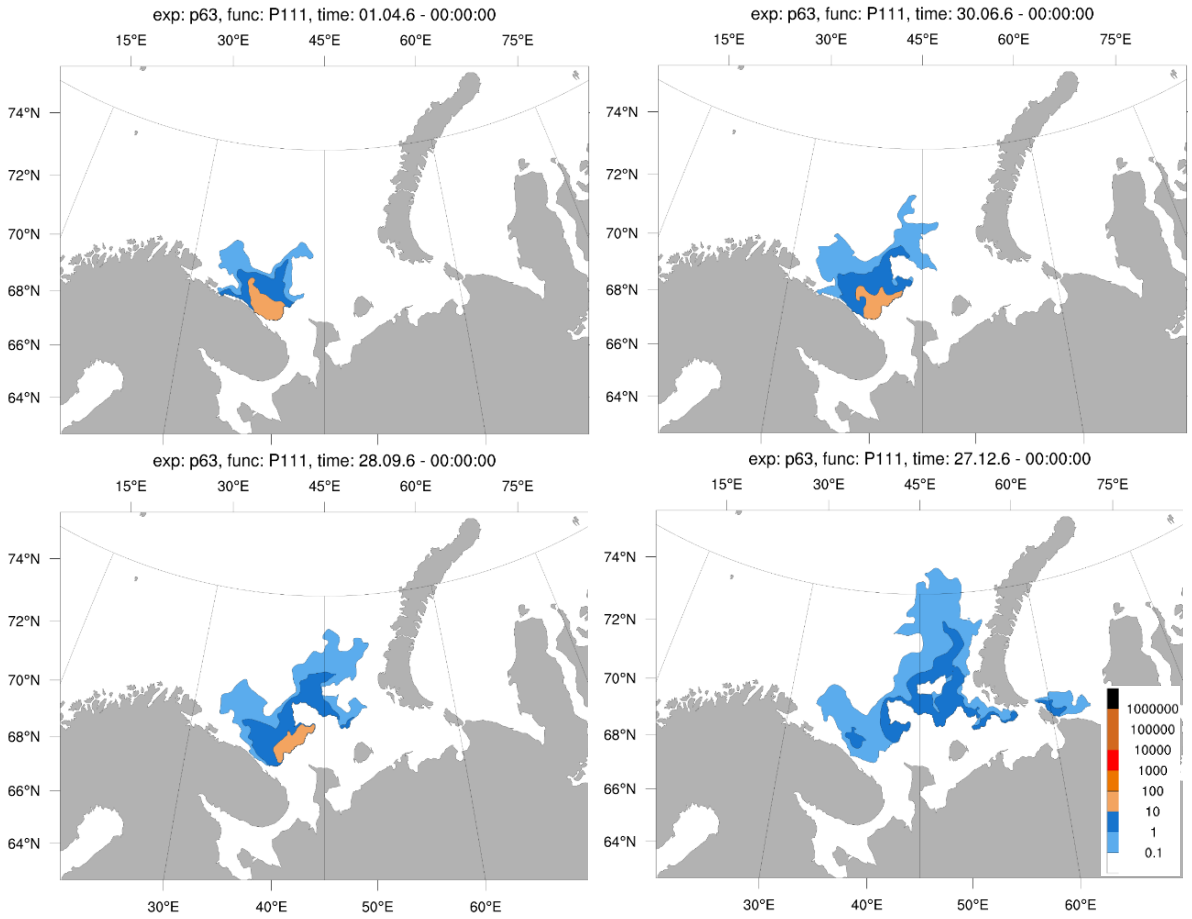

A2.11b. Concentration of ^{137}Cs (Bq/m^3) at a depth of 105 m, following an instantaneous release of 50 TBq at surface in winter. Maps show distribution of the contamination at 3, 6, 9 and 12 months after the release.

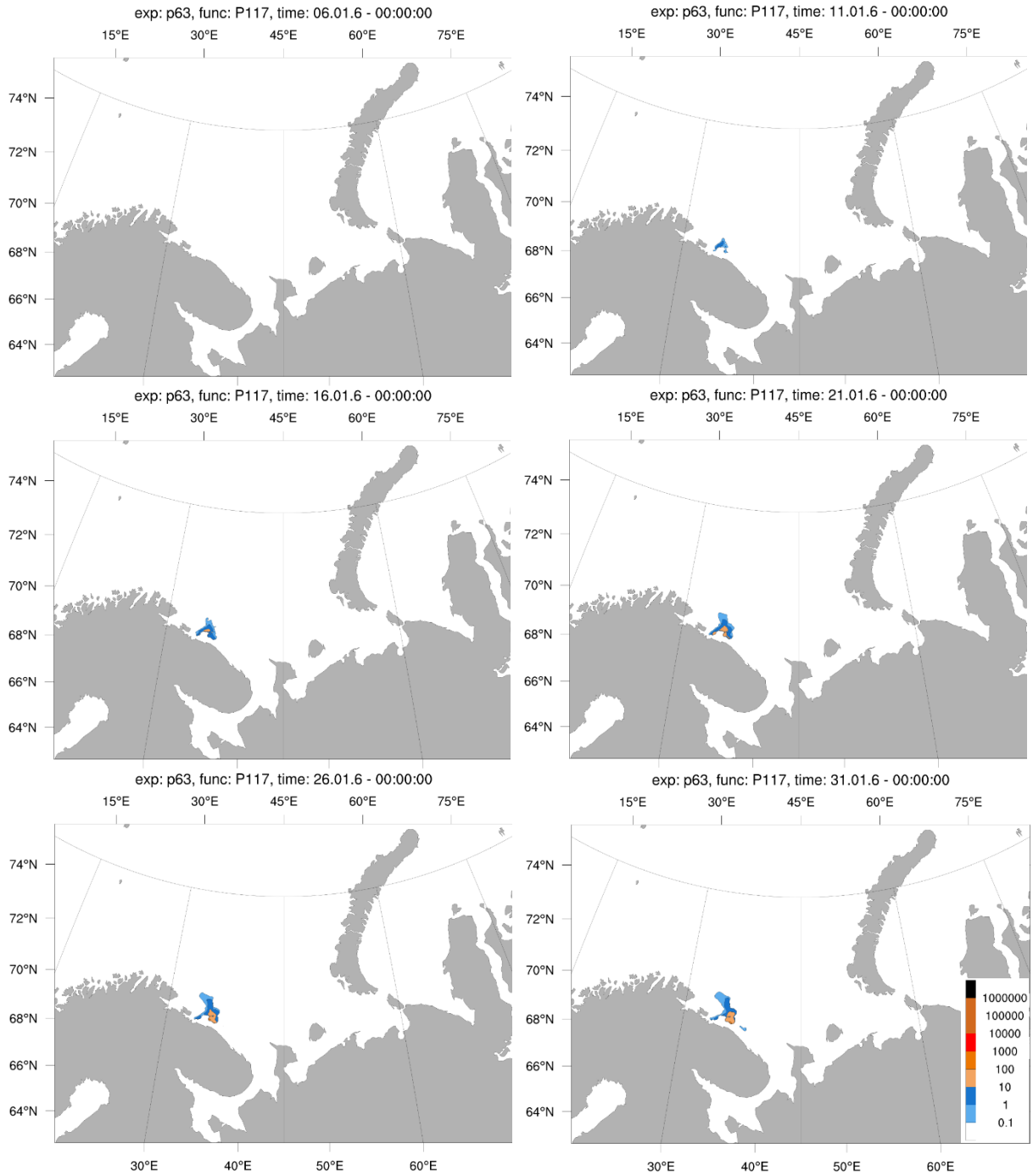

A2.12a. Concentration of ^{137}Cs (Bq/m^3) at a depth of 205 m following an instantaneous release of 50 TBq at surface in winter. Maps show distribution of the contamination at 5, 10, 15, 20, 25 and 30 days after the release.

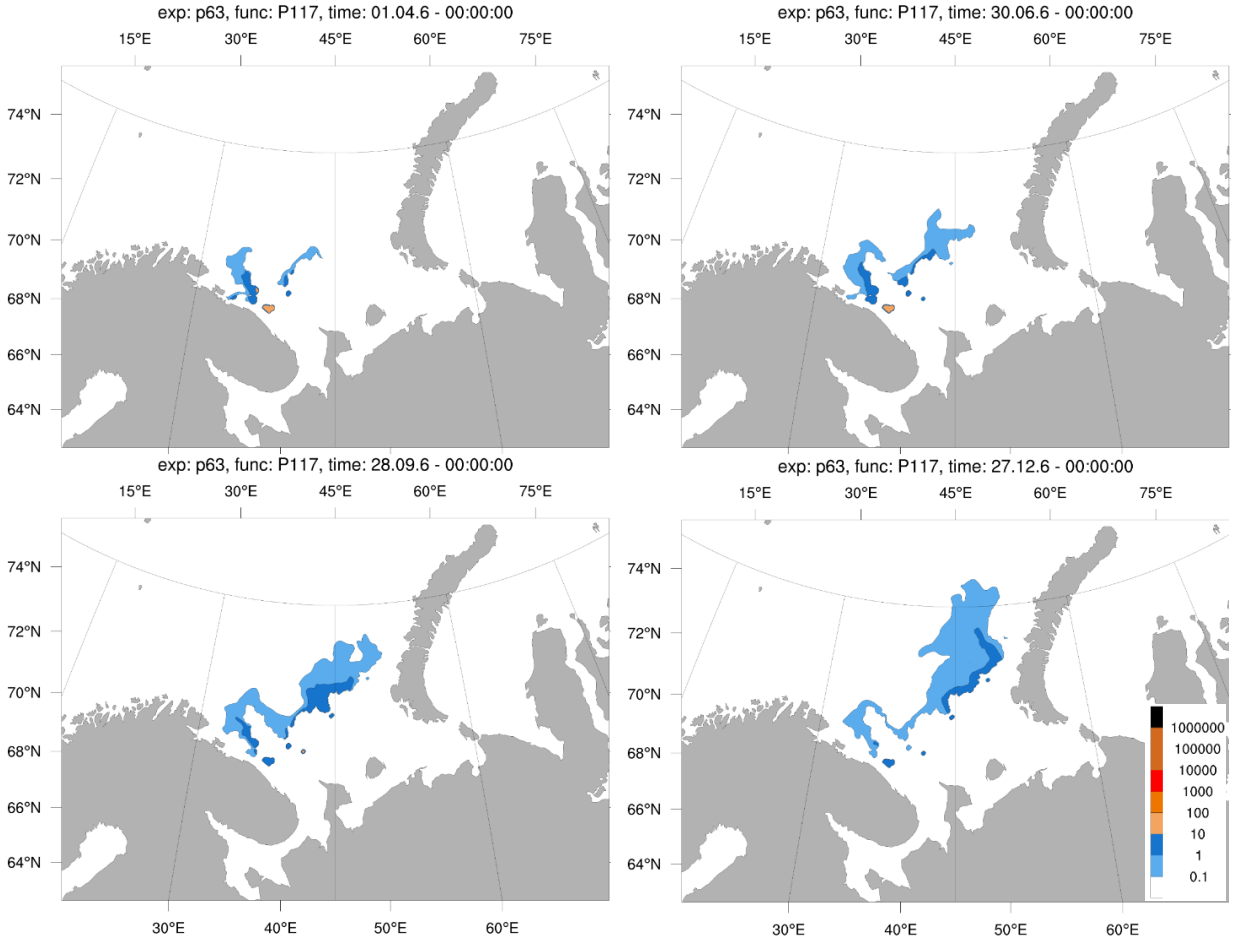

A2.12b. Concentration of ^{137}Cs (Bq/m^3) at a depth of 205 m, following an instantaneous release of 50 TBq at surface in winter. Maps show distribution of the contamination at 3, 6, 9 and 12 months after the release.

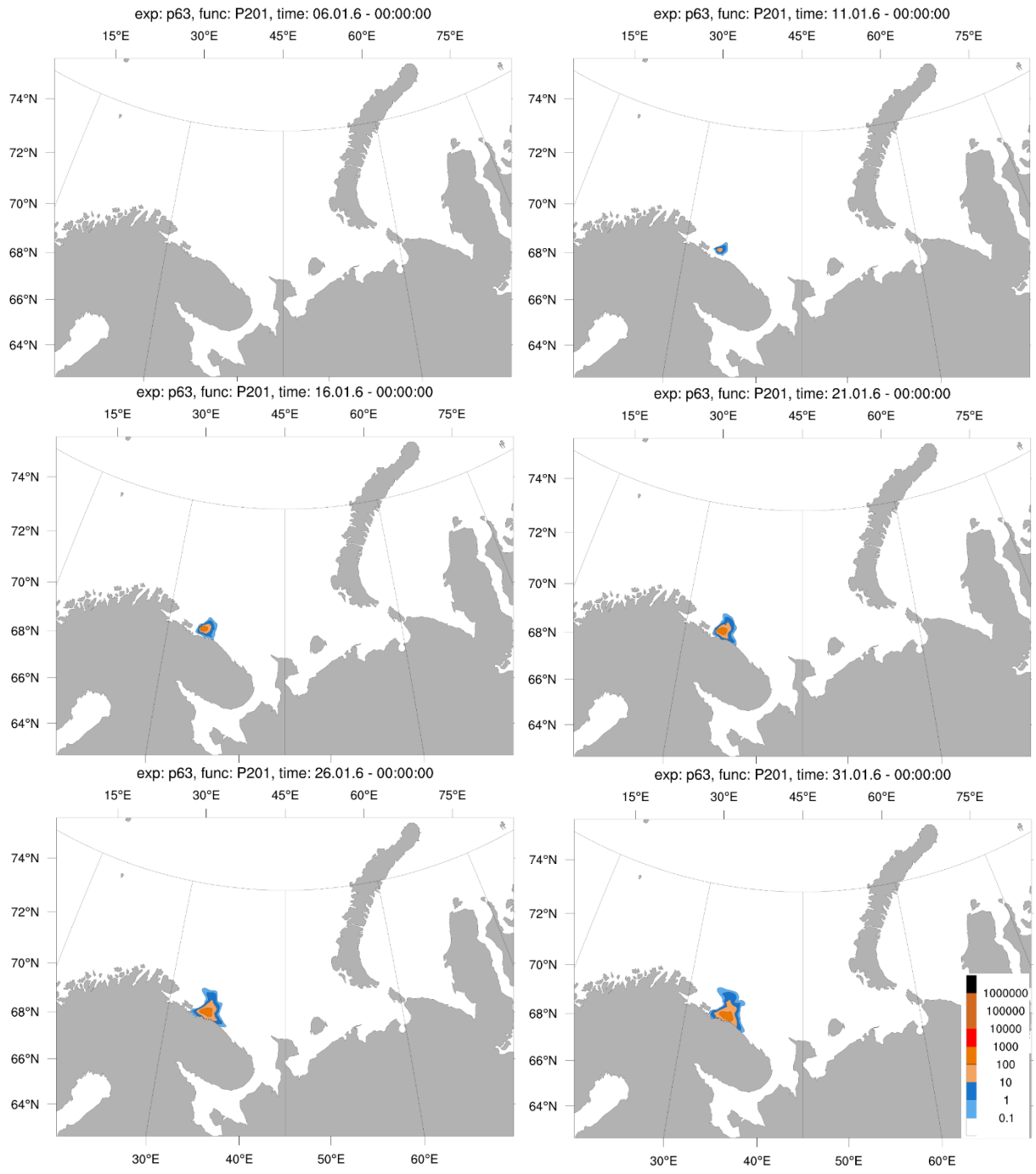

A2.13a. Concentration of ^{137}Cs (Bq/m^3) at the surface following an instantaneous release of 50 TBq at a depth of 205 m in winter. Maps show distribution of the contamination at 5, 10, 15, 20, 25 and 30 days after the release.

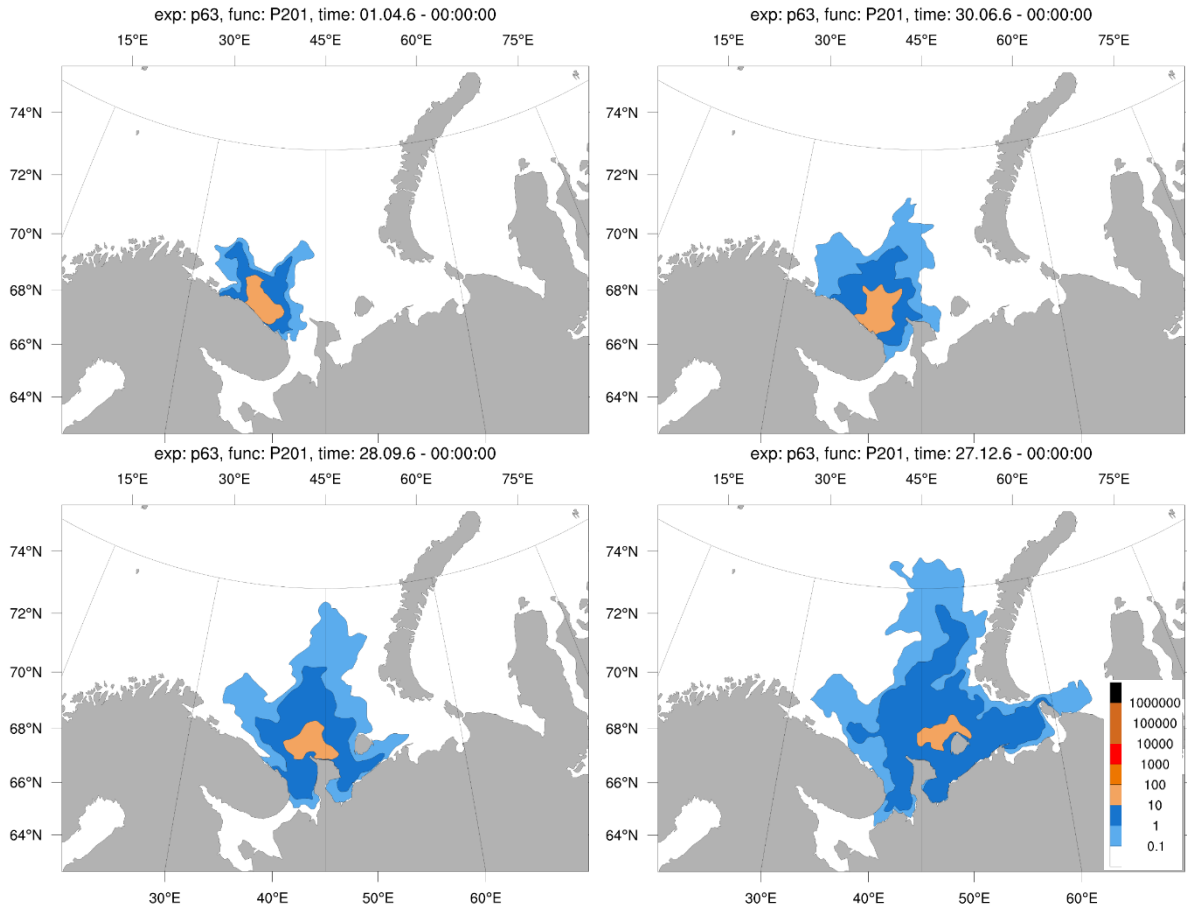

A2.13b. Concentration of ^{137}Cs (Bq/m^3) at the surface following an instantaneous release of 50 TBq at a depth of 205 m in winter. Maps show distribution of the contamination at 3, 6, 9 and 12 months after the release.

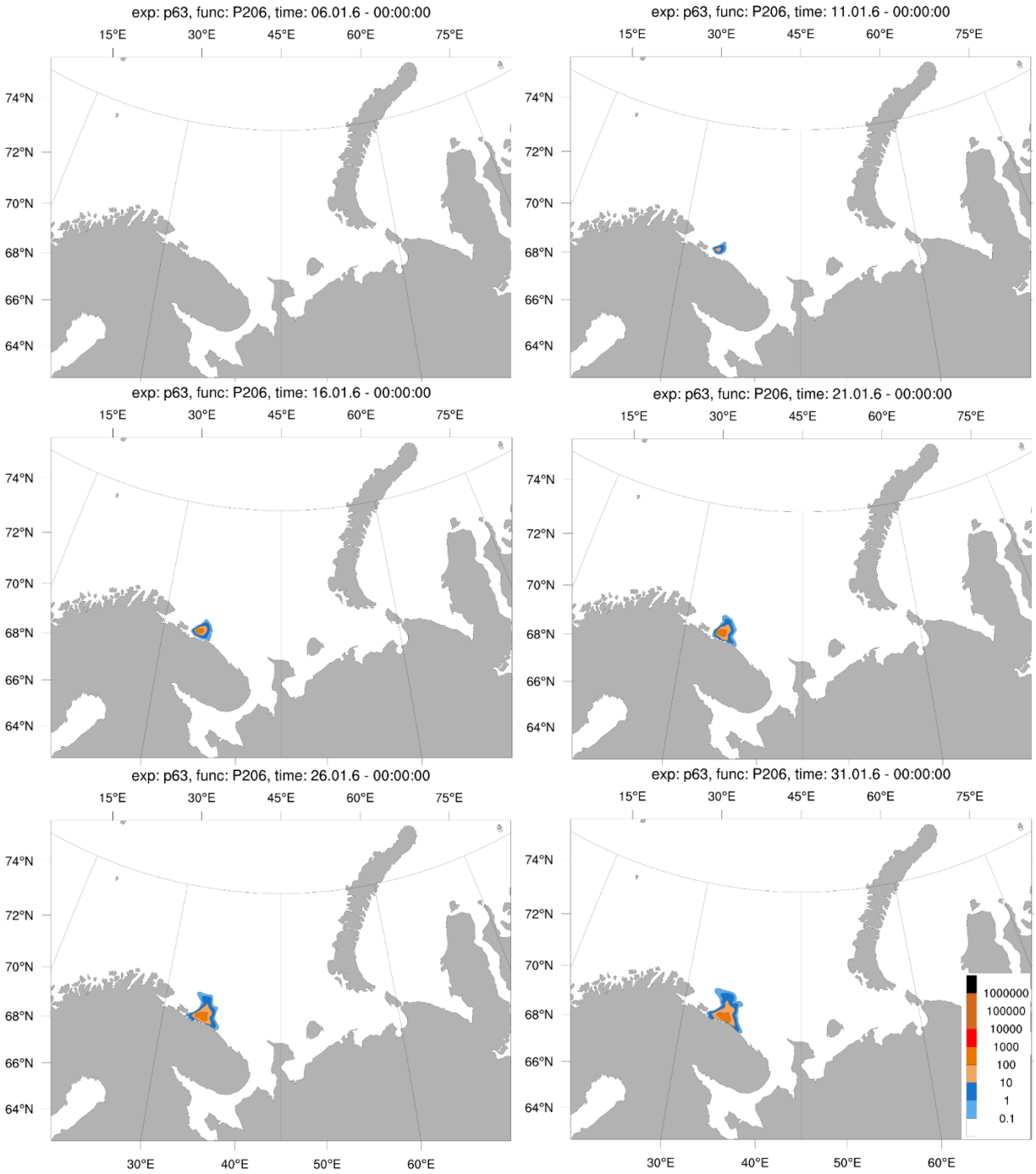

A2.14a. Concentration of ^{137}Cs (Bq/m^3) at a depth of 45 m, following an instantaneous release of 50 TBq at a depth of 205 m in winter. Maps show distribution of the contamination at 5, 10, 15, 20, 25 and 30 days after the release.

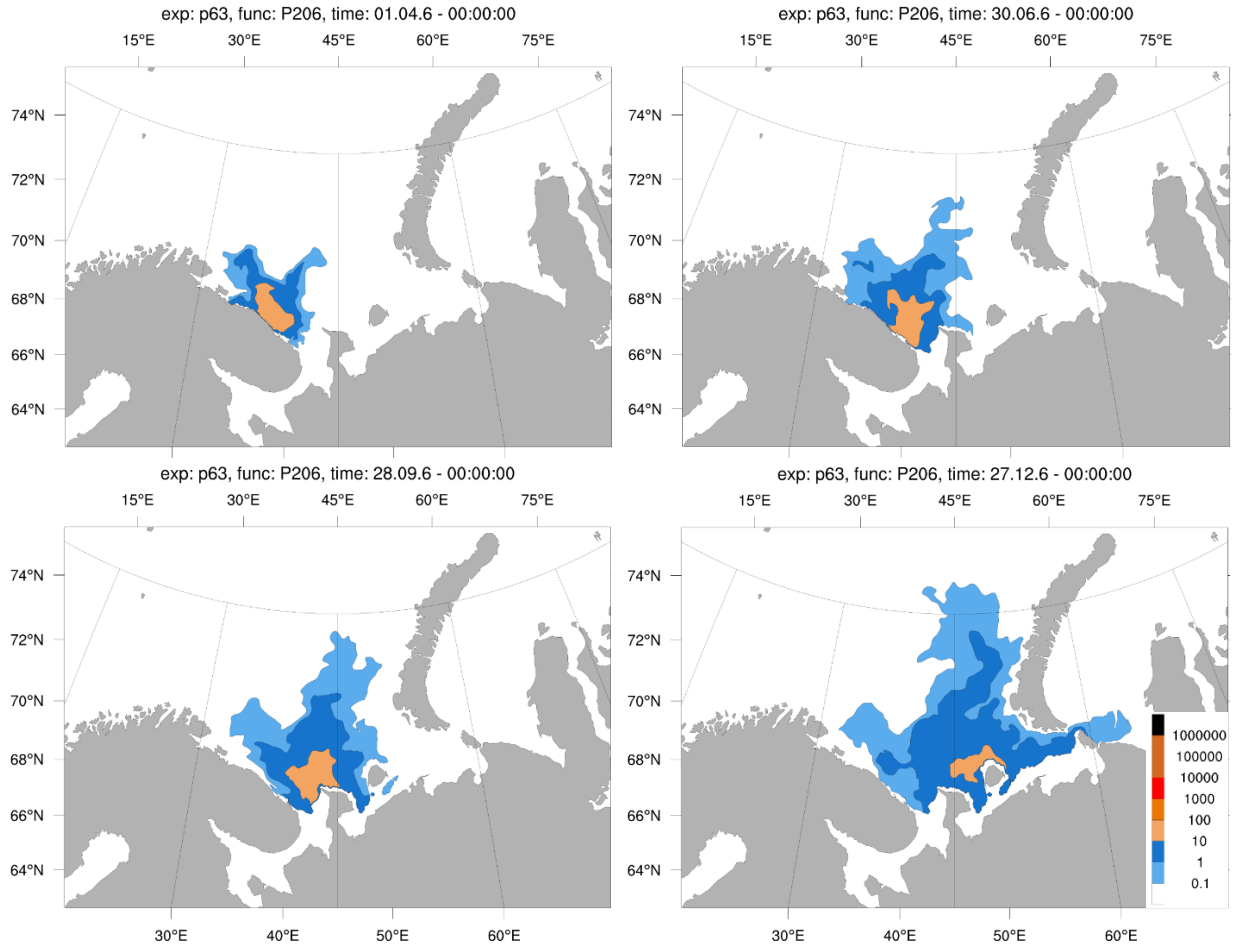

A2.14b. Concentration of ^{137}Cs (Bq/m^3) at a depth of 45 m, following an instantaneous release of 50 TBq at a depth of 205 m in winter. Maps show distribution of the contamination at 3, 6, 9 and 12 months after the release.

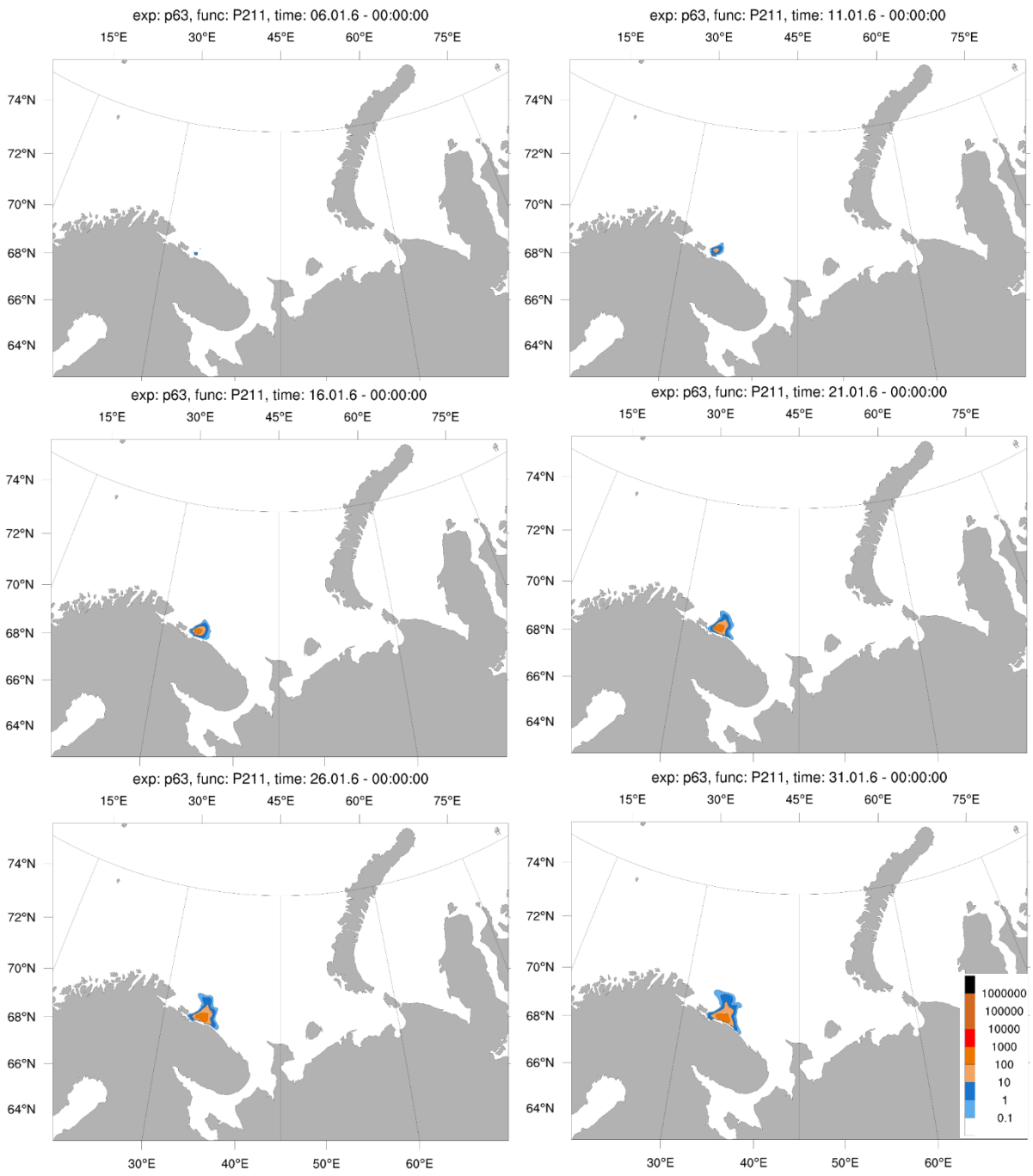

A2.15a. Concentration of ^{137}Cs (Bq/m^3) at a depth of 105 m, following an instantaneous release of 50 TBq at a depth of 205 m in winter. Maps show distribution of the contamination at 5, 10, 15, 20, 25 and 30 days after the release.

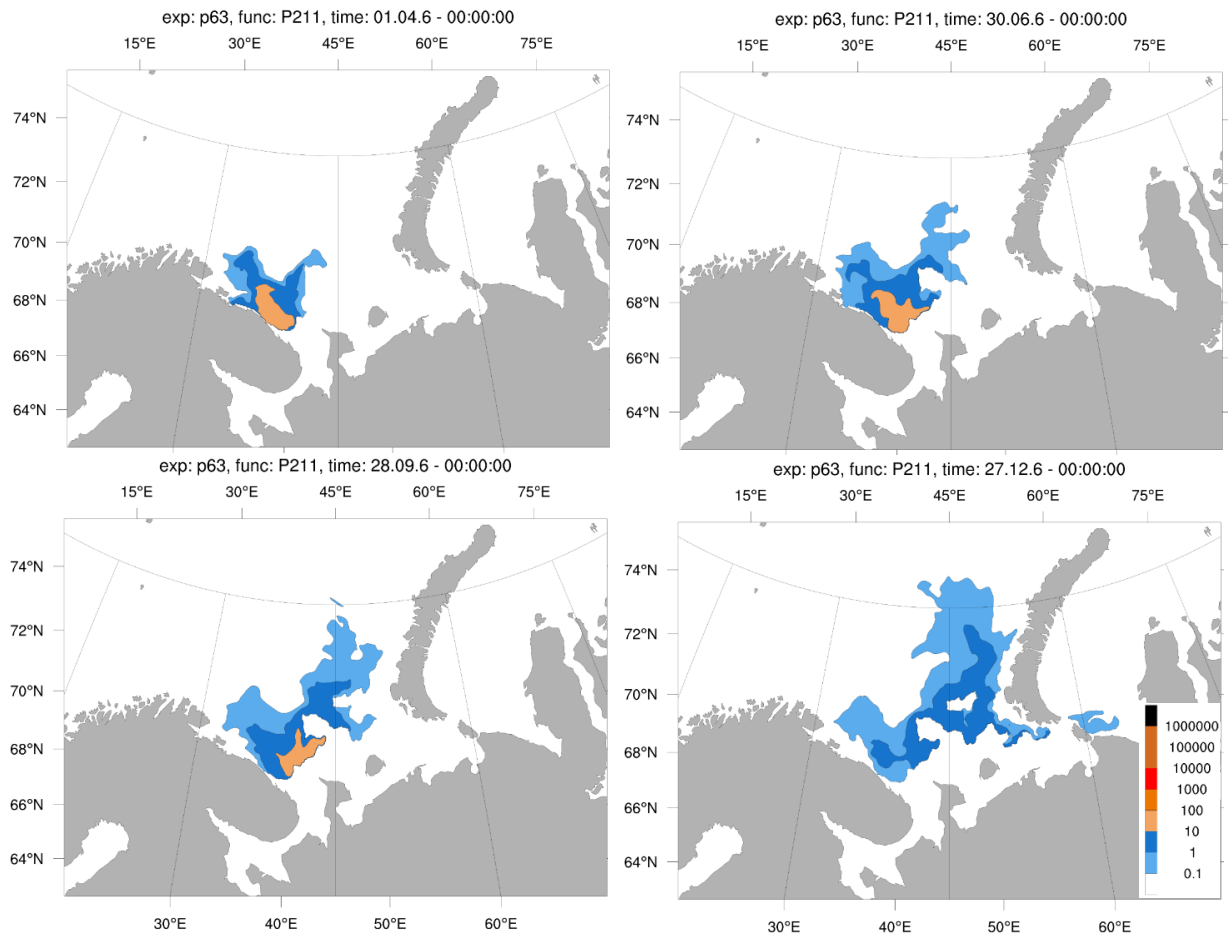

A2.15b. Concentration of ^{137}Cs (Bq/m^3) at a depth of 105 m, following an instantaneous release of 50 TBq at a depth of 205 m in winter. Maps show distribution of the contamination at 3, 6, 9 and 12 months after the release.

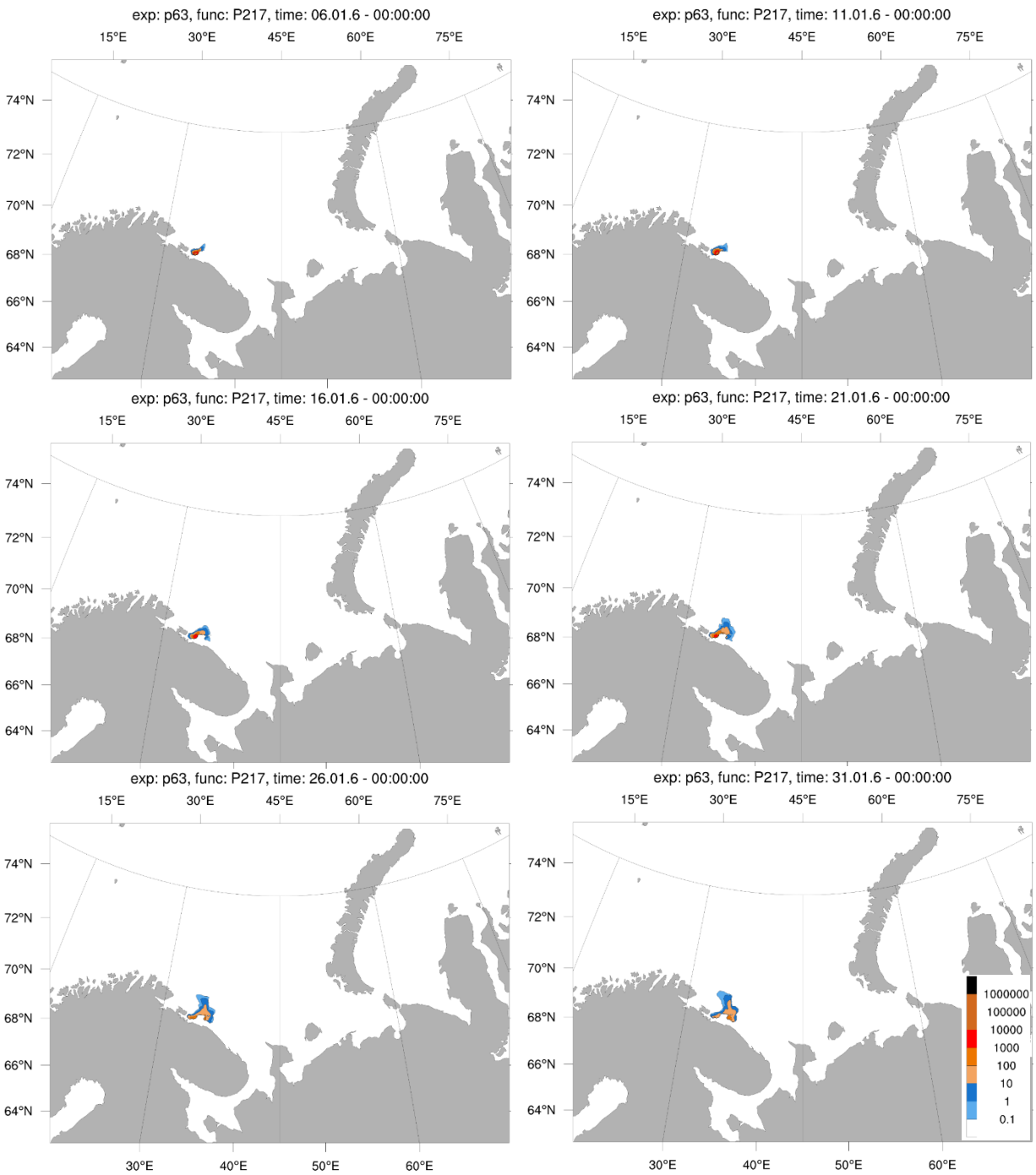

A2.16a. Concentration of ^{137}Cs (Bq/m^3) at a depth of 205 m, following an instantaneous release of 50 TBq at a depth of 205 m in winter. Maps show distribution of the contamination at 5, 10, 15, 20, 25 and 30 days after the release.

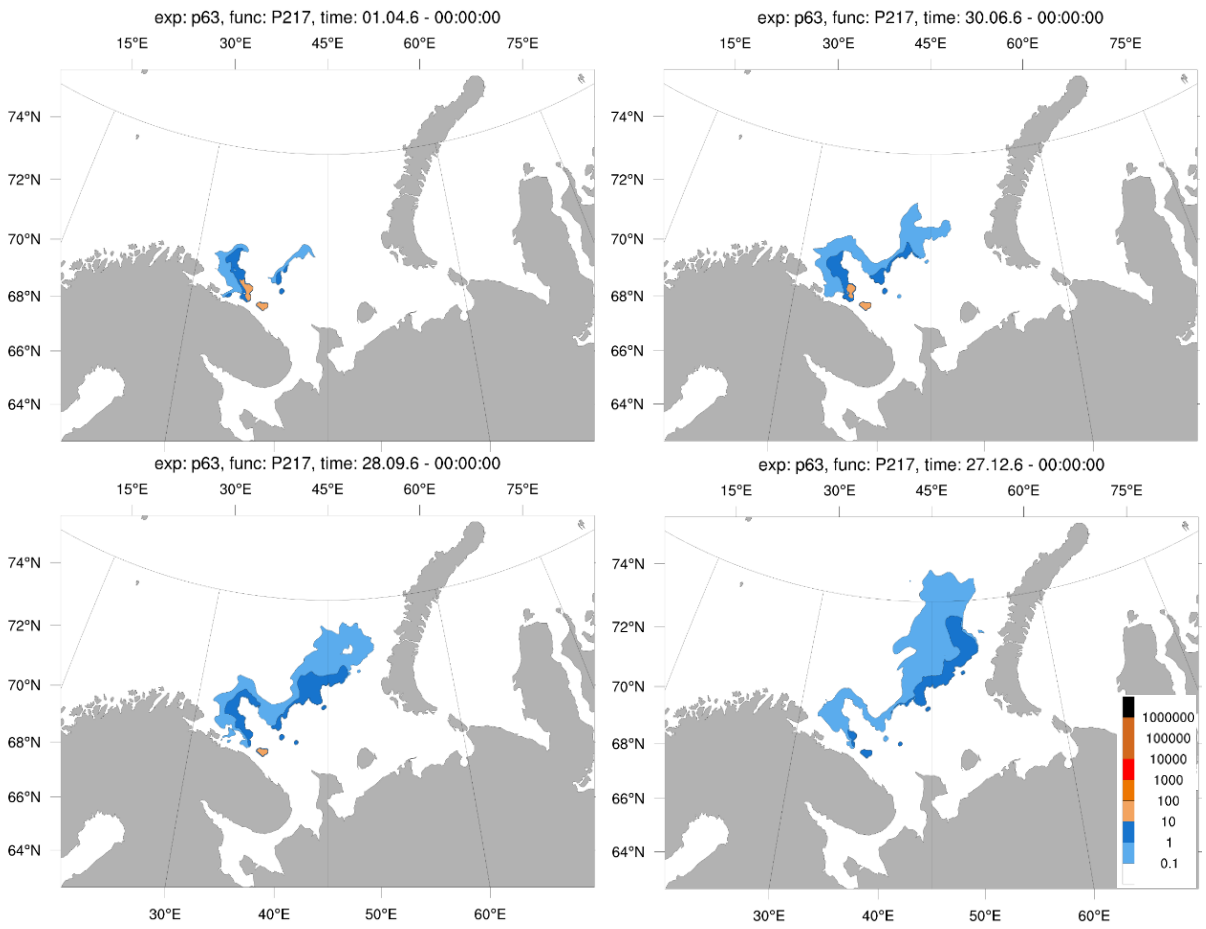

A2.16b. Concentration of ^{137}Cs (Bq/m^3) at a depth of 205 m, following an instantaneous release of 50 TBq at a depth of 205 m in winter. Maps show distribution of the contamination at 3, 6, 9 and 12 months after the release.

Appendix 3: Derivation of a threshold for deposition assessment in atmospheric dispersion modelling

Selecting the (meteorological) worst case scenarios for a given release based on the total deposition over the entire land mass of Norway might be misleading. This means that a worst case may be identified even where maximum deposition levels are relatively low (compared to other cases) because a large fraction of the released material has been deposited over the entire land area. Another way to look at the problem is to set a threshold whereby trivial deposition levels are ignored. This would then focus the analyses on areas where deposition is highest and might lead to the identification of a different suite of worst case meteorological scenarios.

The *de minimis* level of 10 µSv/y is commonly used as means of identifying trivial exposure situations for humans.

Attempts have been made to use a very simple system for establishing the threshold but will need to account for the major human exposure pathways given a deposition event – these being external and internal exposures.

The external component that might contribute to the threshold is the most straightforward. A ^{137}Cs dose conversion coefficient (e.g. µSv/h per Bq/m^2) can be used in conjunction with a 1 year period (essentially assuming a person stood over the contamination continually) to derive the annual dose for a unit Bq deposition. The *de minimis* level is then divided by this value to derive the threshold.

The internal component that might contribute to the threshold is more complicated albeit that numerous simplifying assumptions are also made here. In this case a ^{137}Cs aggregated transfer factor (Bq/kg f.w. per Bq/m^2 deposition) is applied to get the activity in a given food product. In this case reindeer meat has been selected. Thereafter the annual dose for a person is calculated by multiplying by the amount of food ingested annually and applying an (internal) dose conversion coefficient. Finally the threshold is derived by dividing the de *minimis* level by the annual dose per unit deposition. The parameters used have been selected to be conservative, e.g. the initial Tag_0 has been assumed taking no account of a reduction in this value with time.

What is found from the analysis is that the internal component dominates with regards to an effect on influencing the threshold. The threshold itself lies at around approximately 10 Bq/m^2 ^{137}Cs.

Appendix 4: Modelling transfer of radionuclides through food-chains

A. Marine food-chain model description

A model, based on the work of Thomann (1981), Landrum et al. (1992), and Fisher (2002), was used to simulate the uptake of radionuclides via food and water by aquatic organisms and transfer through marine food-chains. Excretion/ elimination rates were assumed to be independent of the uptake route, the assimilation efficiency was assumed to be independent of food type, and predators were assumed not to assimilate the activity concentration in the gut content of their prey. Further assumptions were that the zooplankton were a homogeneous group, described by specified parameter values rather than by ranges, and that the growth rate for all organisms was zero. This last assumption may be a less robust than the others (Thomann, 1981), but the complexity of the weight dynamics for the organisms in question would require further, more detailed study and were anticipated as adding little in terms of yielding more accurate prognoses. The time-dependent transfer of radionuclides to considered marine organisms (molluscs, crustaceans fish, seal and sea bird) within the food chain can be described by simple, first-order differential equations. This approach was adopted as opposed to using only equilibrium based concentration ratios because kinetic models are much better suited to simulating transfer through food-chains when seawater concentrations are changing rapidly as in the case of accidental releases (i.e. steady state/equilibrium conditions are not prevalent). An earlier version of the model is described in Brown et al. (2004) with a condensed explanation provided below:

For prey species (i.e. phytoplankton for mollusk; zooplankton for fish , steady state conditions between radionuclide activity concentrations in biota and water are assumed, allowing the application of concentration ratios[22]:

$$C_p = CR_p \cdot C_w \tag{1}$$

Where:

C_p is the radionuclide activity concentration in prey species (Bq kg^{-1} f.w.);

CR_p is the concentration ratio for prey species (l kg^{-1}); and

C_w is the radionuclide activity concentration in sea water (Bq l^{-1}).

For Fish, accounting for radionuclide uptake via water and food, the following equation is applied:

$$\frac{dC_f}{dt} = AE_f \cdot IR_f \cdot C_P + k_{uf} \cdot C_w - C_f \cdot k_{ef} \tag{2}$$

Where:

[22] Concentration Ratio = Activity concentration within an organism relative to that in (normally filtered) water.

AE_f is the assimilation efficiency (dimensionless) for fish;

IR_f is the ingestion rate per unit mass of fish (kg f.w. d^{-1} per kg f.w.);

k_{uf} is the uptake rate of radionuclide to fish directly from water column (d^{-1});

C_f is the activity concentration in fish (Bq kg^{-1} f.w.);

k_{ef} is the depuration rate from fish (d^{-1}).

Similar equations are used for mollusk and for crustaceans but using parameters appropriate for these organism groups. An overview is provided in Table A4.1 with the provenance of the data given in each case. Modelling the kinetics of radiocaesium transfer for crustaceans was problematic owing to the large and varied diet of this organism group. For the purposes of this work, this category of biota was assumed to be a large crustacean preying on mussels and scavenging on the remains of pelagic organisms. The consistency of prey species has been crudely assumed to be formed from 50 % mollusk and 50 % fish. In practice, this means that the input values of C_p for the crustacean model have been derived from the output of the fish and mollusk models.

One way to consider radionuclide transfer to seals, based on the work of Brown et al. (2004), is through Eq. 3.

$$\frac{dC_s}{dt} = \sum_{1}^{n} (x_i . AE_s \cdot IR_s \cdot C_i) - C_s \cdot k_{es} \qquad (3)$$

Where:

x_i is the fraction of the diet associated with dietary component "i"

$AE_{r,i}$ is the assimilation efficiency (dimensionless) for dietary component "i"

IR is the ingestion rate per unit mass of seal (kg f.w. d^{-1} per kg f.w.)

C_i is the activity concentration in the dietary component "i" (Bq kg^{-1} f.w.)

C_s is the "whole body" activity concentration in the seal (Bq kg^{-1} f.w.)

k_{es} is the effective loss rate from seal (d^{-1}) – incorporating both excretion rate and physical decay of the radionuclide

A similar approach can be adopted to model the time varying activity concentrations in seabirds, C_b, with a requirement to then provide specific values for the parameters IR_b (the ingestion rate per unit mass for seabirds), AE_b (the assimilation efficiency of radiocaesium for seabirds) and k_{eb} (the effective loss rate of radiocaesium for seabirds).

An ingestion rate, IR_s, of 0.072 kg f.w. day^{-1} per kg f.w. seal was derived by Gwynn et al. (2006) using allometric relationships (Nagy, 2001) for carnivora (Eq. 4)

$$FMI = 0.348M^{0.859} \quad (4)$$

where FMI is the fresh matter intake (g/day) and M is the mass of the seal (g).

In a similar way, Nagy (2001) provides the allometric relationship for marine birds (Eq. 5):

$$FMI = 3.221M^{0.658} \quad (5)$$

where FMI is the fresh matter intake (g/day) and M is the mass of the bird (g).

A representative mass of 1.26 kg commensurate with the value used for marine birds in the ERICA Tool (Brown et al., 2008) was used as a default for calculations. This yields an IR_b of 0.28 kg f.w. day^{-1} per kg f.w. seabird.

For seals and sea birds, the assimilation efficiencies for ^{137}Cs were set to unity commensurate with generic values that are normally applied for mammals (Brown et al., 2003b). For the sake of simplicity it was also assumed that the seals and seabirds live entirely off fish. The term x_i =1 in Eq. 3 and C_i is equal to the (time varying) activity concentration in fish derived using the approach outlined earlier. Harp seals, for example, have a varied diet of fish including species such as capelin, polar and Arctic cod and herring. Although they also are known to consume crustaceans, the simplification of the diet was not considered to be unduly problematic. Since a generic group was also being considered in the case of seabirds, similar contentions are valid – assuming the entire diet is based on fish would appear to be a reasonable assumption.

A whole-body biological half-life of 29 days was derived by Gwynn et al. (2006) for ^{137}Cs in an adult ringed seal. This compares to values for grey and harbour seals of 20 days from the Baltic Sea (Holm et al., 2005) and 28 days from the UK and Ireland (Watson et al., 1999). A value of 29 days was adopted in this work as a conservative approximation, i.e. the longer the retention time of a given radionuclide for a specified intake the greater will be the concomitant internal exposure. Deriving biological half-lives for sea birds is a more uncertain process in which recourse was made to the allometric relationships for biological loss provided by Whicker & Shultz (1982) for caesium. The following formula can be applied.

$$k_a = \frac{\ln 2}{18.36\,M^{0.24}}$$

where k_a = the effective loss rate for the animal (d^{-1}), M = mass of animal (kg, f.w.).

This gave a k_b of 0.036 d^{-1} corresponding to a biological half-life of radiocaesium in birds of ca. 19 days. This value appears to be a little on the high side (in view of information concerning other

organism groups) but was likely to provide a conservative estimate of transfer in keeping with accepted approaches to err on the side of caution when model parameters are considered to be uncertain.

An overview of all of the parameters used in the (bio-) kinetic models is presented in Table A4.1.

Table A4.1: Parameters used in the kinetic model for ^{137}Cs in the marine environment

Parameter	**Organism Modelled**	**Value (units)**	**Reference/comment**
CR_p	Fish	130	IAEA (2014); Arithmetic mean value for zooplankton
CR_p	Mollusc	8.5	IAEA (2014); Arithmetic mean value for phytoplankton
AE_f	Fish	0.5 (dimensionless)	Brown et al. (2004)
AE_M	Mollusc	0.5 (dimensionless)	Vive I Batlle et al. (2016); Value form BURN-P model
AE_C	Crustacean	0.5 (dimensionless)	Vives I Batlle et al. (2016); Value from BURN-P model
AE_s	Seal	1 (dimensionless)	Gwynn et al. (2006)
AE_b	(Sea)Bird	1 (dimensionless)	Assumed to be equal to seal
k_{uf}	Fish	0.01 (d^{-1})	Brown et al. (2004)
k_{uM}	Mollusc	1.1 mL g^{-1} (dry) h^{-1} = 26.4d^{-1} = 4.75(d^{-1})	Børretzen & Salbu (2009)
k_{uC}	Crustacean	0.49 (d^{-1})	Brown et al. (2004) for zooplankton
IR_f	Fish	0.009 (kg f.w. d^{-1} per kg f.w.)	Brown et al. (2004)/Large fish
IR_M	Mollusc	0.2 (kg d^{-1} per kg)	Wang et al. (2000) as applied to Mussel (*Perna viridis*)
IR_C	Crustacean	0.027 (kg f.w. d^{-1} per kg f.w.)	Vives I Batlle et al. (2016); Value from K-BIOTA
IR_s	Seal	0.072 (kg f.w. d^{-1} per kg f.w.)	Gwynn et al. (2006)
IR_b	(Sea)Bird	0.28 (kg f.w. d^{-1} per kg f.w.)	Derived allometrically – see main text
k_{ef}	Fish	0.0107 (d^{-1})	ICRP (2009)
k_{eM}	Mollusc	0.04 (d^{-1})	Vives I Batlle et al. (2016); Value derived from D-DAT biological half-life
k_{eC}	Crustacean	0.01 (d^{-1})	Vives I Batlle et al. (2016); Value derived from D-DAT biological half-life
k_{es}	Seal	0.0239 (d^{-1})	Gwynn et al. (2006)
k_{eb}	(Sea)Bird	0.036 (d^{-1})	Derived allometrically – see main text

B. Terrestrial food-chain Model description

A terrestrial food-chain model was used to provide input for both the derivation of ingestion doses for humans and for the assessment of doses to wild plants and animals.

In view of available data, it was most appropriate to split the modeling into flora (Wild grass/grasses, herbs and shrub) and fauna (Deer/herbivorous mammal and rat/burrowing mammal) partly based on the classifications given in UNSCEAR (2008).

Using a variant of the methodology given in UNSCEAR (2008, 2014), the activity concentration in flora can be derived from the total deposition using an expression accounting for interception by foliage, direct deposition onto soil, weathering losses of radionuclides from vegetation and uptake from soil to plant.

In case of an acute deposition the radionuclide content on vegetation at time 't', accumulated via direct deposition from the air, can be calculated (as outlined in Brown et al., 2003b) as:

$$C^{air}_{flora,r} = \frac{f_{flora} \cdot D_{tot,r}}{b_{flora}} \cdot [e^{(-(\lambda_{flw,r}+\lambda_r)\cdot t)}] \qquad (6)$$

where

$C_{flora,r}$ is the radionuclide activity concentration in flora from air deposition (Bq kg^{-1} f.w.)

f_{flora} is the interception fraction for a given flora (dimensionless)

$D_{tot,r}$ is the total deposition of radionuclide 'r' (Bq m^{-2})

$\lambda_{flw,r}$ is the weathering constant for a given flora for radionuclide r(d-1)

λ_r is the decay constant for radionuclide r (d^{-1})

b is standing biomass of the flora(kg m^{-2})

t is time (d)

For the same acute deposition, at time 't', there is also a component of contamination that arises from soil to plant transfer. In this case an assumption is made that for this fraction of the contamination in the plant attributable to root uptake, equilibrium exists between the activity concentration in the plant and the soil.

$$C^{soil}_{flora,r} = \left[\frac{D_{tot,r} \cdot \left[(1 - f_{flora}) + f_{flora} \cdot (1 - e^{-\lambda_{flw,r} t}) \right] \cdot e^{-\lambda_r t}}{\rho_{soil} \cdot d_{soil}} \right] . CR_{flora,r} \qquad (7)$$

where

ρ_{soil} is the dry soil density (kg m^{-3} d.m.)d_{soil} is the depth of soil within which radionuclide r has become mixed (m) $CR_{flora,r}$ is the soil to plant concentration ratio for radionuclide r (dimensionless)

All other parameters have been described above in Eq. (6). Application of this model also allows for time varying deposition rates to be considered. For this more complex situation, the problem can be solved numerically.

There is an assumption in this model that a representative interception fraction 'f' for a given flora type can be applied for the entire simulation period. Data compilations for agricultural systems in relation to this parameter (IAEA, 2010) indicate that the interception fraction depends on whether dry or wet deposition is occurring, the stage of development of the plant and plant type in question, the capacity of the canopy to retain water, elemental properties of the radionuclide, and other factors such as amount and intensity of rainfall in the case of wet deposition and particle sizes of the deposited material. The approach taken here was, therefore, arguably simplistic but in view of the numerous uncertainties involved should at least provide an indication of contamination levels in food-chains following deposition of contamination and at least constitutes an attempt to model the dynamics of interception and loss from flora in contrast to approaches considering soil to plant transfer only. In addition to the interception fraction, biomass, which clearly relates to the stage of development of the plant, also requires further consideration as an important model parameter.

Tømmervik et al. (2009) reported a biomass of 4.13 tonnes/hectare for a 'Field layer' (forbs and grasses) in Northern Finland. This understory biomass would appear to be fairly typical for many other categories of shrub, field, bottom (moss and lichen) layers in mountain birch forests and mountain heaths in this region: Tømmervik et al. (2009) report 1.5 to 5.35 tonnes/hectare for such categories from northern Fenno-scandinavia, including Finnmark). A biomass of 4 tonnes/hectare corresponds to 400 g/m^2. Although Schino et al. (2003) studied grasslands in mountainous areas of central Italy, the work provides an indication of variations in grass biomass that can arise from seasonality and the presence of different species. The recorded range of grass biomass in this aforementioned study was approximately 60 to almost 700 g m^{-2} providing a useful context for our selection of an appropriate biomass value for 'Wild grass/grasses' and for shrubs.

The start and end of the growing seasons (based on data for the period 1982–2002) in the Artic/Alpine and Northern boreal zones to which large areas of Finnmark belong, are June 4-20th and 21-24th September respectively (Karlsen et al., 2006) with a peak in growth occurring towards the end of July/beginning of August. The period selected for the hypothetical release from K-27 was August and September, coinciding with the period where any salvage activity is likely to take place from practical considerations. The deposition would thus occur in the middle of the growing season but following peak growth removing the requirement to model the effect of growth dilution on radionuclide levels. Modelling of this phenomenon would be required were determinations needed for the period coinciding with rapid vegetation biomass increases early in the growing season.

The interception fraction, f, for Cs and grass varies from 0.84 (dry deposition) to 0.027 (wet deposition heavy rain) (IAEA, 2010). A default of 0.43 has been selected for this analysis simply based on the value falling midpoint between the maximum and minimum values reported above. This yields a mass interception fraction f_B of 1.1 (m^2 kg^{-1}) a value which was considered as being typical for Cs deposited on grass following the Chernobyl accident (IAEA, 2010). Owing to the lack of specific information on shrubs, the same default values as grass have been used. As noted by Tømmervik et al. (2009), the shrub layer has a biomass of a similar order of magnitude to the field layer in mid growing season. Although leaf area and surface roughness etc. might be expected to be different between grasses and shrubs the similarity purely in terms of above ground mass available to intercept contaminants render the assumption of similar mass interception fractions a reasonable one. The differences in interception between different elements reflect their different valencies. Plant surfaces are negatively charged and thus may be considered as analogous to a cation exchanger (IAEA, 2009). Therefore, the initial retention of anions such as iodide is less than for polyvalent cations, which seem to be very effectively retained on plant surface. For analyses of data for Chernobyl deposition in Germany, the mass interception factors increase in the order ^{106}Ru, ^{131}I, ^{137}Cs, ^{140}Ba, with these radionuclides having been deposited during the same rainfall event (IAEA, 2009). The highest values were observed for ^{140}Ba, which behaves similarly to strontium. Barium is a bivalent cation, and seems to be more strongly retained on the negatively charged plant surface than the monovalent caesium cation.

A mass interception of 1.4 and 0.7 (m^2 kg^{-1}) for ^{137}Cs and ^{90}Sr has been used by Golikov et al. (2004) in modelling the interception by lichen and subsequent transfer of these radionuclides through Arctic foodchains. Aside from the apparent discrepancy with observation for plants – where the magnitude of f_B is linked with valency – these values constitute a seldom characterization of the apposite process of interception for lichens. Using an assumed lichen biomass of 400 g m^{-2} based loosely on the information of Tømmervik et al. (2009), this information yields interception fractions, of 0.56 and 0.28 for Cs and Sr respectively.

Weathering rates for grass have been derived from the extensive analyses of data undertaken elsewhere (IAEA, 1996). Mitchell (2001) provides an overview of models concerning the transfer radionuclides to fruits. In order to model weathering of radionuclides on plant surfaces, an effective retention half-time was derived for use in the FARMLAND model. A single value of 11 d gave the best fit to experimental data giving a radionuclide independent rate constant of 6.3×10^{-2} d^{-1}. The similarity of this value with those applied for grass has led to the application of the same default values for both vegetation categories. Golikov et al. (2004) modelled the loss of ^{137}Cs and Sr-90 from lichen using short-term and long-term ecological half-lives. For both radionuclides the short-term ecological half-life (1 and 2 years for ^{90}Sr and ^{137}Cs respectively) accounted for losses from the predominant fraction of deposited activity. Longer retention half-lives for ^{137}Cs in lichen have been reported by Kirchner & Daillant (2002), from their own and other studies, falling between 2.6 to 4.9 years. In view of these data and consideration of the fact that the long-term ecological half-life from Golikov et al. (2004) is ca. 20 years for ^{137}Cs and ^{90}Sr, a default weathering loss rate of 5 years, corresponding to the upper end of the values reported by Kirchner & Daillant (2002), has been applied for both radionuclides in our model.

The parameters have been assigned different default values as shown in Table A4.2. Two categories of flora –Wild grass/grasses, and shrubs – taken to be representative of berry plants such as Vaccinium spp.

Table A4.2. Parameters used in Terrestrial food-chain model.

Parameter	Dependencies : flora, radionuclide	Value	Units and notes	References
ρ_{soil}		1550	kg m^{-3} typical soil densities for Finnmarksvidda rnage between 1.4 and 1.7 g cm^{-3}	Uhlig et al. (2004)
d_{soil}		0.05	m, Assumed depth of initial contamination following a deposition event	
f	Wild grass/grasses, Cs Wild grass/grasses, Sr	0.43 0.66	(Unitless) f varies from 0.84 (dry deposition) to 0.027 (wet deposition heavy rain) (IAEA, 2010) Bivalent Sr-90 will have a higher f than monovalent Cs (see main text)	IAEA, 2010 IAEA, 2009
f	Shrub, Cs Shrub, Sr	0.43 0.66	As for grass As for grass	
f	Lichen, Cs Lichen, Sr	0.56 0.28		Golikov et al. (2004)
b	Wild grass/grasses Shrub Lichen	0.4 0.4 0.4	kg m^{-2} kg m^{-2} kg m^{-2}	Tømmervik et al. (2009)
$\lambda_{flw,r}$	Wild grass/grasses, Cs Wild grass/grasses, Sr	5×10^{-2} 5×10^{-2}	d^{-1}, Table VIII, p.37 (IAEA, 1996) d^{-1}, As for Cs (see main text)	IAEA (1996)
$\lambda_{flw,r}$	Shrub, Cs Shrub, Sr	5×10^{-2} 5×10^{-2}	d^{-1}, As for grass d^{-1}, As for grass and Cs	
$\lambda_{flw,r}$	Lichen, Cs Lichen, Sr	4×10^{-4} 4×10^{-4}	d^{-1}, d^{-1},	Kirchner & Daillant (2002) Kirchner & Daillant (2002)

The interception of Sr-90 has been taken to be a factor of (1.7/1.1 based upon the ratio of ^{140}Ba to ^{137}Cs for Chernobyl from IAEA (2009). According to Andersson et al. (2011), there are no clear differences between the weathering rates for grass that can be attributed to radioceasium and radiostrontium. From this observation the same default value has been used for both radionuclides.

Limitations to the use of concentration ratios[23], CRs, arise from an incompatibility of the application of empirical data based on the long term post depositional conditions to the period directly following an accident. The CR values used (Table A4.3) are based on empirical datasets from field investigations collated to avoid inclusion of data pertaining to the period directly following depositional events (global fallout and Chernobyl accident deposition for some radionuclides such as Cs, Pu, Sr and Am) and thus should omit values pertaining to surface contamination of vegetation (Beresford et al., 2008b). These default CR data are generally assumed to correspond to, and thus are applicable for, a contaminated soil depth of 10 cm. There is thus an inconsistency with the observed distributions of radionuclides shortly following deposition. Using the Fukushima accident by way of example, Kato et al., (2012) reported that greater than 86% of total radiocaesium and 79% of total ^{131}I were absorbed in the upper 2.0 cm in a soil profile from a relatively contaminated cultivated area sampled, at the end of April 2011, in proximity to (< 50 km distant, in a northeasterly direction) the Fukushima Dai-ichi site. A default value of 5 cm has been used for the calculations undertaken in the current assessment. Furthermore, bioavailability of radiocaesium has been observed to decrease with time following its introduction to soils (Vidal et al., 1995) with the implication that CRs based upon long term post depositional datasets might not reflect the transfer occurring in the early phase depositional environment appropriately. Indeed this contention is evidenced by reviews of published information on ^{137}Cs in the soil-plant system shortly after the Chernobyl accident (Fesenko et al., 2009). Finally, soil type, as defined by various soil properties, strongly influences transfer to plants (IAEA, 2010) and there will undoubtedly be differences in the soil types upon which the default data are based and the soil types in Finnmark for which the transfer parameters are applied.

Table A4.3 CRs for terrestrial ecosystem from IAEA (2014) – arithmetic mean values

Element	Organism	CR (Bq kg^{-1} f.w. per Bq kg^{-1} d.w)
Cs	Wildgrass/grasses	1.8
Sr	Wildgrass/grasses	1.8
Cs	Shrubs	2.3
Sr	Shrubs	0.5
Cs	Lichen	4.1
Sr	Lichen	4.8

Although some information exists on soil to grass transfer for the short term after accidents (Fesenko et al., 2009) these data are, by the author's own admission, insufficient for adequate (CR) estimation. This, coupled to the knowledge that, with the model constructed and parameterized in its current configuration, direct contamination by fallout dominates the total activity concentration in vegetation in the initial weeks of simulation renders the application of highly uncertain CR values relatively unimportant.

Contaminated lichens may be an important source of radiocaesium to reindeer during summer (Staaland et al., 1995). For this reason the CR data for this biota category is also included in Table A4.3 and for subsequent modelling calculations (see below).

[23] Concentration ratio = activity concentration in whole organism divided by activity concentration in soil

It is important to note that output data for shrubs have been used as input to the assessment of ingestion doses for humans by assuming that shrub contamination levels provide a reasonable proxy for edible berries.

Finally, translocation is often accounted for in assessments with agricultural systems. Translocation is the process leading to the redistribution of a chemical substance deposited on the aerial parts of a plant to other parts that have not been contaminated directly (IAEA, 2010). Since the hypothetical accident has been assumed to coincide with the time of year when berries might be harvested the requirement to account for this process was not obvious and was therefore not attempted.

For mammals, examples of (bio)kinetic model for terrestrial environments have been published in the open literature and one of these, the so-called FASTer model, has been selected for further application (Brown et al., 2003b; Beresford et al., 2010). For herbivorous mammals, the input data used can be those specifying the activity concentrations in grass as expressed above. Details are required regarding biokinetic parameters for various representative animals/fauna as described below.

$$\frac{dC_{r,a}}{dt} = \sum_{i=1}^{i=n}\left(x_i . AE_{r,i} . FMI/M . C_{r,i}\right) - C_{r,a} . \lambda_{r,a} \qquad (8)$$

Where :

x_i is the fraction of the diet associated with dietary component ‘‘i’’;

$AE_{r,i}$ is the assimilation efficiency(dimensionless) for radionuclide “r” within dietary component “i”;

FMI/M is the ingestion rate per unit mass of animal (kg f.w. day^{-1} per kg f.w.);

$C_{r,i}$ is the activity concentration of radionuclide “r” in dietary component ‘‘i’’ (Bq kg^{-1} f.w.);

$C_{r,a}$ is the ‘‘whole-body’’ activity concentration of radionuclide “r” in the animal (Bq kg^{-1} f.w.); and

$\lambda_{r,a}$ is the effective loss rate of radionuclide “r” from animal(day^{-1}) incorporating both excretion rate and physical decay of the radionuclide.

This model has been applied to determine the transfer to deer/herbivorous mammal and rat/burrowing mammal.

Fresh matter ingestion rates, FMI have been derived using allometric relationships of the form given in Eq. 9 as shown in Table A4.4. The masses for Rat/burrowing mammal have been extracted from ICRP (2008). Since for Deer/herbivorous mammal, the obvious candidate for analyses would be Reindeer (*Rangifer tarandus*), it is possible to be more specific with the appropriate masses to

be used. Although selecting a representative mass for an adult of a particular species is not uncontentious, because of uncertainties associated with seasonal changes and differences between the sexes, a value of 100 kg, based on a cursory synthesis of the data collated by Finstad & Prichard (2000), might not be considered entirely groundless. The following allometric relationship can thus be applied:

$$FMI = a.M^{b} \quad (9)$$

where :

a is the multiplication constant in the allometric relationship for fresh matter intake for animal [kg d^{-1}] b is the exponent in the allometric relationship for fresh matter intake for animal [relative units] M is mass of the animal (kg).

Table A4.4 : Fresh matter ingestion rates, FMI, for the various animals selected for study

Organism	**FMI (kg/d)**	**Comments and references**
Deer/herbivorous mammal	3.6E+00	Mass = 100 kg (Finstad. & Prichard (2000)); FMI for herbivores (kg d^{-1}) = $0.1995M^{0.628}$ from Nagy (2001)
Rat/burrowing mammal	8.4E-02	Mass = 0.314 kg (ICRP, 2008); FMI for Rodentia (kg d^{-1}) = $0.2296M^{0.864}$ from Nagy (2001)

Similarly, $\lambda_{r,a}$ the effective loss rate of radionuclide "r" from animal, a, can be derived using allometric relationships (Table A4.5) along with the animal masses specified above (Table A4.4).

Table A4.5 : Allometric equations used to derive effective loss rates (d^{-1}) for studied animals from mass of animals (kg) (Brown et al., 2003b).

Radionuclide	***Allometric equ.s***
Cs	$\lambda_{r,a} = \frac{\ln 2}{18.36\, M^{0.24}}$
Sr	$\lambda_{r,a} = \frac{\ln 2}{645\, W^{0.26}}$

The various parameters required in the model runs are thus specified in Table A4.6.

Table A4.6. parameters used in dynamic model runs

Parameter	Dependencies : fauna, flora,radionuclide	Value	Units	Notes (references)
x_i	Grass (Deer) Lichen (Deer)	0.75 0.25	dimensionless dimensionless	Åhman (2007)
AE	Deer, Cs Deer, Sr	1 0.3	dimensionless dimensionless	USDoE (2002); USDoE(2002), ICRP 1979 (Part 1)
FMI/M	Deer Rat	3.6E-02 2.7E-01	kg f.w. day^{-1} per kg kg f.w. day^{-1} per kg	(FMI/M) (FMI/M)
$\lambda_{r,a}$	Deer, Cs Deer, Sr Rat, Cs Rat, Sr	1.3E-02 3.2E-04 5.0E-02 1.5E-03	d^{-1} d^{-1} d^{-1} d^{-1}	Table vv; Mass = 100 kg Table vv; Mass = 100 kg Table vv; Mass = 0.314 kg Table vv; Mass = 0.314 kg

The fraction dietary intake of lichen, grass and other vegetation in the diet of reindeer for the period in question is of course unknown but an assumption of 75 % grass intake by mass for September, as adopted by Åhman (2007), and assuming the rest of the diet comprises of lichen can be considered a reasonable first estimate. The inclusion of lichen in the summer diet will have the tendency to yield a conservative estimate of transfer to reindeer.

References

Åhman B (2007). Modelling radiocaesium transfer and long-term changes in reindeer. Journal of Environmental Radioactivity 2007; 98(1-2): 153-165.

AMAP (1998). AMAP assessment report: Arctic pollution issues. Oslo: Arctic Monitoring and assessment programme (AMAP), 1998.

AMEC (2007). Salvage and marine operations IPT/DCS, AMEC Project 1.12 survey of B159. Reference: S&MO/274/5/6, 2007.

Andersson KG, Nielsen SP, Thørring H et al (2011). Revision of deposition and weathering parameters for the ingestion dose module (ECOSYS) of the ARGOS and RODOS decision support systems. Journal of Environmental Radioactivity 2011; 102(11): 1024-1031.

Antipov SV, Bilashenko VP, Vysotskii VL, Kalantarov VE, Kobrinskii MN, Sarkisov AA et al (2015). Prediction and evaluation of the radioecological consequences of a hypothetical accident on the sunken nuclear submarine B-159 in the Barents Sea. Atomic Energy 2015: 119(2): 132-141.

Avila R, Beresford NA, Aguero A, Broed R, Brown J, Iosjpje M et al (2004). Study of the uncertainty in estimation of the exposure of non-human biota to ionising radiation. Journal of Radiological Protection 2004; 24(4A): A105–A122.

Avila R, Broed R, Pereira A (2005) ECOLEGO - A toolbox for radioecological risk assessment. In: Proceedings of the International Conference on the Protection from the Effects of Ionizing Radiation, Stockholm (Sweden) 6.-10. October 2003. IAEA-CN-109/80. Vienna: International Atomic Energy Agency, 2003: 229-232.

Bartnicki J, Haakenstad H, Hov Ø 2011. Operational SNAP model for remote applications from NRPA. Met report 12. Oslo: Norwegian Meteorological Institute, 2011.

Bartnicki J, Amundsen I, Brown J, Hosseini A, Hov Ø, Haakenstad H et al 2016. Atmospheric transport of radioactive debris to Norway in case of a hypothetical accident related to the recovery of the Russian submarine K-27. Journal of Environmental Radioactivity 2016; 151(2): 404-416.

Beresford NA, Barnett CL, Brown JE, Cheng JJ, Copplestone D, Gaschak S et al (2010). Predicting the radiation exposure of terrestrial wildlife in the Chernobyl exclusion zone: an international comparison of approaches. Journal of Radiological Protection 2010; 30(2): 341–373.

Beresford NA, Barnett CL, Jones DG, Wood MD, Appelton JD, Breward N et al (2008a). Background exposure rates of terrestrial wildlife in England and Wales. Journal of Environmental Radioactivity 2008; 99(9): 1430–1439.

Beresford NA, Barnett CL, Howard BJ, Scott WA, Brown JE, Copplestone D (2008b). Derivation of transfer parameters for use within the ERICA Tool and the default concentration ratios for terrestrial biota. Journal of Environmental Radioactivity 2008; 99(9): 1393-1407.

Bondur VG, Ibrayev RA, Grebenyuk Yu V, Sarkisyan GA 2008. Modeling the sea currents in open basins: The case study for the Hawaiian Island region. Izvestiya, Atmospheric and Oceanic Physics 2008; 44(2): 225-235.

Børretzen P, Salbu B (2009). Bioavailability of sediment-associated and low molecular-mass species of radionuclides/trace metals to the mussel Mytilus edulis. Journal of Environmental Radioactivity 2009; 100(4): 333–341.

Brown J, Hosseini A, Børretzen P, Iosjpe M (2003a). Environmental impact assessments for the marine environment: transfer and uptake of radionuclides. StrålevernRapport 2003:7. Østerås: Statens strålevern, 2003.

Brown J, Strand P, Hosseini A, Børretzen P (2003b). Handbook for assessment of the exposure of biota to ionising radiation from radionuclides in the environment. FASSET deliverable 5. https://wiki.ceh.ac.uk/display/rpemain/FASSET+reports (09.11.2017)

Brown JE, Alfonso B, Avila R, Beresford NA, Copplestone D, Pröhl G et al (2008). The ERICA tool. Journal of Environmental Radioactivity 2008; 99(9): 1371-1383.

Brown J, Børretzen P, Dowdall M, Sazykina T, Kryshev I (2004). The derivation of transfer parameters in the assessment of radiological impacts to Arctic marine biota. Arctic; 57(3): 279-289.

Brown J, Amundsen I, Bartnicki J, Dowdall M, Dyve J, Hosseini A et al (2016a). Impacts on the terrestrial environment in case of a hypothetical accident involving the recovery of the dumped Russian submarine K-27. Journal of Environmental Radioactivity 2016; 165: 1-12.

Brown JE, Alfonso B, Avila R, Beresford NA, Copplestone D, Hosseini A (2016b). A new version of the ERICA tool to facilitate impact assessments of radioactivity on wild plants and animals. Journal of Environmental Radioactivity 2016; 153: 141-148.

Bryan K (1969). A numerical method for the study of the circulation of the World Ocean. Journal of Computational Physics 1969; 4(3): 347-376.

Buesseler KO (2012). Fishing for answers off Fukushima. Science 2012; 338(6106): 480-482.

Chernyaev AM, Kazennov A Yu, Vysotskiy VL et al (2003). Main results of radiation monitoring close the light hull of the sunken nuclear submarine «K-159» and adjacent region. Field research October-November 2003. Report of RRC Kurchatov Institute, NIKIET, IBRAE RAS, Russian Navy, Severodvinsk. (In Russian).

Dee DP, Uppala SM, Simmons AJ, Berrisford P, Poli P, Kobayashi S et al (2011). The ERA-Interim reanalysis: configuration and performance of the data assimilation system. Quarterly Journal of the Royal Meteorological Society 2011; 137(656 Part A), 553-597.

Dozhdikov SI, Zhuravkov AM, Zolotkov AA (1991). Corrosion resistance of spent nuclear fuel in sea water. In: Nuclear power at sea. Ecology and safety. Proceedings of the international conference of the Nuclear Society of the USSR on atomic power at sea. September 24-28, 1990, Murmansk. Moscow: Kurchatov Institute, 1991: 337-342. (In Russian).

ENES (2003). Efficiency assessment of the protection barriers of the FA claddings and burnup absorbers of VM-A reactors of NS B-159 in the sea water environment. Report no. 23.7603. Moscow: Engineering Center of Nuclear Equipment Strength (ENES), 2003. (In Russian).

ETOPO5 (1988). Data announcement 88-MGG-02. Digital relief of the surface of the earth. Boulder, Colorado: National Oceanic and Atmospheric Administration (NOAA). National Geophysical Data Center, 1988.

Fesenko S, Sanzharova N, Tagami K (2009). Evolution of plant contamination with time. In: Quantification of radionuclide transfer in terrestrial and freshwater environments for radiological assessments. IAEA-TECDOC 1616. Vienna: International Atomic Energy Agency (IAEA), 2009: 259-263.

Finstad GL, Prichard AK (2000). Growth and body weight of free-range reindeer in western Alaska. Rangifer 2000; 20(4): 221-227.

Fisher NS (2002). Advantages and problems in the application of radiotracers for determining bioaccumulation of contaminants in aquatic organisms. In: Børretzen P, Jølle T, Strand P (eds). Proceedings of the International conference on radioactivity in the environment, Monaco 1–5 September 2002. Østerås: Norwegian Radiation Protection Authority, 2002: 573–576.

Frey, HC (1992). Quantitative analysis of uncertainty and variability in environmental policy making. Research Associate Centre for Energy and Environmental Studies, Department of Engineering and Public Policy. Pittsburg, Carnegie Mellon University, 1992.

Golikov V, Logacheva I, Bruk G, Shutov V, Balonov M, Strand P et al (2004). Modelling of long-term behaviour of caesium and strontium radionuclides in the Arctic environment and human exposure. Journal of Environmental Radioactivity 2004; 74(1-3): 159–169.

Gómez-Ros JM, Pröhl G, Ulanovsky A, Lis M (2008). Uncertainties of internal dose assessment for animals and plants due to non-homogeneously distributed radionuclides. Journal of Environmental Radioactivity 2008; 99(9): 1449-1455.

Gwynn JP, Brown J, Kovacs KM, Lydersen G (2006). The derivation of radionuclide transfer parameters for and dose-rates to an adult ringed seal (Phoca hispida) in an Arctic environment. Journal of Environmental Radioactivity 2006; 90(3): 197-209.

Heldal HE, Vikebø F, Johansen GO (2013). Dispersal of the radionuclide caesium-137 (^{137}Cs) from point sources in the Barents and Norwegian Seas and its potential contamination of the Arctic marine food chain: coupling numerical ocean models with geographical fish distribution data. Environmental Pollution 2013; 180: 190-198.

Holm E, Leisvik M, Ranebo Y (2005). Radioactivity in seals from the Swedish coast. In: Bréchignac F, Howard BJ (eds.). Scientific trends in radiological protection of the environment. ECORAD 2004. , Paris: Lavoisier, 2005: 85-95.

Hosseini A, Beresford NA, Brown JE, Jones DG, Phaneuf M, Thørring H et al (2010). Background dose-rates to reference animals and plants arising from exposure to naturally occurring radionuclides in aquatic environments. Journal of Radiological Protection 2010; 30(2): 235–264.

Hosseini A, Amundsen I, Brown J, Dowdall M, Karcher M, Kauker F et al (2017). Impacts on the marine environment in the case of a hypothetical accident involving the recovery of the dumped Russian submarine K-27, based on dispersion of 137 Cs. Journal of Environmental Radioactivity 2017; 167: 170-179.

Howard BJ, Wright SM, Salbu B, Skuterud KL, Hove K, Loe R (2004). Long-term consequences for Northern Norway of a hypothetical release from the Kola nuclear power plant. Science of the Total Environment 2004; 327(1-3): 53–68.

Hunke EC, Lipscomb WH (2010). CICE: the Los Alamos Sea ice model. Documentation and software user's manual. Version 4.1.
http://oceans11.lanl.gov/trac/CICE/attachment/wiki/WikiStart/cicedoc.pdf

Hunke EC, Lipscomb WH, Turner AK, Jeffery N, Elliott S (2015). CICE: the Los Alamos Sea ice model documentation and software user's manual. Version 5.1 LA-CC-06-012. Los Alamos: Los Alamos National Laboratory, 2015.

IAEA (1996). Modelling of radionuclide interception and loss processes in vegetation and of transfer in semi-natural ecosystems: second report of the VAMP terrestrial working group. IAEA-TECDOC-857. Vienna: International Atomic Energy Agency, 1996.

IAEA (1998). Radiological conditions of the Western Kara Sea: assessment of the radiological impact of the dumping of radioactive waste ion the Arctic Seas. Radiological assessment reports series 4. Vienna: IAEA, 1998.

IAEA (1999). Inventory of radioactive waste disposals at sea. IAEA-TECDOC-1105. Vienna: International Atomic Energy Agency, 1999.

IAEA (2004). Sediment distribution coefficients and concentration factors for biota in the marine environment. Technical reports series 422. Vienna: International Atomic Energy Agency, 2004.

IAEA (2009). Quantification of radionuclide transfer in terrestrial and freshwater environments for radiological assessments. IAEA-TECDOC-1616. Vienna: International Atomic Energy Agency, 2009.

IAEA (2010). Handbook of parameter values for the prediction of radionuclide transfer in terrestrial and freshwater environments. IAEA technical report series 472. Vienna: International Atomic Energy Agency, 2010.

IAEA (2014). Handbook of parameter values for the prediction of radionuclide transfer to wildlife. IAEA technical report series 479. Vienna: International Atomic Energy Agency, 2014.

IAEA (2015). Determining the suitability of materials for disposal at sea under the London Convention 1972 and London Protocol 1996: a radiological assessment procedure. IAEA-TECDOC-1759. Vienna: International Atomic Energy Agency, 2014.

Ibrayev RA, and Kurdyumov DG (2003). Sensitivity of seasonal variability of the Caspian Sea circulation to the parametrization of vertical mixing in a hydrodynamic model. Izvestiya, Atmospheric and Oceanic Physics 2003; 39(6): 768-774.

Ibrayev RA, Sarkisyan AS, Trukhchev DI (2001). Seasonal variability of circulation in the Caspian Sea reconstructed from normal hydrological data. Izvestiya, Atmospheric and Oceanic Physics 2001; 37(1): 96-104.

Ibrayev RA (2001). A study of the sensitivity of the model of the Black Sea current dynamics to the surface boundary conditions. Oceanology 2001; 41(5): 615-621.

Ibrayev RA (2008). Numerical modeling of thermodynamical processes of the Caspian Sea. Moscow: GEOS Publ., 2008. (In Russian).

Ibrayev RA, Ozsoy E, Schrum C, Sur HI (2010). Seasonal variability of the Caspian Sea three-dimensional circulation, sea level and air-sea interaction. Ocean Science 2010; 6: 311-329.

Ibrayev RA, Kalmykov VV, Ushakov KV, Khabeev RN (2011). Eddy-resolving 1/10º model of the world ocean. In: Ivanov VA (ed.). Ecological safety of coastal and shelf zones and comprehensive use of shelf resources: Collected scientific papers. Sevastopol: Marine Hydrophysical Intstitute, 2011; 2(25).

Ibrayev RA, Khabeev RN, Ushakov KV (2012). Eddy-resolving 1/10º model of the world ocean. Izvestiya, Atmospheric and Oceanic Physics 2012; 48(1): 37-46.

ICRP (1979). Limits for intakes of radionuclides by workers. ICRP publication 30 (Part 1). Annals of the ICRP 1979; 2(3-4).

ICRP (1995a). Age-dependent doses to members of the public from intake of radionuclides - part 3 ingestion dose coefficients. ICRP publication 69. Annals of the ICRP 1995; 25(1).

ICRP (1995b). Age-dependent doses to members of the public from intake of radionuclides - part 4 inhalation dose coefficients. ICRP publication 71. Annals of the ICRP 1995; 25(3-4).

ICRP (2007). The 2007 recommendations of the International Commission on Radiological Protection. ICRP publication 103. Annals of the ICRP 2007; 37(2-4).

ICRP (2008). Environmental protection: the concept and use of reference animals and plants. ICRP publication 108. Annals of the ICRP 2008; 38(4-6).

ICRP (2009). Environmental protection: transfer parameters for reference animals and plants. ICRP publication 114. Annals of the ICRP 2009; 39(6).

ICRP (2014). Protection of the environment under different exposure situations. ICRP publication 124. Annals of the ICRP 2014; 43(1).

IPCS (2014). Guidance document on evaluating and expressing uncertainty in hazard characterization. Harmonization project document 11. Geneva: World Health Organization, 2014.

JNREG (in prep.). Joint Norwegian-Russian Expert Group expedition to the site of the sunken nuclear submarine K-159 in the Barents Sea. Edited by Justin P Gwynn and Vyacheslav I Shpinkov.

Kalmykov VV, Ibrayev RA. The overlapping algorithm for solving shallow water equations on massively-parallel architectures with distributed memory. Vestnik UGATU 2013; 17(5): 252-259. (In Russian).

Karlsen SR, Elvebakk A, Høgda KA, Johansen B (2006). Satellite based mapping of the growing season and bioclimatic zones in Fennoscandia. Global Ecology and Biogeography 2006; 15(4): 416–430.

Kato H, Onda Y, Teramage M (2012). Depth distribution of ^{137}Cs, ^{134}Cs, and ^{131}I in soil profile after Fukushima Dai-ichi nuclear power plant accident. Journal of Environmental Radioactivity 2012; 111: 59-64.

Kazennov A Yu (2007). Radiation monitoring of the NS B-159. Moscow: Materials of the Russian-British Expert Group, August 15, 2007. (In Russian).

Killworth PD, Stainforth D, Webb DJ, Paterson S (1991). The development of a free surface Bryan-Cox-Semtner model. Journal of Physical Oceanography 1991; 21(9): 1333-1348.

Kirchner G, Daillant O (2002). The potential of lichens as long-term biomonitors of natural and artificial radionuclides. Environmental Pollution 2002; 120(1): 145–150.

Knysh VV, Ibrayev RA, Korotaev GK, Inyushina NV (2008). Seasonal variability of climatic currents in the Caspian Sea reconstructed by assimilation of climatic temperature and salinity into the model of water circulation. Izvestiya, Atmospheric and Oceanic Physics 2008; 44(2), 236-249.

Kocher DC (1987). A proposal for a generally applicable de minimis dose. Health Physics 1987; 53(2): 117-121.

Kristiansen NI, Stohl A, Olivié DJL, Croft B, Søvde OA, Klein H et al (2016). Evaluation of observed and modelled aerosol lifetimes using radioactive tracers of opportunity and an ensemble of 19 global models. Atmospheric Chemistry and Physics 2016; 16: 3525-3561.

Landrum PF, Lydy HL, Lee H (1992). Toxicokinetics in aquatic systems: model comparison and use in hazard assessment. Environmental Toxicology and Chemistry 1992; 11(12): 1709–1725.

Large W, Yeager S (2004). Diurnal to decadal global forcing for ocean and sea-ice models: the data sets and flux climatologies. NCAR technical note: NCAR/TN-460+STR. Boulder, Colorado: CGD Division of the National Center for Atmospheric Research, 2004.

Large W, Yeager S (2009). The global climatology of an interannually varying air–sea flux data set. Climate Dynamics 2009; 33(2-3): 341-364.

Large WG, McWilliams JC, Doney SC (1994). Oceanic vertical mixing: A review and a model with a nonlocal boundary layer parameterization. Reviews of Geophysics 1994; 32(4): 363– 403.

Larsson CM (2008). An overview of the ERICA Integrated Approach to the assessment and management of environmental risks from ionising contaminants. Journal of Environmental Radioactivity 2008; 99(9): 1364-1370.

Liland A, Lochard J, Skuterud L (2009). How long is long-term? Reflections based on over 20 years of post-Chernobyl management in Norway. Journal of Environmental Radioactivity 2009; 100(7): 581-584.

MALACHITE 2007. Survey of the NS B-159. Report TO -050-83-07. St. Petersburg: St. Petersburg Marine Design Bureau MALACHITE, 2007. (In Russian).

Marchesiello P, McWilliams JC, Shchepetkin AF (2001). Open boundary conditions for long-term integration of regional ocean models. Ocean Modelling 2001; 3(1-2): 1-20.

Marchuk GI, Sarkisyan AS (1988). Mathematical modelling of ocean circulation. Berlin: Springer-Verlag, 1988.

Marchuk GI, Dymnikov VP, Lykossov VN, Zalesny VB, Galin V Ya (1984). Mathematical modeling of general circulation of the atmosphere and ocean. Leningrad: Gidrometeoizdat, 1984. (In Russian).

Mitchell NG (2001). Models for radionuclide transfer to fruits and data requirements. Journal of Environmental Radioactivity 2001; 52(2-3): 291-307.

Monin AS (1956). Semi-empirical theory of turbulent diffusion. Trudy Geofiziceskogo Instituta. Instituta Adademii Nauk SSSR Academy of Science 1956; 33(160). (In Russian).

Nagy KA (2001). Food requirements of wild animals: predictive equations for free-living mammals, reptiles, and birds. Nutrition Abstracts and Reviews Series B, Livestock Feeds and Feeding 2001; 71(10): 21R–32R.

NES (2013). Sunken K-27 Nuclear Submarine Recovery: Risk Overview. Nuclear and Environmental Safety Magazine 2013; 1.

NFB (2014). Protective measures in early and intermediate phases of a nuclear or radiological emergency: Nordic guidelines and recommendations. The Radiation Protection Authorities in Denmark, Finland, Iceland, Norway and Sweden, 2014.

NRPA (2006). K-159: Havariet av den russiske atomubåten K-159 og den norske atomberedskaps organisasjonens håndtering av ulykken. StrålevernRapport 2006:8. Østerås: Statens strålevern, 2008.

NRPA (2014). Joint Norwegian-Russian expedition to investigate the sunken nuclear submarine K-159 in the Barents Sea. NRPA Bulletin 2014:4. Østerås: Statens strålevern, 2014.

NRPA (2015). Inventory and source term evaluation of the dumped nuclear submarine K-27. StrålevernRapport 2015:6. Østerås: Statens strålevern, 2015.

NRPA (2016). Environmental modelling and radiological impact assessment associated with hypothetical accident scenarios for the nuclear submarine K-27. StrålevernRapport 2016:8. Østerås: Statens strålevern, 2016.

Obukhov AM (1946). Turbulence in a temperature-inhomogeneous atmosphere. Trudy Instituta teoretičeskoj geofiziki. Instituta Adademii Nauk SSSR Academy of Science 1946; 1: 95-115. (In Russian).

Rearden BT, Jessee MA (2016). SCALE Code System, ORNL/TM-2005/39, Version 6.2.1. Oak Ridge, Tennessee: Oak Ridge National Laboratory, 2016.

Reistad M, Breivik Ø, Haakenstad H, Aarnes OJ, Furevik BR, Bidlot J-R (2011). A high resolution hindcast of wind and waves for the North Sea, the Norwegian Sea and the Barents Sea. Journal of Geophysical Research 2011; 116(C5): C05019.

Salbu B (2016). Environmental impact and risk assessments and key factors contributing to the overall uncertainties. Journal of Environmental Radioactivity 2016; 151(2): 352-360.

Sarkisov AA, Sivintsev YV, Vysotskiy VL, Nikitin VS (2009). Atomic legacy of the cold war at the Arctic seabed: radioecological consequences and technical and economic problems of radiation remediation at the Arctic Seas. Moscow: Nuclear Safety Institute, 2009.

Sarkisyan AS (1991). Modelling of ocean dynamics. St. Petersburg, 1991. (In Russian).

Sarkisyan AS (1977). Numerical analysis and forecast of sea currents. Leningrad: Gidrometeoizdat, 1977. (In Russian).

Sarkisyan AS (1966). On dynamics of currents in the Equatorial Atlantic. In: Proceedings of the Symposium on the oceanography and fisheries resource of the Tropical Atlantic. Paris: UNESCO, 1966.

Sarkisyan AS, Ibrayev RA, Iakovlev NG (2010). High resolution and four-dimensional analysis as a prospect for ocean modelling. Russian Journal of Numerical Analysis and Mathematical Modelling 2010; 25(5): 477-496.

Schino G, Borfecchia F, De Cecco L, Dibari C, Iannetta M, Martini S et al (2003). Satellite estimate of grass biomass in a mountainous range in central Italy. Agroforestry Systems 2003; 59(2): 157–162.

Shishkin VA, Vasyukhno VP, Orlov Yu V et al (2007). Radiation monitoring of NS B-159 using TLD dosimeters. Moscow: N.A. Dollezhal Research and Development Institute of Power Engineering, 2007. (In Russian).

Sivintsev YuV, Vakulovskiy SM, Vasil'ev AP et al (2005). Human-made radionuclides in seas surrounding Russia. In: Radiological consequences of radioactive waste release into Arctic and Far-East Seas («White Book-2000»). Moscow: IzdAT, 2005. (In Russian).

Sivintsev Yu V, Vysotskiy VL, Danilyan VA. Radiological consequences of the severe radiation accident at the nuclear submarine in Chazhma Bay in 1985. Atomnaya Energiya 1994; 76(2): 158-160. (In Russian).

Staaland H, Garmo TH, Hove K, Pedersen Ø (1995). Feed selection and radiocaesium intake by reindeer, sheep and goats grazing alpine summer habitats in southern Norway. Journal of Environmental Radioactivity 1995; 29(1): 39-56.

Stiansen JE, Korneev O, Titov O, Arneberg P et al (2009). Joint Norwegian-Russian environmental status 2008. Report on the Barents Sea ecosystem. Part II – complete report. IMR/PINRO Joint Report Series 2009(3). Bergen: Institute of Marine Research Polar Research Institute of Marine Fisheries and Oceanography, 2009.

Strand P, Aono T, Brown J, Garnier-Laplace J, Hosseini A, Sazykina T et al (2014). Assessment of Fukushima-derived radiation doses and effects on wildlife in Japan. Environmental Science and Technology Letters 2014; 1(3): 198–203.

Terziev FS, Girduk GV, Zykova GG, Dzhenyuk SL (Eds.). Hydrometeorological conditions. In: Hydrometeorology and hydrochemistry of seas of the USSR. Volume 1. The Barents Sea. Leningrad: Gidrometeoizdat, 1990 (in Russian).

Thomann RV (1981). Equilibrium model of fate of microcontaminants in diverse aquatic food-chains. Canadian Journal of Fisheries and Aquatic Sciences 1981; 38(3): 280-296.

Thørring H, Hosseini A, Skuterud L (2004). Kostholdsundersøkelser 1999 og 2002. Reindriftsutøvere i Midt-Norge. StrålevernRapport 2004:14. Østerås: Statens strålevern, 2004.

Thørring H, Skuterud L (2012). Radioaktiv forurensning i befolkningen: reindriftsutøvere og andre personer i Kautokeino 1965-2010. StrålevernRapport 2012:11. Østerås: Statens strålevern, 2012.

Thørring H, Ytre-Eide MA, Liland A (2010). Consequences in Norway after a hypothetical accident at Sellafield: Predicted impacts on the environment. StrålevernRapport 2010:13. Østerås: Statens strålevern, 2010.

Tolstykh M, Ibrayev R, Volodin E, Ushakov K, Kalmykov V, Shlyaeva A et al (2013). Global atmosphere and world ocean models: Algorithms and supercomputing technologies, manual. Supercomputer Education. Moscow: Moscow University Publishing House, 2013. (In Russian).

Tømmervik H, Johansen B, Riseth JÅ, Karlsen SR, Solberg B, Høgda KA (2009). Above ground biomass changes in the mountain birch forests and mountain heaths of Finnmarksvidda, Northern Norway, in the period 1957–2006. Forest Ecology and Management 2009; 257(1): 244–257.

Uhlig C, Sveistrup TE, Schjelderup I (2004). Impacts of reindeer grazing on soil properties on Finnmarksvidda, northern Norway. Rangifer 2004; 24(special issue 15): 83-91.

Ulanovsky A, Pröhl G (2006). A practical method for assessment of dose conversion coefficients for aquatic biota. Radiation and Environmental Biophysics 2006; 45(3): 203-214.

Ulanovsky A, Pröhl G, Gómez-Ros JM (2008). Methods for calculating dose conversion coefficients for terrestrial and aquatic biota. Journal of Environmental Radioactivity 2008; 99(9): 1440-1448.

Undén P, Rontu L, Järvinen H, Lynch P, Calvo J, Cats G et al (2002). HIRLAM-5 Scientific Documentation, HIRLAM-5 Project. Norrköping, Sweden: Swedish Meteorological and Hydrological Institute, 2002.

UNSCEAR (2008). Sources and effects of ionizing radiation, UNSCEAR 2008 report: Volume II: Annex E: Effects of ionizing radiation on non-human biota. New York: United Nations, 2008.

UNSCEAR (2014). Sources, effects and risks of ionizing radiation, UNSCEAR 2013 report: Volume I: Annex A: Levels and effects of radiation exposure due to the nuclear accident after the 2011 great east-Japan earthquake and tsunami. New York: United Nations, 2014.

USDoE (2002). A graded approach for evaluating radiation doses to aquatic and terrestrial biota. Technical standard DOE-STD-1153-2002. Washington, DC: U.S. Department of Energy, 2002.

Van der Sluijs JP (2007). Uncertainty and precaution in environmental management: Insights from the UPEM conference. Environmental Modelling & Software 2007; 22(5): 590 -598.

Vidal M, Roig M, Rigol A, Montserrat L, Rauret G, Wauters J et al (1995). Two approaches to the study of radiocaesium partitioning and mobility in agricultural soils form the Chernobyl area. Analyst 1995; 120(6): 1785-1791.

Vives i Batlle J, Aono T, Brown JE, Hosseini A, Garnier-Laplace J, Sazykina T et al (2014). The impact of the Fukushima nuclear accident on marine biota: retrospective assessment of the first year and perspectives. Science of the Total Environment 2014; 487: 143-153.

Vives i Batlle J, Beresford NA, Beaugelin-Seiller K, Bezhenar R, Brown J, Cheng J-J et al (2016). Inter-comparison of dynamic models for radionuclide transfer to marine biota in a Fukushima accident scenario. Journal of Environmental Radioactivity 2016; 153: 31-50.

Vives i Batlle J, Wilson RC, Watts SJ, Jones SR, McDonald P, Vives-Lynch S (2008). Dynamic model for the assessment of radiological exposure to marine biota. Journal of Environmental Radioactivity 2008; 99(11): 1711-1730.

Walker, WE, Harremoës, P, Rotmans, J et al (2003). Defining uncertainty: A onceptual basis for uncertainty management in model-based decision support. Integrated Assessment 2003; 4(1): 5–17.

Wang WX, Ke CH, Yu KN, Lam PKS (2000). Modelling the bioaccumulation of radiocesium in a marine food chain. Marine Ecology Progress Series 2000; 208:41–50.

Watson WS, Sumner DJ, Baker JR, Kennedy S, Reid R, Robinson I (1999). Radionuclides in seals and porpoises in the coastal waters around the UK. Science of the Total Environment 1999; 234(1-3): 1-13.

Whicker FW, Schultz V (1982). Kinetics of compartment systems. In: Radioecology: nuclear energy and the environment, volume II. Boca Raton, FL: CRC Press, 1982: 64-117.

WOA 2009. World Ocean Atlas 2009. www.nodc.noaa.gov/OC5/WOA09/pr_woa09.html (09.11.2017)

Statens strålevern
Norwegian Radiation Protection Authority

2017

StrålevernRapport 2017:1
Årsrapport 2016

StrålevernRapport 2017:2
Ionising radiation metrology infrastructure in Europe

StrålevernRapport 2017:3
Radon i nye boliger

StrålevernRapport 2017:4
Stråledoser til øyelinsen for intervensjons-personell

StrålevernRapport 2017:5
Persondosimetritjenesten ved Statens strålevern

StrålevernRapport 2017:6
Faglige anbefalinger for strålebehandling ved ikke-småcellet lungekreft

StrålevernRapport 2017:7
Faglige anbefalinger for kurativ stråle-behandling ved småcellet lungecancer

StrålevernRapport 2017:8
Faglige anbefalinger for lindrende stråle-behandling ved lungecancer

StrålevernRapport 2017:9
Environmental Impact Assessment Of The Removal of Spent Nuclear Fuel (SNF) From Andreeva Bay

StrålevernRapport 2017:10
Radioaktivitet i norsk mat

StrålevernRapport 2017:11
Radioaktivitet i utmarksbeitende dyr 2016

StrålevernRapport 2017:12
Radiological impact assessment for hypothetical accident scenarios involving the Russian nuclear submarine K-159

ISSN 1891-5191 (online)
ISSN 0804-4910 (print)